In-medium properties of ω mesons

In-Medium-Eigenschaften von ω-Mesonen

- Diplomarbeit -

vorgelegt von

Fabian Eichstädt

aus Wettenberg

Institut für Theoretische Physik
Justus-Liebig-Universität Gießen

Gießen, den 07.09.2006

Für Jan und Lena

Contents

Introduction

There has been an ongoing interest in modifications of hadron properties in a nuclear medium for quite some time now. This interest has its main origin in experiments which showed changes of masses and widths of hadrons when put into a strongly interacting medium. Especially mass changes are possibly connected to the restoration of chiral symmetry, which is spontaneously broken in the vacuum. A deeper look into this can be found in [RW00].

In the past a lively discussion has been going on about a possible mass shift of the ω-meson in a nuclear medium. While there seems to be a general agreement that the ω aquires a width of about 40 MeV in the medium, the matter of mass shift is not so commonly agreed on. While some groups have predicted a dropping mass, e.g. [Re02], [Kl97], [Kl99], there have also been suggestions for a rising mass [DM01], [PM01], [SL06], [Zs02] or even a structure with several peaks [Lu02], [Mu06]. In this context a recent experiment by the CBELSA/TAPS collaboration is of particular interest, since they were the first to observe a modification of the product of the spectral function and the relative decay width, indicating a downward shift of the mass of the ω-meson in a nuclear medium [Tr05]. Since Klingl et al. [Kl97] were one of the first to predict this downward shift it is worthwhile to look into their approach in further detail.

In the course of the present work the effective Lagrangian approach of [Kl97] is picked up and examined further. The authors combined vector meson dominance with SU(3) chiral symmetry for coupling nucleons, pseudovector mesons and vector mesons, but no direct ω-nucleon-resonance interaction was included. To examine the importance of such direct resonance-couplings the $S_{11}(1535)$ resonance is included in this work and the effects of this additional coupling are shown in section 7.1.3 and 7.2.

In this framework the authors calculated the ωN forward-scattering amplitude connected it to the ω-selfenergy via the low density theorem. The inelastic processes $\omega N \to \pi N$ and $\omega N \to 2\pi N$, that are relevant for these calculations, were only treated at tree level. A discussion of this approach can be found in section 7.5. In the present work these calculations are reexamined.

The authors used a heavy baryon limit, on behalf of which several possible diagrams at tree level were not included. This is introduced and reviewed rigorously in sections 4.4, 7.1.2 and 7.5 and drastic changes are found when this limit is not considered.

This work is structured as follows: In Part I several mathematical methods are introduced that will be helpful for the later calculations in the present work. In the next few lines a short roadmap of the approach taken is presented, which motivates the inclusion of these mathematical tools. The aim of the present work is a description of the in-medium properties of the ω meson. These properties can be found in the spectral function of the ω. The spectral function itself now is a function of the in-medium selfenergy of the ω, which is discussed in detail in section 3.6. To calculate this selfenergy one can make use of the low density theorem, which connects the selfenergy with the forward-scattering amplitude of the process where the probe (in this the case the ω) is scattered at the constituents of the medium (in this case the nucleons). This is described further in section 3.7. In general the forward-scattering amplitude is a very complex object. However given a specific hadronic model one can calculate the imaginary part of the forward-scattering amplitude at the one-loop level by using Cutkosky's Cutting Rules [PS95]. The mathematical basics for this approach along with Cutkosky's Cutting Rules are introduced in Chapter 1. To obtain the full selfenergy it is now necessary to calculate the real part of the forward-scattering amplitude. Since the real part needs to be regularized [PS95] and since one wants to preserve the analyticity of the scattering amplitude [BD93], this is done by using dispersion relations which connect the real part via a principal value integration with the imaginary part. This is examined in detail in Chapter 2.

Part II introduces the model of [Kl97] which is the underlying framework for all following calculations. Chapter 3 includes the Lagrangians and the model parameters. Here also the derived vertex functions and the form factors are given that are employed in later calculations to account for the inner structure of the baryons and mesons. The connection between the in-medium spectral function of the ω and the ωN forward-scattering amplitude using the low density theorem is also motivated at this point. Chapter 4 is a picture gallery of all the diagrams that were included in this work to calculate the forward-scattering amplitudes and the heavy baryon limit that was used in [Kl97], [Kl98], [Kl99] is introduced.

Part III covers the calculations and results. In Chapter 5 the Feynman rules for the calculations and technicalities concerning the imaginary and real parts of the scattering amplitudes are given. Several representations of the ρ meson vacuum spectral function are needed (the reason for this is discussed in detail in section 5.2.2), which are introduced in Chapter 6. The results for the amplitudes in the different channels together with a comparison with previous calculations are shown in Chapter 7 and the corresponding scattering lengths and cross sections are calculated. Here also the calculated in-medium ω spectral function is presented and finally discussed in section 7.5. Finally there is a summary and an outlook in Chapter 8.

The appendix contains information about the notational and technical conventions and the numerical routines used for the calculations, and the analytic expressions for the scattering amplitudes are given as well as a summary in German language.

Part I

Mathematical tools

Chapter 1

Imaginary parts of Feynman amplitudes

1.1 Propagator descriptions

1.1.1 Φ^4 theory

Quantum Field Theory is the theoretical framework that describes elementary particles and their interactions. Particles are described as excitations of matter fields and interactions by exchange of particles. A simple theory to study basic concepts in this framework is the so called Φ^4 theory. This theory knows just one scalar (spin 0) particle of mass m and involves only one interaction, namely one of four such particles. The Lagrangian looks as follows [PS95]:

$$\mathcal{L} = \frac{1}{2}\left(\partial_\mu \Phi\right)^2 - \frac{1}{2}m^2\Phi^2 - \frac{\lambda}{4!}\Phi^4 \ . \tag{1.1}$$

From this one can derive the Feynman rules in momentum-space to obtain $i\mathcal{M}$, where $\mathcal{M}$ is the transition matrix element:

- for every external particle assign a factor of 1
- for every internal scalar line assign a factor

$$D(q) = \frac{i}{q^2 - m^2 + i\epsilon}$$

- for every vertex assign a factor of $(-i\lambda)$
- impose four-momentum conservation on each vertex
- integrate over every internal momentum, i.e. $\int \frac{d^4p}{(2\pi)^4}$
- divide by the symmetry factor

$D(q)$ is the so-called (Feynman) propagator of Φ^4 theory. Since propagators are an important concept that will be exploited later in this work it is useful to look into their properties a little further. Before doing that, however, it is helpful to denote that the propagation amplitude for a particle in the vacuum to move without interaction from y to x in space-time is given by

$$\langle 0| \Phi(x)\Phi(y) |0\rangle = \int \frac{d^3p}{(2\pi)^3} \frac{1}{2E_p} e^{-ip(x-y)}\bigg|_{p_0=E_p} \quad . \tag{1.2}$$

1.1.2 Feynman propagator

The (Feynman) propagator $D_F(x-y)$ describes the time-ordered propagation of a virtual particle from a space-time point y to a point x, i.e. for $y_0 < x_0$ it describes the propagation of the particle from $\vec{y}$ to $\vec{x}$ and vice versa for $x_0 < y_0$. It is nothing else but the two-point Green's function:

$$D_F(x-y) = \langle \Omega| T\Phi(x)\Phi(y) |\Omega\rangle \ . \tag{1.3}$$

Here $|\Omega\rangle$ denotes the ground state of the theory which generally is different from the state $|0\rangle$, the ground state of the free theory. The Φ represents the field corresponding to the propagating particle and T is the time-ordering symbol.
Now I will show that in the free case the Feynman propagator in position-space has the form

$$D_F(x-y)_{free} = \int \frac{d^4p}{(2\pi)^4} \frac{i}{p^2 - m^2 + i\epsilon} e^{-ip(x-y)} \quad . \tag{1.4}$$

Obviously this is just the Fourier transform of

$$D_F(p) = \frac{i}{p^2 - m^2 + i\epsilon} \ , \tag{1.5}$$

the free propagator in momentum space. For small enough ϵ the poles of $D_F(p)$ are at $p_0 = \pm\sqrt{\vec{p}^{\,2} + m^2 - i\epsilon} = \pm(E_p - i\epsilon)$, meaning one pole is in the upper half-plane and one in the lower half-plane. Therefore the dp_0-integration in equation 1.4 can be evaluated as follows:
For $x^0 > y^0$ the exponential drops to 0 for Im $p^0 \to -\infty$, thus one can close the integration contour in the lower half-plane and gets $\langle 0| \Phi(x)\Phi(y) |0\rangle$. Similarly for $x^0 < y^0$ one can close the contour in the upper half-plane and gets $\langle 0| \Phi(y)\Phi(x) |0\rangle$ (see figure 1.1). Therefore equation (1.4) gives

$$\begin{aligned} D_F(x-y) &= \Theta(x^0 - y^0) \langle 0| \Phi(x)\Phi(y) |0\rangle + \Theta(y^0 - x^0) \langle 0| \Phi(y)\Phi(x) |0\rangle & (1.6)\\ &= \langle 0| T\Phi(x)\Phi(y) |0\rangle \ . & (1.7) \end{aligned}$$

The time-ordering symbol T in the last line implies that the Feynman propagator always transports a particle forward in time.

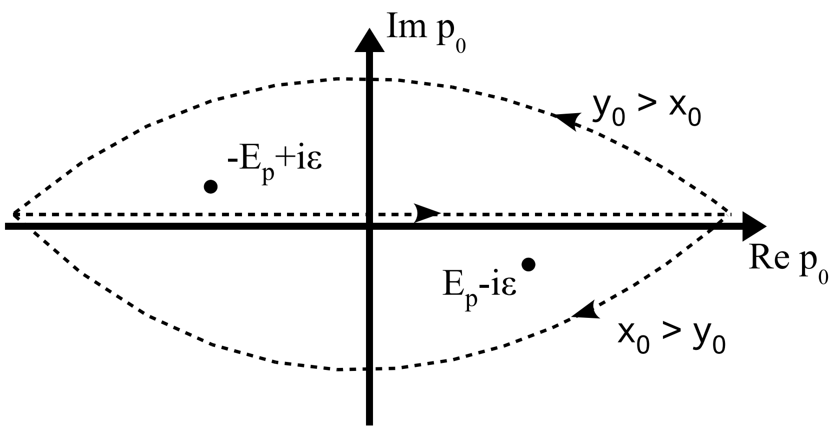

Figure 1.1: Poles of the Feynman propagator and integration contours for different time-ordering.

1.1.3 Retarded and advanced propagator

In section 1.1.5 we will take a look at an example and it will prove very useful to have two additional propagator descriptions at hand, namely the retarded and advanced propagators introduced here. Since they are connected to the Feynman propagator in a special way as shown in section 1.1.4 they will allow for an easy calculation of the imaginary part of the scattering amplitude of the example process.

Similarly to the Feynman propagator one can define the retarded propagator D_R [PS95]:

$$D_R(x-y)_{free} = \int \frac{d^4p}{(2\pi)^4} \frac{i}{p^2 - m^2 + i\epsilon p_0} e^{-ip(x-y)} \ . \tag{1.8}$$

Again one can identify the retarded propagator in momentum space as:

$$D_R(p) = \frac{i}{p^2 - m^2 + i\epsilon p_0} \ . \tag{1.9}$$

This time the poles of $D_R(p)$ are located at $p_0 = \pm E_p - i\epsilon$, i.e. both in the lower half-plane. Therefore the integration yields 0 for $y_0 > x_0$ because we have to close the contour in the upper half-plane. In the case $x_0 > y_0$ however one picks up both poles (see figure 1.2) and gets:

$$\begin{aligned} D_R(x-y) &= \int \frac{d^3p}{(2\pi)^3} \left[\frac{1}{2E_p} e^{-ip(x-y)} + \frac{1}{-2E_p} e^{-ip(y-x)} \right] & (1.10) \\ &= \Theta(x_0 - y_0) \left(\langle 0| \Phi(x)\Phi(y) |0\rangle - \langle 0| \Phi(y)\Phi(x) |0\rangle \right) & (1.11) \\ &= \Theta(x_0 - y_0) \langle 0| [\Phi(x), \Phi(y)] |0\rangle \ . & (1.12) \end{aligned}$$

This quantity vanishes for $x_0 < y_0$ which is the reason why it is called "retarded" propagator. Since the excitation starts at y_0, no effect appears before that point in time.

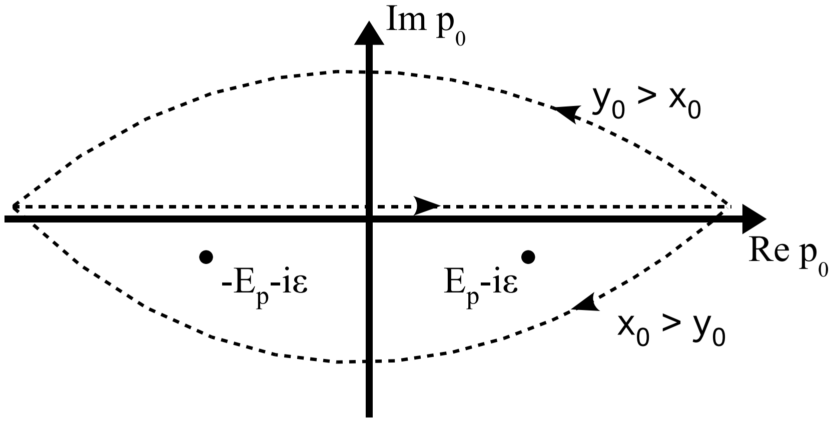

Figure 1.2: Poles of the retarded propagator and integration contours for different time-ordering.

In total analogy one can introduce the advanced propagator [PS95]

$$D_A(x-y)_{free} = \int \frac{d^4p}{(2\pi)^4} \frac{i}{p^2 - m^2 - i\epsilon p_0} e^{-ip(x-y)} \ , \tag{1.13}$$

which in momentum space looks

$$D_A(p) = \frac{i}{p^2 - m^2 - i\epsilon p_0} \ , \tag{1.14}$$

The poles are at $p_0 = \pm E_p + i\epsilon$ in the upper half plane and thus the integration (see figure 1.3) gives:

$$D_A(x-y) = \Theta(y_0 - x_0) \langle 0| [\Phi(y), \Phi(x)] |0\rangle \ . \tag{1.15}$$

It vanishes for $y_0 < x_0$ giving it the name "advanced" propagator.

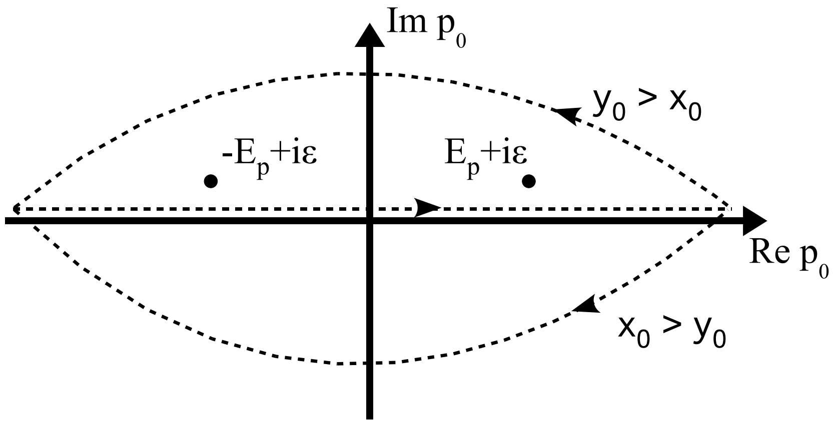

Figure 1.3: Poles of the advanced propagator and integration contours for different time-ordering.

1.1.4 Connection between propagators

For the calculations following below it is useful to take a closer look at the different propagators shown above and to figure out how they are connected to each other. For simplicity we will divide the i out of the propagators, thus looking at $-iD$. Starting with the free Feynman propagator in momentum-space (1.5) and using $x = p^2 - m^2$ we see:

$$-iD_F = \frac{1}{x + i\epsilon} = \frac{x - i\epsilon}{x^2 + \epsilon^2} = \frac{x}{x^2 + \epsilon^2} - i\frac{\epsilon}{x^2 + \epsilon^2} \ . \tag{1.16}$$

Taking ϵ to 0 this yields [PS95]

$$-iD_F \overset{\epsilon \to 0}{=} P\frac{1}{x} - i\pi\delta(x) \ , \tag{1.17}$$

where P denotes that in a following integration the principal value has to be calculated.

In complete analogy one gets for the retarded (1.9) and advanced (1.14) propagators:

$$-iD_{R/A} = \frac{1}{x + i\epsilon(\pm p_0)} \tag{1.18}$$

$$= \frac{x - i\epsilon(\pm p_0)}{x^2 + \epsilon^2 p_0^2} \tag{1.19}$$

$$= \frac{x}{x^2 + \epsilon^2 p_0^2} - i\frac{\epsilon(\pm p_0)}{x^2 + \epsilon^2 p_0^2} \ . \tag{1.20}$$

While in the first term for small enough ϵ the p_0^2 factor does not change the result, we pick up the sign in the second term:

$$-iD_{R/A} = P\frac{1}{x} - i\pi\delta(x) \cdot \text{sgn}(\pm p_0) \ . \tag{1.21}$$

The signum function can now be rewritten:

$$\text{sgn}(p_0) = 1 - 2\Theta(-p_0) \ , \tag{1.22}$$

$$\text{sgn}(-p_0) = 1 - 2\Theta(p_0) \ . \tag{1.23}$$

Substituting for sgn in (1.21) using equations (1.22) and (1.23) we have

$$\begin{aligned} -iD_{R/A} &= P\frac{1}{x} - i\pi\delta(x) \cdot (1 - 2\Theta(\mp p_0)) && (1.24) \\ &= P\frac{1}{x} - i\pi\delta(x) + 2i\pi\delta(x) \cdot \Theta(\mp p_0) && (1.25) \\ &\overset{(1.17)}{=} -iD_F + 2\pi i\delta(x) \cdot \Theta(\mp p_0) \ . && (1.26) \end{aligned}$$

Therefore the Feynman propagator is connected to the advanced and retarded propagator in a simple way:

$$-iD_F(p) = -iD_{R/A}(p) - 2\pi i\delta(p^2 - m^2)\Theta(\mp p_0) \ . \tag{1.27}$$

1.1.5 Illustrative example

The usefulness of the previously deduced propagator relations can now be easily exploited in the following example. Figure 1.4 shows an elementary process in Φ^4 theory, namely the forward-scattering of one particle at another.

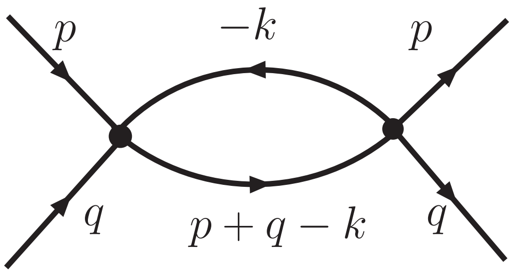

Figure 1.4: Forward scattering of two particles in Φ^4 theory.

According to the Feynman rules of Φ^4 theory we can now calculate the transition amplitude for this process (omitting the symmetry factor):

$$i\mathcal{M} = (-i\lambda)^2 \int \frac{d^4k}{(2\pi)^4} \frac{i}{k^2 - m^2 + i\epsilon} \frac{i}{(p+q-k)^2 - m^2 + i\epsilon} \ . \tag{1.28}$$

The imaginary part of this complex 4-dimensional integral can now be easily evaluated. The idea is to rewrite the Feynman propagators according to equation (1.27) and then to look at the imaginary part of this expression:

$$\mathcal{M} = -\frac{1}{i}\lambda^2 \int \frac{d^4k}{(2\pi)^4} D_F(k) D_F(p+q-k) \ . \tag{1.29}$$

$$\begin{aligned} D_F(k)D_F(p+q-k) = &\left[D_R(k) + 2\pi\delta(k^2-m^2)\ \Theta(-k_0)\right] \\ &\times \left[D_A(p+q-k) + 2\pi\delta((p+q-k)^2-m^2)\right. \\ &\quad \left.\times\ \Theta(p_0+q_0-k_0)\right] \end{aligned}$$

Multiplying this out one ends up with four terms. The first one gives just

$$\mathcal{M}_1 = -\frac{1}{i}\lambda^2 \int \frac{d^4k}{(2\pi)^4} D_R(k) D_A(p+q-k) \ . \tag{1.30}$$

Now looking at the k_0-integration we see that $D_R(k)$ has its poles in the lower half-plane as shown above. $D_A(p+q-k)$ also has its poles in the lower half-plane because the four-momentum k has a minus sign in front of it. Our aim is to close the integration contour in equation (1.30) in the upper half-plane and get 0. This is indeed possible, since one can show that the contribution of the upper half-circle vanishes. This goes as follows: One can rewrite both propagators in equation (1.30) as a Fourier transform of their corresponding propagators in position-space.

$$\mathcal{M}_1 = -\frac{1}{i}\lambda^2 \int \frac{d^4k}{(2\pi)^4} \int d^4x \hat{D}_R(x) e^{ikx} \int d^4y \hat{D}_A(y) e^{i(p+q-k)y} \tag{1.31}$$

$$= -\frac{1}{i}\lambda^2 \int d^4x \int d^4y \int \frac{d^4k}{(2\pi)^4} \hat{D}_R(x)\hat{D}_A(y) e^{i(p+q)y} e^{ik(x-y)} \tag{1.32}$$

As shown in equations (1.12) and (1.15) $D_R(x)$ vanishes for $x_0 < 0$ and $D_A(y)$ vanishes for $y_0 > 0$. Therefore in equation (1.32) one has $x_0 - y_0 > 0$ and the last exponential drops to 0 when $k_0 \to +i\infty$. This means that the contribution of the upper half-circle of the integration indeed vanishes and that one can close the integration contour in the upper half-plane, as we wanted to show.

Thus we are left with the integration over the three remaining terms. Now we look at the imaginary part of $\mathcal{M}$ only:

$$\begin{aligned} \mathrm{Im}\mathcal{M} = \lambda^2 \int \frac{d^4k}{(2\pi)^4} \quad &[\quad \mathrm{Re}D_R(k) 2\pi\delta((p+q-k)^2-m^2)\ \Theta(p_0+q_0-k_0) \\ &+\quad \mathrm{Re}D_A(p+q-k)2\pi\delta(k^2-m^2)\ \Theta(-k_0) \\ &+\quad (2\pi)^2\delta(k^2-m^2)\ \Theta(-k_0)\delta((p+q-k)^2-m^2) \\ &\qquad \times\ \Theta(p_0+q_0-k_0)\ ]\ . \end{aligned} \tag{1.33}$$

Using (1.21), (1.22) and (1.23) one can substitute for the real parts of the propagators in the last equation:

$$\begin{aligned} \mathrm{Re} D_R(k) &= \pi\delta(k^2-m^2)(1-2\Theta(-k_0)) \ , & (1.34)\\ \mathrm{Re} D_A(p+q-k) &= \pi\delta((p+q-k)^2-m^2)(1-2\Theta(p_0+q_0-k_0)) \ . & (1.35)\end{aligned}$$

Therefore we have

$$\begin{aligned} \mathrm{Im}\mathcal{M} = \lambda^2 \int \frac{d^4k}{(2\pi)^4} \quad & [\quad 2\pi^2\delta(k^2-m^2)\delta((p+q-k)^2-m^2) \\ & \quad \times(\Theta(p_0+q_0-k_0)+\Theta(-k_0)) \\ & - \quad (2\pi)^2\delta(k^2-m^2)\delta((p+q-k)^2-m^2) \\ & \quad \times\Theta(p_0+q_0-k_0)\Theta(-k_0) \ ] \ . \qquad (1.36)\end{aligned}$$

With $\Theta(x) \equiv \Theta^2(x)$:

$$\begin{aligned} \mathrm{Im}\mathcal{M} = \lambda^2 \int \frac{d^4k}{(2\pi)^4} \quad & 2\pi^2\delta(k^2-m^2)\delta((p+q-k)^2-m^2) \\ & \times[\ \Theta^2(p_0+q_0-k_0)+\Theta^2(-k_0) \\ & -2\Theta(p_0+q_0-k_0)\Theta(-k_0) \ ] \ . \qquad (1.37)\end{aligned}$$

Arriving at the final formula, we get:

$$\begin{aligned} 2i\ \mathrm{Im}\mathcal{M} = -\frac{1}{i}(-i\lambda)^2 \int \frac{d^4k}{(2\pi)^4} \quad & (-2\pi i)^2\delta(k^2-m^2)\delta((p+q-k)^2-m^2) \\ & \times(\Theta(p_0+q_0-k_0)-\Theta(-k_0))^2 \ . \qquad (1.38)\end{aligned}$$

In the last equation factors of i have been introduced to make a comparison with the following cutting rules easier. Note here that the square of the difference of the Θ-functions states nothing else but that the intermediate particles must have positive energy ($k_0 > 0$) and cannot have more energy than is actually brought into the process by the incoming particles ($k_0 < p_0 + q_0$). Note also that in general an expression like equation (1.28) requires renormalization [PS95]. The expression $\mathrm{Im}\mathcal{M}$ given in equation (1.38), however, is finite (see also section 1.2.3 below). Instead of the propagators in equation (1.28) only δ-functions appear in equation (1.38). They limit the k integrations such that no divergence appears any more and one can see that only particles that are on-shell will contribute to the imaginary part. In the next chapter we will make use of this and actually calculate the imaginary part of the scattering amplitude of the example diagram in figure 1.4. Reducing the propagators to δ-functions has been achieved by showing that (1.30) vanishes and by using equations (1.34) and (1.35). In contrast to $\mathrm{Im}\mathcal{M}$ the real part $\mathrm{Re}\mathcal{M}$ needs renormalization.

1.2 Cutkosky's Cutting Rules

1.2.1 The Rules

In the last section we have calculated the imaginary part of the scattering amplitude by using propagator relations. Another possible approach is to look at the discontinuity of the diagram [PS95]: Let us go back to our example diagram (1.4). Let s be the Mandelstam variable which is just the square of the sum of the four-momenta of the incoming particles and let s_0 be the threshold energy squared for the production of the intermediate particles. If $s < s_0$ the propagators in equation (1.28) cannot go on-shell, which means that e.g. in the first propagator $p^2 - m^2 \neq 0$ and thus the ϵ can be put to zero. (The $+i\epsilon$ description is only necessary to prevent division by 0.) Therefore $\mathcal{M}$ is purely real. This gives just the following relation:

$$\mathcal{M}(s) = [\mathcal{M}(s^*)]^* \ . \tag{1.39}$$

Since $\mathcal{M}$ is an analytic function of s it can be continued to the entire complex plane. The last equation then implies:

$$\text{Re } \mathcal{M}(s + i\epsilon) = \text{Re } \mathcal{M}(s - i\epsilon) \ , \tag{1.40}$$
$$\text{Im } \mathcal{M}(s + i\epsilon) = -\text{Im } \mathcal{M}(s - i\epsilon) \ . \tag{1.41}$$

We have a branch cut across the real axis starting at the threshold energy. The discontinuity across the cut is given by

$$\begin{aligned} \text{Disc } \mathcal{M}(s) &= \mathcal{M}(s + i\epsilon) - \mathcal{M}((s + i\epsilon)^*) \\ &= \mathcal{M}(s + i\epsilon) - \mathcal{M}(s - i\epsilon) \\ \Rightarrow \text{Disc } \mathcal{M}(s) &= 2i \text{ Im } \mathcal{M}(s + i\epsilon) \ . \end{aligned} \tag{1.42}$$

In the last line equations (1.40) and (1.41) have been used. The $(s + i\epsilon)$ in the last equation indicates that the imaginary part has to be evaluated above the branch cut.

Cutkosky proved [Cu60] that the discontinuity of any given Feynman diagram can be calculated with a simple set of cutting rules [Po03]:

- Cut through the diagram in all possible ways so that the cut propagators can simultaneously be put on-shell.
- For every cut through a propagator line corresponding to a stable particle, replace $(p^2 - m^2 + i\epsilon)^{-1}$ by $-2\pi i \ \delta(p^2 - m^2)$.
- For every cut through a propagator line corresponding to a broad particle, replace $(p^2 - m^2 - \Pi)^{-1}$ by $-2\pi i \ A(p^2)$, where $A(p^2)$ is the spectral function of the particle (see section 3.6).
- Sum over all cuts.

1.2.2 Example revisited

Having these rules in mind we can look again at the previous example diagram (1.4). There is only one way this diagram can be cut, namely by cutting the propagators as illustrated in figure (1.5).

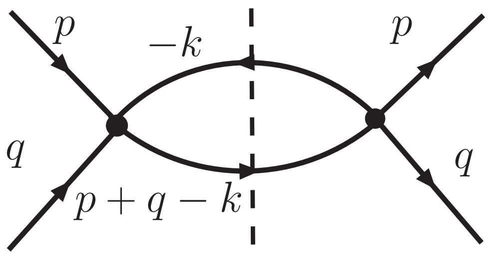

Figure 1.5: Cut through simple example diagram in Φ^4 theory.

Now we can simply apply the cutting rules. Again we start with equation (1.28):

$$i\mathcal{M} = (-i\lambda)^2 \int \frac{d^4k}{(2\pi)^4} \frac{i}{k^2 - m^2 + i\epsilon} \frac{i}{(p+q-k)^2 - m^2 + i\epsilon} \ . \tag{1.43}$$

We have to replace the two cut propagators:

$$2i \ \mathrm{Im} \ \mathcal{M} = -\frac{1}{i}(-i\lambda)^2 \int \frac{d^4k}{(2\pi)^4} (-2\pi i)^2 \delta(k^2 - m^2) \delta((p+q-k)^2 - m^2) \ . \tag{1.44}$$

Now we see that equation (1.44) is equivalent to equation (1.38) except for the Θ-functions. They are omitted in the cutting rules for simplicity and oneself has to take care of proper values of (in our case) k_0. (The conditions of the Θ-functions are partially included in the first rule, which states that one can only cut propagators that can be put on-shell.)

1.2.3 Final evaluation of the example diagram

To obtain the imaginary part of $\mathcal{M}$ the integration over the δ-functions has to be carried out. In the center-of-mass frame we have

$$p = (\frac{\sqrt{s}}{2}, \vec{p}) \ , \tag{1.45}$$

$$q = (\frac{\sqrt{s}}{2}, -\vec{p}) \ , \tag{1.46}$$

$$(p+q)^2 = s \ , \tag{1.47}$$

$$\vec{p}^{\,2} = \frac{s}{4} - m^2 \ . \tag{1.48}$$

Now we will use the first δ-function to cancel the k_0-integration (remember at this point, that here we actually have a condition involving Θ-functions, which were left out in the cutting rules, but which have to be inserted by hand, as mentioned above)

$$\delta(k^2 - m^2) \cdot (\Theta(p_0 + q_0 - k_0) - \Theta(-k_0))^2 = \frac{\delta(k_0 - \hat{k_0})}{2\hat{k_0}}; \; \hat{k_0} = \sqrt{\vec{k}^2 + m^2} \quad (1.49)$$

and the second δ function to cancel the $|\vec{k}|$-integration

$$\delta((p + q - k)^2 - m^2) = \frac{\delta(|\vec{k}| - \hat{k})\sqrt{\hat{k}^2 + m^2}}{2\sqrt{s}\;\hat{k}}; \; \hat{k} = \sqrt{\frac{s}{4} - m^2}\; . \quad (1.50)$$

By substituting these δ-functions in equation (1.44) this yields:

$$2i \; \mathrm{Im}\; \mathcal{M}(s) = i(-i\lambda)^2 \int \frac{d^4k}{(2\pi)^4}(-2\pi i)^2 \frac{\delta(k_0 - \hat{k}_0)}{2\hat{k}_0} \frac{\delta(|\vec{k}| - \hat{k})\sqrt{\hat{k}^2 + m^2}}{2\sqrt{s}\;\hat{k}}\;, \quad (1.51)$$

$$\mathrm{Im}\; \mathcal{M}(s) = \frac{\lambda^2}{8} \int \frac{d^3k}{(2\pi)^2} \frac{\sqrt{\hat{k}^2 + m^2}}{\hat{k}_0 \hat{k} \sqrt{s}} \delta(|\vec{k}| - \hat{k}) = \frac{\lambda^2}{8\pi}\sqrt{\frac{1}{4} - \frac{m^2}{s}}\; . \quad (1.52)$$

In this chapter we have learned how to calculate the imaginary part of a forward-scattering amplitude in the framework of Φ^4-theory. Two seperate methods to do this were demonstrated: One which used the relations between time-ordered, retarded and advanced propagators and one which exploited the analyticity of the scattering amplitude in the complex plane with the exception of a branch cut and then calculated the discontinuity across the cut. The second method was proved by Cutkosky to be valid for any given Feynman diagram and thus it is subsumed in so-called Cutkosky's Cutting Rules, which were given above. These rules will be used in section 5.2 to calculate the imaginary parts of the scattering amplitudes that we will encounter there. Keep in mind that by using this method one obtains a finite expression for Im $\mathcal{M}$ (provided there are no further loops in the cut diagram) as one can see in equation (1.52).

Chapter 2

Dispersion relations

As already mentioned in the introduction the real part of the scattering amplitude that will be calculated in section 7.2 needs renormalization. To preserve the analyticity of the scattering amplitude this is handled here by employing dispersion relations, which are now introduced in this chapter.

2.1 Contour integrals

In complex analysis one very important concept are contour integrals. A contour integral is defined in the following way [Ja99]: Let $U \subset \mathbb{C}$ and let $f : U \to \mathbb{C}$ be continous and let $\gamma : [t_0, t_1] \to U$ be a continously differentiable curve. Then

$$\int_\gamma f(z)dz := \int_{t_0}^{t_1} f(\gamma(t))\frac{d\gamma}{dt}dt \tag{2.1}$$

is the contour integral of f along γ. Cauchy proved that the value of a holomorphic function at a certain point z is basically given by the contour integral over the function along the boundary of a open connected subset which includes z: Let $G \subset \mathbb{C}$ be an open connected subset and let $f : G \to \mathbb{C}$ be holomorphic in G. Let $\gamma : [t_0, t_1] \to G$ be a closed continously differentiable curve, that runs counter-clockwise around $z \in G$ exactly once. Then for this z we have

$$f(z) = \frac{1}{2\pi i}\int_\gamma \frac{f(z')}{z' - z}dz' \ . \tag{2.2}$$

This is a generalization of so-called Cauchy's integral formula.

2.2 Principal values

Let $I \subset \mathbb{R}$ be a finite or infinite interval, $p \in I\backslash\partial I$ and $f : I\backslash p \to \mathbb{C}$. Although the integral

$$\int_I f(x)dx \tag{2.3}$$

might not exist because of a possible singularity at p it is still possible that for *arbitrary* $\epsilon > 0$

$$\int_{I\setminus(p-\epsilon,p+\epsilon)} f(x)dx \tag{2.4}$$

exists. If in this case the limit

$$\lim_{\delta\to+0}\left[\int_{p-\epsilon}^{p-\delta} f(x)dx \ + \ \int_{p+\delta}^{p+\epsilon} f(x)dx\right] =: \mathcal{P}\int_{p-\epsilon}^{p+\epsilon} f(x)dx \tag{2.5}$$

exists, it is called the principal value of the integral over f and so

$$\mathcal{P}\int_I f(x)dx := \int_{I\setminus(p-\epsilon,p+\epsilon)} f(x)dx + \mathcal{P}\int_{p-\epsilon}^{p+\epsilon} f(x)dx \ . \tag{2.6}$$

If f is holomorphic at p then obviously one has:

$$\mathcal{P}\int_I f(x)dx = \int_I f(x)dx \ . \tag{2.7}$$

In the simple case that a holomorphic f has a single pole at p one can calculate the following principal value:

$$\begin{aligned}
\mathcal{P}\int_{p-\epsilon}^{p+\epsilon}\frac{dx}{x-p} &= \lim_{\delta\to+0}\left[\int_{p-\epsilon}^{p-\delta}\frac{dx}{x-p} \ + \ \int_{p+\delta}^{p+\epsilon}\frac{dx}{x-p}\right] && (2.8)\\
&= \lim_{\delta\to+0}\left[\int_{-p+\epsilon}^{-p+\delta}\frac{dx}{x+p} \ + \ \int_{p+\delta}^{p+\epsilon}\frac{dx}{x-p}\right] && (2.9)\\
&= \lim_{\delta\to+0}\left[[\ln(x+p)]_{-p+\epsilon}^{-p+\delta} \ + \ [\ln(x-p)]_{p+\delta}^{p+\epsilon}\right] && (2.10)\\
&= \lim_{\delta\to+0}[\ln(\delta)-\ln(\epsilon) \ + \ \ln(\epsilon)-\ln(\delta)] && (2.11)\\
\mathcal{P}\int_{p-\epsilon}^{p+\epsilon}\frac{dx}{x-p} &= 0 \ . && (2.12)
\end{aligned}$$

Then one can write $f(z) = \frac{c_{-1}}{z-p} + g(z)$ with the Laurent coefficient c_{-1} and a g which is holomorphic at p. Inserting equation (2.12) into (2.6) then just gives:

$$\begin{aligned}
\mathcal{P}\int_I f(x)dx &= \int_{I\setminus(p-\epsilon,p+\epsilon)} f(x)dx + \mathcal{P}\int_{p-\epsilon}^{p+\epsilon} f(x)dx && (2.13)\\
&= \int_{I\setminus(p-\epsilon,p+\epsilon)} f(x)dx + \int_{p-\epsilon}^{p+\epsilon} g(x)dx \ . && (2.14)
\end{aligned}$$

2.3 Dispersion integrals

2.3.1 Simple dispersion relation

Using equation (2.2) one can now connect real and imaginary part of a holomorphic function [BD93]. Let $f : \mathbb{C} \to \mathbb{C}$ be a holomorphic function in the upper halfplane and let z be a point with $\mathrm{Im} z > 0$. Then by Cauchy's integral formula the value of f at z is simply given by

$$f(z) = \frac{1}{2\pi i} \int_C \frac{f(\omega')}{\omega' - z} d\omega' \ , \tag{2.15}$$

with an appropiate contour C in the upper halfplane (see figure 2.1). If we now take z very close to the real axis ($\epsilon > 0$) we get with an appropriate $R > 0$

$$f(\omega + i\epsilon) = \frac{1}{2\pi i} \int_{-R}^{R} \frac{f(\omega')}{\omega' - \omega - i\epsilon} d\omega' \ + \ \frac{1}{2}\mathcal{C}(R) \ . \tag{2.16}$$

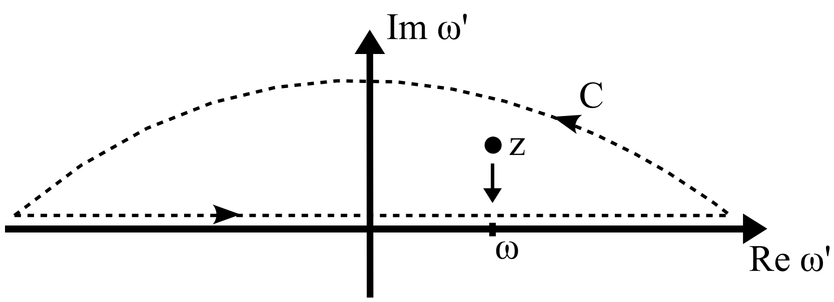

Figure 2.1: Integration contour C with pole at $z = \omega + i\epsilon$ above the real axis.

Here $\mathcal{C}(R)$ is the contribution of the loop of the integral in the upper halfplane. Taking ϵ to 0 the pole in the integrand hits the integration contour. Therefore one has to correct for this by calculating the principal value at the pole ω and by changing the integration contour with a half-circle γ around ω (see figure 2.2):

$$f(\omega) = \lim_{\epsilon \to +0} f(\omega + i\epsilon) = \frac{1}{2\pi i}\mathcal{P} \int_{-R}^{R} \frac{f(\omega')}{\omega' - \omega} d\omega' \ + \frac{1}{2\pi i} \int_\gamma \frac{f(\omega')}{\omega' - \omega} d\omega' \ + \ \frac{1}{2}\mathcal{C}(R) \ . \tag{2.17}$$

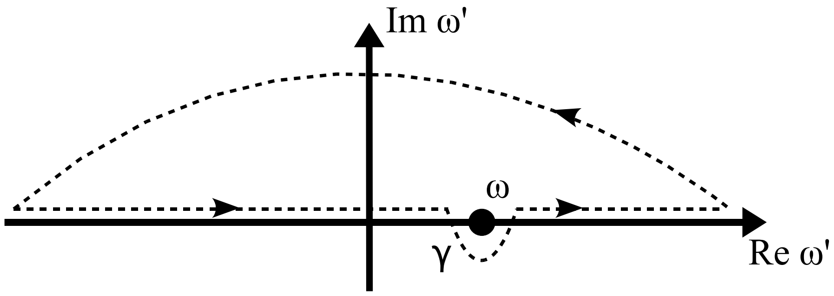

Figure 2.2: Integration contour C with half-circle γ to compensate for the pole on the real axis.

Since

$$\mathcal{P}\int_{-R}^{R}\frac{f(\omega')}{\omega'-\omega}d\omega' \;=\lim_{\delta\to 0}\left(\int_{-R}^{\omega-\delta}\frac{f(\omega')}{\omega'-\omega}d\omega' \;+\int_{\omega+\delta}^{R}\frac{f(\omega')}{\omega'-\omega}d\omega'\right)\;, \tag{2.18}$$

we only have to evaluate f along the half-circle $\gamma(t)=\omega+\delta e^{-i\pi(1-t)}$ with $t=0...1$. In an infinitesimal small circle ($\delta\to 0$) around ω one can rewrite $\frac{f(\omega')}{\omega'-\omega}=\frac{f(\omega)}{\omega'-\omega}+g(\omega')$ with a function g holomorphic at ω. The residual of $\frac{f(\omega')}{\omega'-\omega}$ at ω is simply $f(\omega)$. Thus

$$\int_\gamma\frac{f(\omega')}{\omega'-\omega}d\omega'=f(\omega)\int_\gamma\frac{d\omega'}{\omega'-\omega}+\int_\gamma g(\omega')d\omega'\;. \tag{2.19}$$

Now

$$f(\omega)\int_\gamma\frac{d\omega'}{\omega'-\omega}=f(\omega)\int_0^1\frac{\delta i\pi e^{-i\pi(1-t)}}{\delta e^{-i\pi(1-t)}}dt \tag{2.20}$$

$$=f(\omega)\int_0^1 i\pi dt \tag{2.21}$$

$$=f(\omega)i\pi\;. \tag{2.22}$$

And finally we get

$$\lim_{\delta\to 0}\int_\gamma\frac{f(\omega')}{\omega'-\omega}d\omega'=f(\omega)i\pi\;, \tag{2.23}$$

since g is holomorphic at ω and so the integral over g vanishes when δ goes to zero. Inserting the last line in equation (2.17) yields

$$f(\omega)=\frac{-i}{\pi}\mathcal{P}\int_{-R}^{R}\frac{f(\omega')}{\omega'-\omega}d\omega' \;+\mathcal{C}(R)\;. \tag{2.24}$$

Finally taking the real part of equation (2.24) yields:

$$\mathrm{Re} f(\omega) = \frac{1}{\pi}\mathcal{P}\int_{-R}^{R} \frac{\mathrm{Im} f(\omega')}{\omega' - \omega} d\omega' \ + \mathrm{Re}\ \mathcal{C}(R)\ . \tag{2.25}$$

Now taking R to infinity gives the dispersion relation:

$$\mathrm{Re} f(\omega) = \frac{1}{\pi}\mathcal{P}\int_{-\infty}^{\infty} \frac{\mathrm{Im} f(\omega')}{\omega' - \omega} d\omega' \ + \lim_{R\to\infty} \mathrm{Re}\ \mathcal{C}(R)\ . \tag{2.26}$$

If $f(\omega)$ does go to 0 for $\omega \to \infty$ the closing half-circle in the upper halfplane contributes nothing and $\mathrm{Re}\,\mathcal{C}(R)$ vanishes. However if $f(\omega)$ approaches a constant value for $\omega \to \infty$ there is a non-zero contribution of the half-circle. In this special case one can handle this appropriately by making use of a so-called subtracted dispersion relation, i.e. looking at $g(\omega) = \frac{f(\omega)}{\omega}$ instead of $f(\omega)$. Then g approaches 0 for $\omega \to \infty$ and again the contribution of the half-circle vanishes. This comes at a price however, as one can see in the following section.

2.3.2 Subtracted dispersion relation

We utilize equation (2.25) and first calculate the following difference:

$$\mathrm{Re} f(\omega) - \mathrm{Re} f(0) = \frac{1}{\pi}\mathcal{P}\int_{-R}^{R} \frac{\mathrm{Im} f(\omega')}{\omega' - \omega} d\omega' \ - \ \frac{1}{\pi}\mathcal{P}\int_{-R}^{R} \frac{\mathrm{Im} f(\omega')}{\omega'} d\omega'. \tag{2.27}$$

Note that through this subtraction the contribution of the half-circle is no longer present in the last equation. Now one can take R to infinity:

$$\mathrm{Re} f(\omega) - \mathrm{Re} f(0) = \frac{1}{\pi}\mathcal{P}\int_{-\infty}^{\infty} \frac{\mathrm{Im} f(\omega')}{\omega' - \omega} d\omega' \ - \ \frac{1}{\pi}\mathcal{P}\int_{-\infty}^{\infty} \frac{\mathrm{Im} f(\omega')}{\omega'} d\omega' \tag{2.28}$$

$$= \frac{\omega}{\pi}\mathcal{P}\int_{-\infty}^{\infty} \frac{\mathrm{Im} f(\omega')}{\omega'(\omega' - \omega)} d\omega'\ . \tag{2.29}$$

Now comparing equations (2.26) and (2.29), one sees that the last equation is a dispersion relation for $\frac{f(\omega)}{\omega}$. The constant $\mathrm{Re} f(0)$, that is subtracted from $\mathrm{Re} f(\omega)$, is the price one has to pay for this so-called subtracted dispersion relation, since it has to be known. However this subtracted dispersion relation allows to have a function $f(\omega)$ that approaches a constant for $\omega \to \infty$ and the integral in equation (2.29) still converges. If the divergence of f is of the order $o(\omega)$ or even worse when $\omega \to \infty$, then one in general needs additional subtractions, each one introducing another subtraction constant that has to be known (basically these are the derivatives of f at $\omega = 0$). However if f abides

$$f(-\omega) = f^*(\omega)\ , \tag{2.30}$$

one has

$$\mathrm{Im}f(-\omega) = -\mathrm{Im}f(\omega) \tag{2.31}$$

and so one can exploit this symmetry to write down a dispersion relation with only one subtraction constant that allows for an $f(\omega)$ that is of the order $o(\omega)$ when $\omega \to \infty$. This works as follows:

$$\begin{aligned}
\mathrm{Re}f(\omega) &= \mathrm{Re}f(0) + \frac{\omega}{\pi}\mathcal{P}\int_{-\infty}^{\infty} \frac{\mathrm{Im}f(\omega')}{\omega'(\omega'-\omega)}d\omega' && (2.32)\\
&= \mathrm{Re}f(0) + \frac{\omega}{\pi}\mathcal{P}\int_{-\infty}^{0} \frac{\mathrm{Im}f(\omega')}{\omega'(\omega'-\omega)}d\omega' \; + \frac{\omega}{\pi}\mathcal{P}\int_{0}^{\infty} \frac{\mathrm{Im}f(\omega')}{\omega'(\omega'-\omega)}d\omega' && (2.33)\\
&\overset{(2.31)}{=} \mathrm{Re}f(0) - \frac{\omega}{\pi}\mathcal{P}\int_{0}^{\infty} \frac{\mathrm{Im}f(\omega')}{\omega'(\omega'+\omega)}d\omega' \; + \frac{\omega}{\pi}\mathcal{P}\int_{0}^{\infty} \frac{\mathrm{Im}f(\omega')}{\omega'(\omega'-\omega)}d\omega' && (2.34)\\
\mathrm{Re}f(\omega) &= \mathrm{Re}f(0) + \frac{2\omega^2}{\pi}\mathcal{P}\int_{0}^{\infty} \frac{\mathrm{Im}f(\omega')}{\omega'(\omega'^2-\omega^2)}d\omega' \quad . && (2.35)
\end{aligned}$$

Looking at the behavior of the integrand for large ω one can see that the integral is convergent as long as $f(\omega)$ does rise slower than ω^2 for large values of ω (since then the integrand falls quicker than $\frac{1}{\omega}$). To derive the last equation was the goal of this section, since it is the once subtracted dispersion relation that will later be used for all the dispersion calculations.

Part II

The Model

Chapter 3

An effective Lagrangian

3.1 Introduction

Since the late sixties Vector Meson Dominance (VMD) is known to yield a very good description of the electromagnetic interaction of hadrons [Fe72],[Sa69]. Especially the annihilation of e^+e^- pairs into hadrons in the low energy regime up to $\sqrt{s} \sim 1$ GeV is described very well [Kl97]. The cross section of this annihilation is proportional to the imaginary part Im Π of the current-current (CC) correlation function:

$$\frac{\sigma(e^+e^- \to \text{hadrons})}{\sigma(e^+e^- \to \mu^+\mu^-)} = -\frac{12\pi}{s}\text{Im}\Pi(s) \ . \tag{3.1}$$

The CC correlation function and its details are given in [Kl97], equations (1) - (7).

As one can see in figure 3.1 VMD gives a very good description in this case of the isoscalar (ω) channel of the electromagnetic current. Based on this finding an effective Lagrangian was constructed which adds chiral SU(3) dynamics [Kl97] to the already successful VMD-model. In the following sections the different parts of this Lagrangian will be introduced and the appearing vertex function which are necessary for the following calculations will be given.

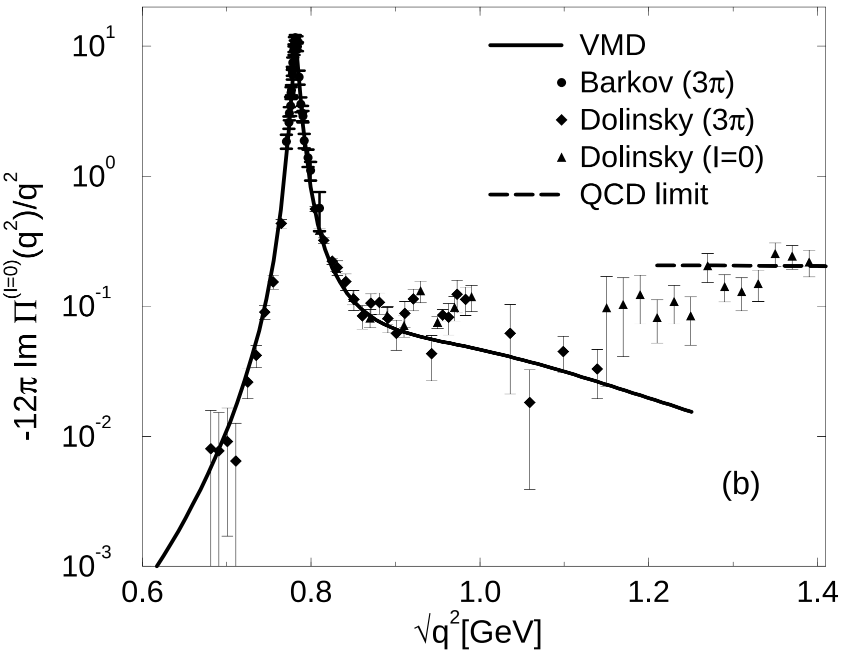

Figure 3.1: $\sigma(e^+e^- \to \text{hadrons})/\sigma(e^+e^- \to \mu^+\mu^-)$ as a function of c.m.-energy in the isoscalar channel. Up to $\sqrt{q^2} \sim 1$ GeV VMD proves to be a sensible model for the electromagnetic hadron interaction. The dashed line represents the pertubative QCD limit. (figure taken from [Kl97])

3.2 Effective Lagrangian

In this section we exploit the fact that for SU(3) symmetry one can introduce a 3X3 matrix representation (details can be found in [Mo99]), which proves here to be more convenient than using e.g. an 8-dimensional vector to describe the baryon octet. All the Lagrangians and matrix fields in this section are taken from [Kl98] (in the form (Kl-#)) and the according equation numbers are given for easy comparison (many of the details can also be found in [Kl96]). The matrix fields in the following Lagrangians will be used for simplicity. As shown in equation (Kl-2.10) the neutral vector meson components of the vector meson nonet [PD02] look as follows:

$$V^\mu \equiv \begin{pmatrix} \rho + \omega & 0 & 0 \\ 0 & -\rho + \omega & 0 \\ 0 & 0 & \sqrt{2}\Phi \end{pmatrix}^\mu . \tag{3.2}$$

The matrix field of the baryon octet is given by equation (Kl-4.46):

$$B \equiv \begin{pmatrix} \frac{\Lambda}{\sqrt{6}} + \frac{\Sigma^0}{\sqrt{2}} & \Sigma^+ & p \\ \Sigma^- & \frac{\Lambda}{\sqrt{6}} - \frac{\Sigma^0}{\sqrt{2}} & n \\ \Xi^- & \Xi^0 & -\frac{2}{\sqrt{6}}\Lambda \end{pmatrix} \ . \tag{3.3}$$

The electromagnetic charge matrix (SU(3)-form) is (equation (Kl-2.31)):

$$Q = \begin{pmatrix} \frac{2}{3} & 0 & 0 \\ 0 & -\frac{1}{3} & 0 \\ 0 & 0 & -\frac{1}{3} \end{pmatrix} \ . \tag{3.4}$$

And the pseudo-scalar meson octet reads (equation (Kl-1.32)):

$$\Phi \equiv \sqrt{2} \begin{pmatrix} \frac{\pi^0}{\sqrt{2}} + \frac{\eta}{\sqrt{6}} & \pi^+ & K^+ \\ \pi^- & \frac{-\pi^0}{\sqrt{2}} + \frac{\eta}{\sqrt{6}} & K^0 \\ K^- & \bar{K}^0 & -\frac{2\eta}{\sqrt{6}} \end{pmatrix} \ . \tag{3.5}$$

The SU(3)-Lagrangian for the interaction of the pseudo-scalar mesons and the baryons is given by equation (Kl-4.45):

$$\mathcal{L}_{\Phi B} = F\ tr\left(\bar{B}\gamma_\mu\gamma_5 \left[u^\mu, B\right]\right) + D\ tr\left(\bar{B}\gamma_\mu\gamma_5 \left\{u^\mu, B\right\}_+\right) \ . \tag{3.6}$$

$$u^\mu = -\frac{1}{2f_\pi}\left(\partial^\mu\Phi - ie\left[Q, \Phi\right] A^\mu\right) \tag{3.7}$$

is given in equation (Kl-4.47) and contains the minimal gauge invariant coupling of the pseudo-scalar meson octet Φ with the photon field A_μ. $F \simeq 0.51$ and $D \simeq 0.75$ fulfill $g_A = F + D = 1.26$, where g_A is the axial-vector coupling constant of the nucleon. The direct vector meson-nucleon coupling is given by equation (Kl-4.50). However the relative sign between the first and second term is presumably a typing error, since with a minus sign the SU(3)-relation for the vector meson-nucleon coupling constants $g \equiv g_{\rho N} = \frac{1}{3} g_{\omega N}$ would not be fulfilled. The correct version is:

$$\mathcal{L}_{VB} = \frac{g}{2}\left(tr(\bar{B}\gamma_\mu \left[V^\mu, B\right]) + tr(\bar{B}\gamma_\mu B) tr(V^\mu)\right) \ . \tag{3.8}$$

Proof: Since we are only interested in the vector meson-nucleon coupling we can disregard all the elements in the matrix of the baryon octet (equation (3.3)) except for the proton and the neutron. Then we have:

$$[V^\mu, B] = \left[\begin{pmatrix} \rho+\omega & 0 & 0 \\ 0 & -\rho+\omega & 0 \\ 0 & 0 & \sqrt{2}\Phi \end{pmatrix}^\mu , \begin{pmatrix} 0 & 0 & p \\ 0 & 0 & n \\ 0 & 0 & 0 \end{pmatrix} \right] \tag{3.9}$$

$$= \begin{pmatrix} 0 & 0 & (\rho+\omega)p \\ 0 & 0 & (-\rho+\omega)n \\ 0 & 0 & 0 \end{pmatrix}^\mu - \begin{pmatrix} 0 & 0 & \sqrt{2}\Phi p \\ 0 & 0 & \sqrt{2}\Phi n \\ 0 & 0 & 0 \end{pmatrix}^\mu \tag{3.10}$$

$$= \begin{pmatrix} 0 & 0 & (\rho+\omega-\sqrt{2}\Phi)p \\ 0 & 0 & (-\rho+\omega-\sqrt{2}\Phi)n \\ 0 & 0 & 0 \end{pmatrix}^\mu \tag{3.11}$$

and so

$$tr(\bar{B}\gamma_\mu [V^\mu, B]) = tr\left(\begin{pmatrix} 0 & 0 & 0 \\ 0 & 0 & 0 \\ \bar{p} & \bar{n} & 0 \end{pmatrix} \gamma_\mu \begin{pmatrix} 0 & 0 & (\rho+\omega-\sqrt{2}\Phi)p \\ 0 & 0 & (-\rho+\omega-\sqrt{2}\Phi)n \\ 0 & 0 & 0 \end{pmatrix}^\mu \right) \tag{3.12}$$

$$= tr \begin{pmatrix} 0 & 0 & 0 \\ 0 & 0 & 0 \\ 0 & 0 & \bar{p}\gamma_\mu(\rho+\omega-\sqrt{2}\Phi)^\mu p + \bar{n}\gamma_\mu(-\rho+\omega-\sqrt{2}\Phi)^\mu n \end{pmatrix} \tag{3.13}$$

$$= (\bar{p}\gamma_\mu p - \bar{n}\gamma_\mu n)\rho^\mu + (\bar{p}\gamma_\mu p + \bar{n}\gamma_\mu n)\omega^\mu - (\bar{p}\gamma_\mu p + \bar{n}\gamma_\mu n)\sqrt{2}\Phi^\mu . \tag{3.14}$$

In addition we have

$$tr\left(\bar{B}\gamma_\mu B\right) = \bar{p}\gamma_\mu p + \bar{n}\gamma_\mu n \tag{3.15}$$

and

$$tr\,(V^\mu) = 2\omega^\mu + \sqrt{2}\Phi^\mu \ . \tag{3.16}$$

Now inserting into equation (3.8) yields:

$$\mathcal{L}_{VB} = \frac{g}{2}(\bar{p}\gamma_\mu p - \bar{n}\gamma_\mu n)\rho^\mu + \frac{3g}{2}(\bar{p}\gamma_\mu p + \bar{n}\gamma_\mu n)\omega^\mu \ . \tag{3.17}$$

The last equation shows the correct behavior as described in [Kl98]: There is no direct ΦN-coupling and the SU(3)-relation $g = g_{\rho N} = \frac{1}{3}g_{\omega N}$ is fulfilled. However having a minus sign between the first and second term in equation 3.8 would lead to the *wrong* result:

$$\mathcal{L}_{VB}^{\mathrm{WRONG}} = \frac{g}{2}(\bar{p}\gamma_\mu p - \bar{n}\gamma_\mu n)\rho^\mu - \frac{g}{2}(\bar{p}\gamma_\mu p + \bar{n}\gamma_\mu n)\omega^\mu - \frac{g}{2}2\sqrt{2}(\bar{p}\gamma_\mu p + \bar{n}\gamma_\mu n)\Phi^\mu \ . \tag{3.18}$$

Obviously the last line does NOT fulfill the conditions given above and therefore the plus sign in equation (3.8) is correct.

Corrections by the anomalous vector meson-nucleon tensor coupling are also taken into account (equation (Kl-4.51)):

$$\mathcal{L}_{VN} = \frac{g\kappa_\rho}{4M_N}\bar{N}\vec{\tau}\sigma_{\mu\nu}N\partial^\mu\vec{\rho}^\nu + \frac{g\kappa_\omega}{4M_N}\bar{N}\sigma_{\mu\nu}N\partial^\mu\omega^\nu \ . \tag{3.19}$$

Finally there is a $\rho\omega\pi$-interaction whose Lagrangian is taken from [Kl96] equation (Kl-3.13):

$$\mathcal{L}_{V\Phi} = \frac{g_{\rho\omega\pi}}{4f_\pi}\epsilon^{\mu\nu\alpha\beta}tr\left(\partial_\mu V_\nu V_\alpha \partial_\beta \Phi\right) \ . \tag{3.20}$$

In the present work the constants given above have the following values:

$$\begin{aligned} g_A &= 1.26, \\ g &= 6.05, \\ f_\pi &= 0.0924 \text{ GeV}, \\ \kappa_\rho &= 6.0, \\ \kappa_\omega &= 0, \\ g_{\rho\omega\pi} &= 1.2, \\ M_N &= 0.93827 \text{ GeV}. \end{aligned}$$

While the first four constants are taken directly from [Kl98], setting κ_ω to 0 resembles the fact that the ωN tensor-coupling is neglected in this work for simplicity. Looking at the very small value of 0.1 given for κ_ω in [Kl98] this seems to be a valid simplification. $g_{\rho\omega\pi}$ was chosen to match the 1π-channel of [Kl99] as shown in section 7.1.1. In [Kl99] however a value $g_{\rho\omega\pi} = -1.2$ was found. With this value we cannot reproduce the results for the 1π-channel, however with the opposite sign as chosen above we can. The nucleon mass is taken from [PD02].

3.3 Vertex functions

In this section the vertex functions that are needed in the later calculations and that have to be derived from the effective Lagrangians above are shown in the following figures. They were taken from [Kl97] and checked. Figure 3.2 shows the πN vertex function.

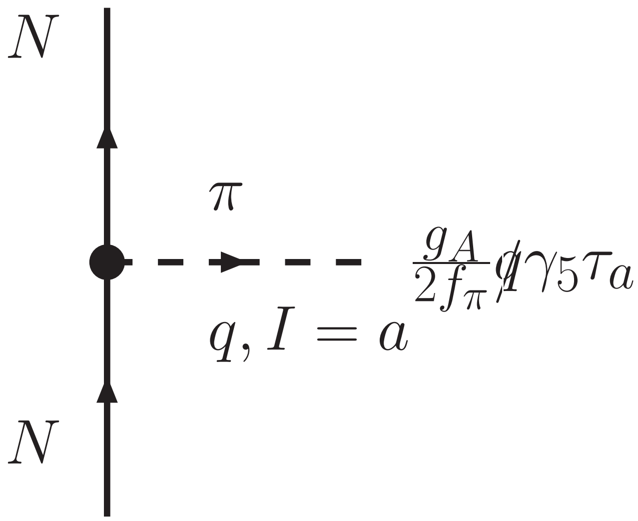

Figure 3.2: Vertex function for a pion interacting with a nucleon. The pion carries isospin a and momentum q (taken from [Kl97]).

The ρN vertex is illustrated in figure 3.3.

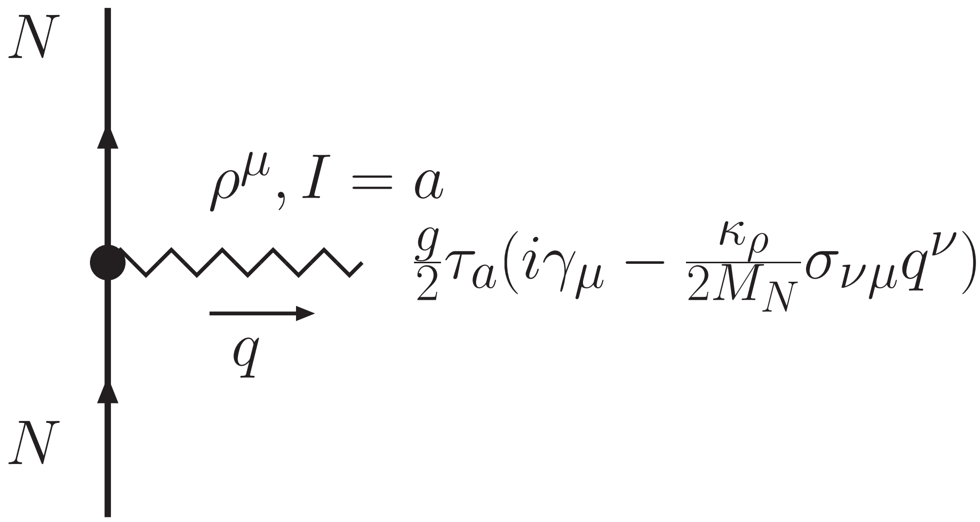

Figure 3.3: Vertex function for a ρ meson interacting with a nucleon. The ρ carries isospin a and momentum q (taken from [Kl97]).

For the ωN coupling see figure 3.4.

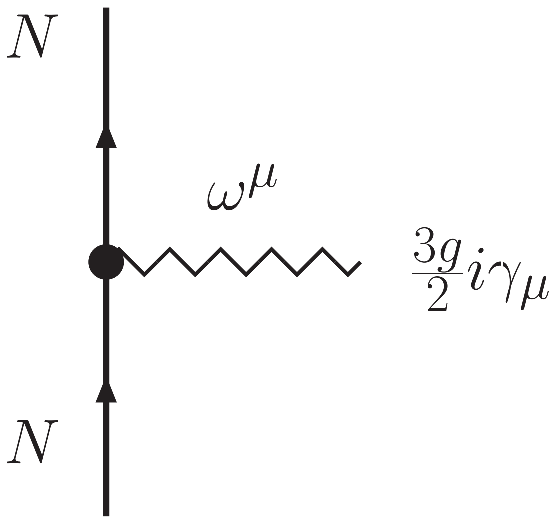

Figure 3.4: Vertex function for an ω meson interacting with a nucleon (taken from [Kl97]).

Finally the vertex function for the $\rho\omega\pi$ interaction is shown in figure 3.5.

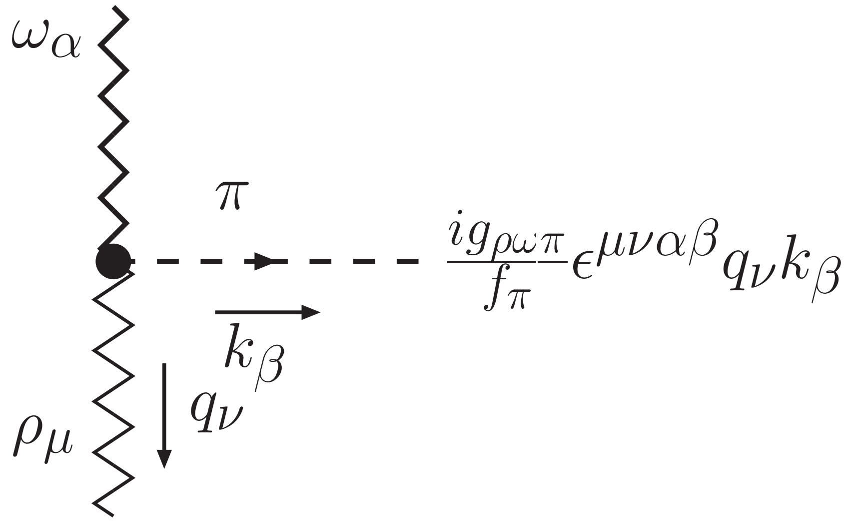

Figure 3.5: Vertex function for an ω meson interacting with a ρ meson and a pion. The ρ carries momentum q, the pion carries momentum k (taken from [Kl97]).

3.4 Resonance interaction

In addition to the model employed by Klingl in [Kl98] the present work also includes an additional resonance interaction. Specifically a coupling of the ωN

system to the $S_{11}(1535)$ resonance is included. The Lagrangian for this interaction is extracted from [PM02] (equation C8) and looks as follows:

$$\mathcal{L}_{RN\omega} = -\bar{u}_R\,(-i\gamma_5)\left(g_1\gamma_\mu - \frac{g_2}{2M_N}\sigma_{\mu\nu}\partial_\omega^\nu\right)u_N\omega^\mu \ . \tag{3.21}$$

The coupling constants are taken from [Sh05] (table IV):

$$g_1 = 3.79,$$
$$g_2 = 6.50.$$

3.5 Form factors

Since in this work a hadronic model is employed the inner structures of the participating particles is not taken into account. Therefore we expect our model to be valid only for energies up to 1 GeV, since at higher energies this inner structure would be resolved. To compensate for this deficiency, form factors are introduced that lead to a suppression at higher energies. For the pion-nucleon vertex the axial form factor from [Kl97] is used:

$$G_A(k^2) = \frac{g_A}{(1-\frac{k^2}{\Lambda_A^2})^2} \ . \tag{3.22}$$

Here k is the four-momentum of the pion and $\Lambda_A \simeq 1$ GeV [Ki83].
For the vector meson-baryon coupling we use

$$F_{VB}(k^2) = \frac{\lambda_V^2 - m_V^2}{\lambda_V^2 - k^2} \ . \tag{3.23}$$

Here k is the four-momentum and m_V the mass of the vector meson. $\Lambda_V \simeq 1.6$ GeV is chosen [Kl97]. How exactly these form factors are employed is described below in section 5.2 together with the corresponding calculations.

3.6 Spectral function and selfenergy

The aim of the present work is a calculation of the ω spectral function in a nuclear medium. Therefore it is worthwhile at this point to look into the technical details of spectral functions a little further. The in-medium spectral function $A(q)$ of the ω is given by [Po03]

$$A_{med}(q) = -\frac{1}{\pi}\mathrm{Im}\frac{1}{q^2 - (m_\omega^0)^2 - \Pi_{vac}^{ret}(q) - \Pi_{med}^{ret}(q)}, \tag{3.24}$$

with the bare mass m_ω^0 of the ω. Since in the present work the full retarded propagator is defined as (compare with section 1.1.3)

$$D^{ret}(q) = \frac{i}{q^2 - m^2 - \Pi^{ret}(q)}, \tag{3.25}$$

we have

$$A_{med}(q) = -\frac{1}{\pi}\text{Re } D^{ret}_{med}(q). \tag{3.26}$$

The last line implies that one has to calculate the (real part of the) retarded in-medium propagator to obtain the spectral function. As one can see from equation (3.25) the retarded propagator depends on the retarded selfenergy Π^{ret}. In the nuclear medium this selfenergy can be decomposed into the vacuum contribution Π^{ret}_{vac} and the medium contribution Π^{ret}_{med} [Po03].

The details of the vacuum contribution of the selfenergy for the ω-meson are presented in section 7.4. The contribution of the nuclear medium can be calculated using the low density theorem, which is introduced in the next section.

3.7 ω mesons at rest and low density theorem

In the present work we are looking at a nuclear medium with density $\rho \neq 0$ and temperature $T = 0$ which is moving with a constant four-velocity. Then we can choose a frame where the nuclear medium is at rest, i.e. its three-momentum is 0. Since the aim of the present work is a calculation of the in-medium ω mass, it is useful to look at the case $q = (\omega, 0)$ where the ω is at rest inside the nuclear medium. This is a valid approximation since a bound ω meson is expected to have very small three-momentum. In [Kl97] it is shown that for this case the forward-scattering amplitude is given by

$$T(\omega) = -\frac{1}{3} g_{\mu\nu} T^{\mu\nu}(\omega, \vec{q} = 0) \ . \tag{3.27}$$

Here $T^{\mu\nu}$ is the forward-scattering tensor in analogy to the Comptontensor of the forward-scattering of a virtual photon at a free nucleon. The scattering process is depicted in figure 3.6.

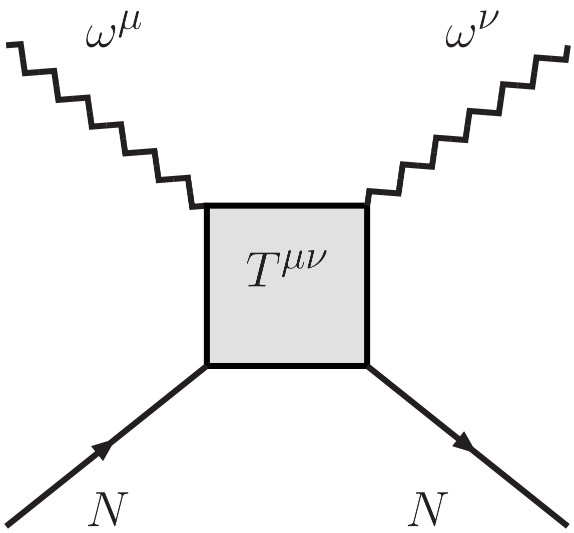

Figure 3.6: General picture of the ωN forward-scattering tensor.

The scattering graph in figure (3.6) is connected to the selfenergy (or better polarization) graph in figure (3.7). It can be obtained by cutting the nucleon line in the selfenergy graph.

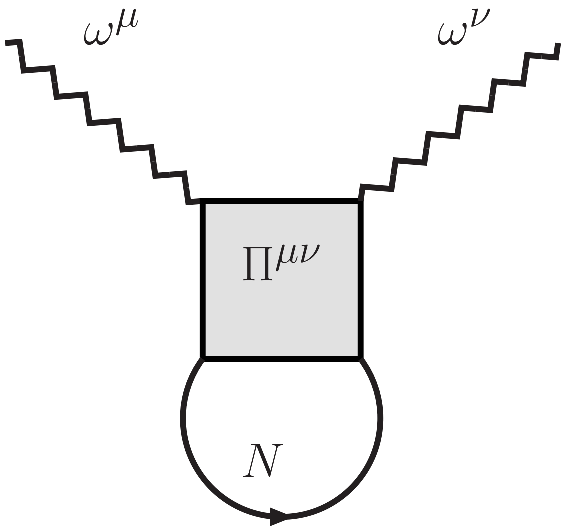

Figure 3.7: Selfenergy graph of the ω.

Equation (3.27) is basically an average over the polarizations of the ω.

If the density ρ is small enough one can neglect the momentum-dependence of the scattering tensor [Mu06] and apply the low density theorem [Kl97]:

$$\Pi^{ret}_{med}(\omega, \vec{q} = 0; \rho) = -\rho T^{ret}(\omega) \ . \tag{3.28}$$

Note here, that T^{ret} is a retarded *vacuum* forward-scattering amplitude. However in [Po03] it is shown that in the vacuum case there are simple relations for time-ordered and retarded quantities:

$$\text{Re } \Pi^F(q) = \text{Re } \Pi^{ret}(q) \ , \tag{3.29}$$

$$\text{Im } \Pi^F(q) = \text{sgn}(q_0)\text{Im } \Pi^{ret}(q) \ . \tag{3.30}$$

In total analogy one can now treat the retarded vacuum forward-scattering amplitude in equation (3.28) and see that it fulfills the same relations. This is the reason why it is sufficient to calculate the imaginary part of the Feynman forward-scattering amplitude in section 5.1. Since the retarded amplitude is analytic in the upper half-plane, so is the time-ordered amplitude for positive energies ($q_0 > 0$). This is important, since this allows us to calculate the real part of the scattering amplitude via a dispersion relation as introduced in Chapter 2.

Chapter 4

Diagrams

As motivated in the introduction and in section 3.7 we are interested in the vector meson-nucleon forward-scattering amplitude at the one-loop-level. To obtain the imaginary part of this amplitude via Cutkosky's Cutting Rules one needs as input the inelastic reactions $\omega N \to \pi N$ (1π-channel) and $\omega N \to 2\pi N$ (2π-channel). The corresponding diagrams for these two channels are presented in this chapter. In addition one more diagram including the $S_{11}(1535)$ resonance is included to study its influence on the behavior of the ω in a nuclear medium, as already mentioned in the introduction. Finally the heavy baryon limit that was employed in [Kl97], [Kl99] is introduced.

4.1 1π-channel

In this section all the diagrams calculated in this work which contribute to the $\omega N \to \pi N$ decay channel are shown. They are exactly the same as mentioned in [Kl98] (section 4.2.3).

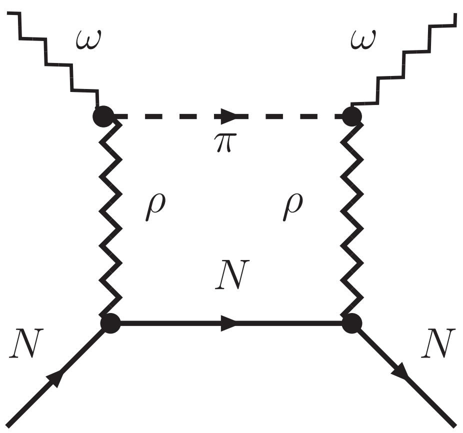

Figure 4.1: Diagram a)

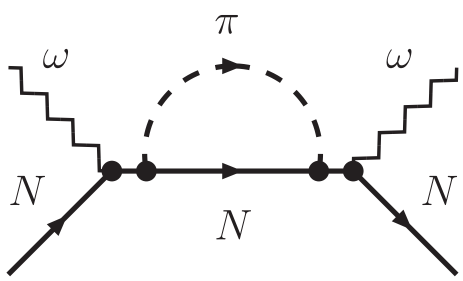

Figure 4.2: Diagram b)

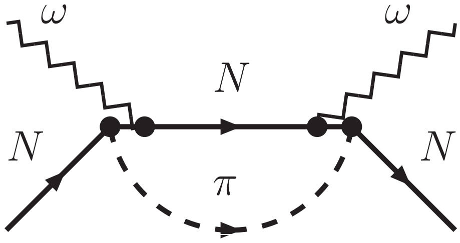

Figure 4.3: Diagram c)

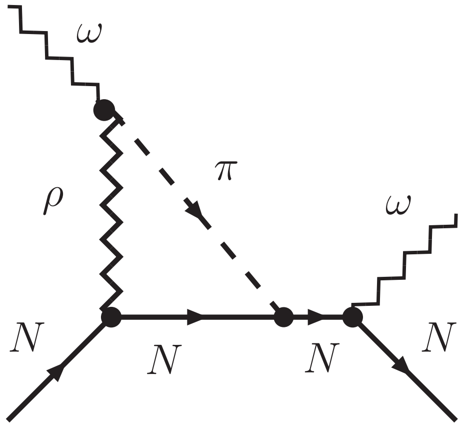

Figure 4.4: Diagram d)

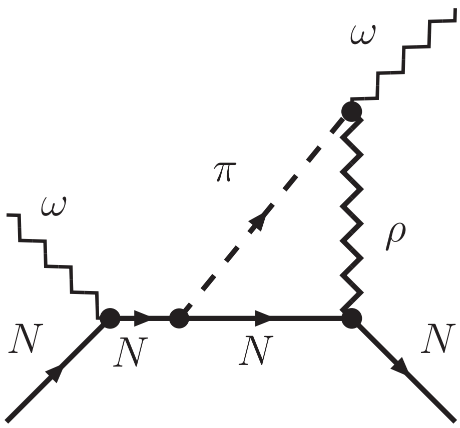

Figure 4.5: Diagram e)

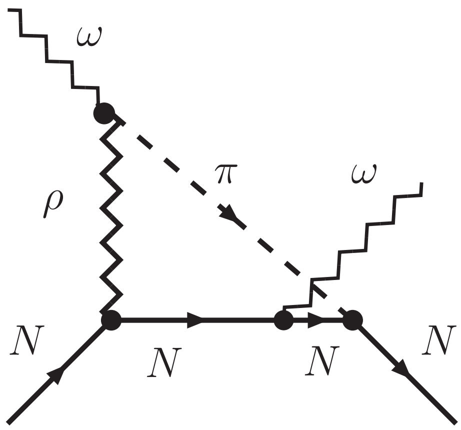

Figure 4.6: Diagram f)

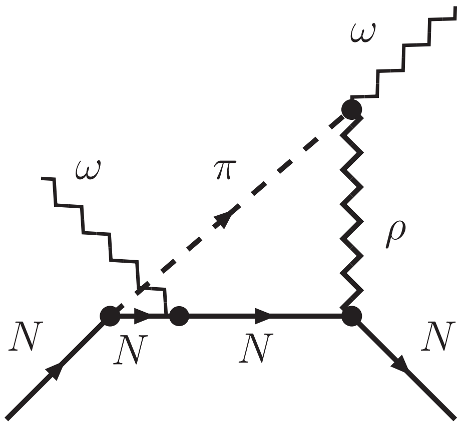

Figure 4.7: Diagram g)

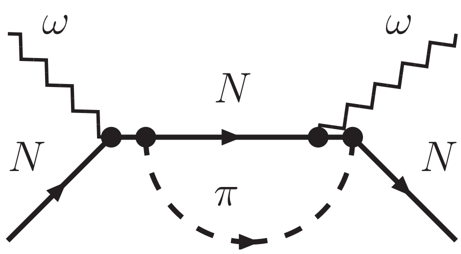

Figure 4.8: Diagram h)

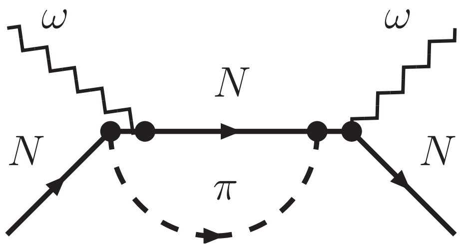

Figure 4.9: Diagram i)

4.2 2π-channel

In this section all the diagrams included in this work which contribute to the $\omega N \to 2\pi N$ decay channel are shown. While in the last section there was always one pion and one nucleon in the intermediate state here we have always one ρ and one nucleon. The ρ primarily decays into two pions (thus 2π-channel) which is described in this work by the spectral function of the ρ (see Chapter 6).

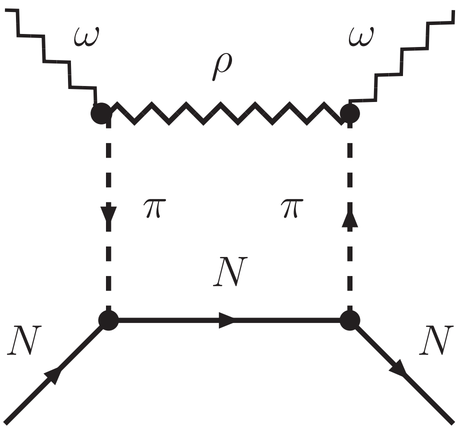

Figure 4.10: Diagram j)

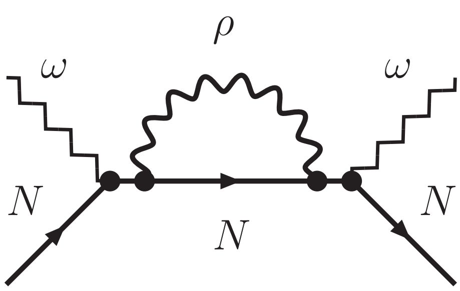

Figure 4.11: Diagram k)

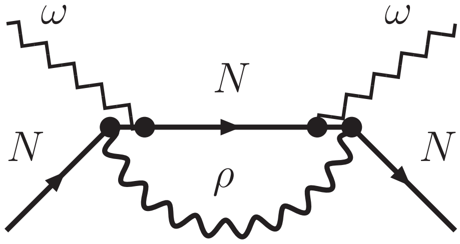

Figure 4.12: Diagram l)

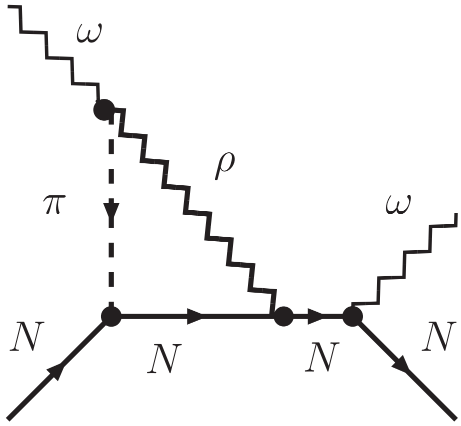

Figure 4.13: Diagram m)

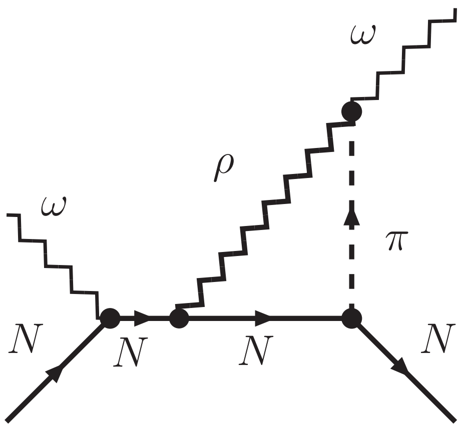

Figure 4.14: Diagram n)

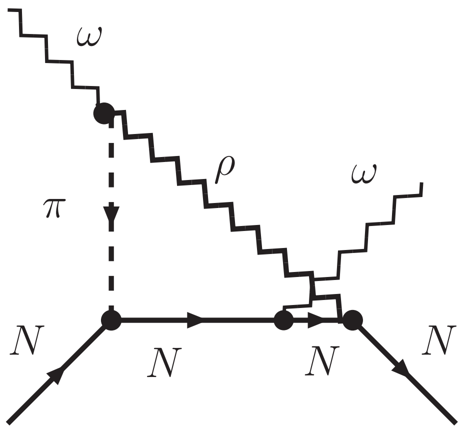

Figure 4.15: Diagram o)

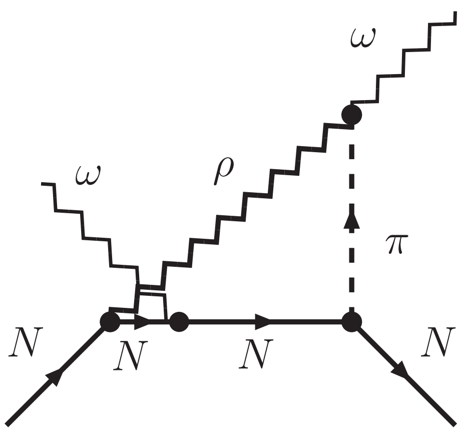

Figure 4.16: Diagram p)

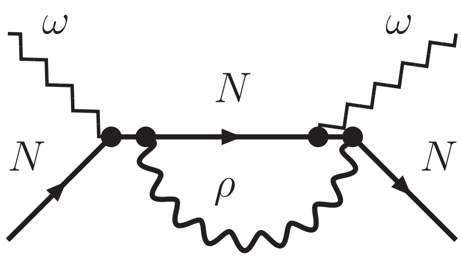

Figure 4.17: Diagram q)

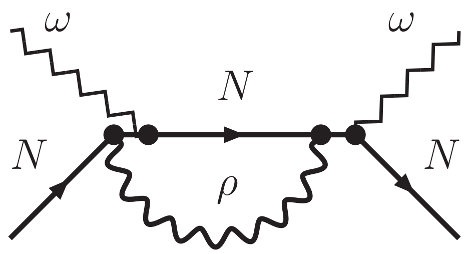

Figure 4.18: Diagram r)

4.3 S_{11} - resonance

Given the interaction of equation (3.21) one further s-channel diagram for the ωN forward-scattering amplitude is included in this work:

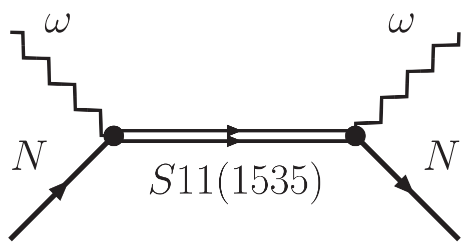

Figure 4.19: Diagram s)

4.4 Heavy baryon limit

In [Kl97] it is mentioned, that in the limit of heavy baryon masses diagrams k), l), q) and r) vanish and only contribute very little to the total scattering amplitude even with the large coupling $g_\omega \simeq 17$. Furthermore it is stated, that the dominant contribution in the 2π-channel comes from the box diagram j). This is in disagreement with [Kl98], where it is explained, that diagrams k), l), q) and r) vanish in the heavy baryon limit, *but* in a relativistic calculation still contribute a lot to the total scattering amplitude due to the large coupling g_ω. Even with this finding it is still claimed here, that diagram j) gives the most important contribution to the 2π-channel. In both cases the heavy baryon limit can also be applied to the inferences of diagrams j) + k) and j) + l). These interferences are just the diagrams m) - p) and they should also vanish in the limit of heavy baryon masses. In sections 7.1.2 and 7.2 we will compare the contributions of the different diagrams in the 2π-channel to the imaginary and real part of the scattering amplitude and we will review the heavy baryon limit.

Part III

Calculations and Results

Chapter 5

Calculation of scattering amplitudes

5.1 Feynman rules

In this section the Feynman rules for the evaluation of all the diagrams given in Chapter 4 are presented. The general structure of all those diagrams is illustrated in figure (3.6). The forward-scattering tensor $T^{\mu\nu}$ (as introduced in section 3.7) can now be calculated using the following set of rules:

- For an incoming nucleon with momentum p', spin state s' and isospin state I' assign
$$u_{s'}(p')\chi_{I'} \ ,$$
where $u_{s'}(p')$ is the nucleon spinor and $\chi_{I'}$ is the isospin vector of the nucleon [PS95].

- For an outgoing nucleon with momentum p, spin state s and isospin state I assign
$$\bar{u}_s(p)\chi_I^\dagger \ .$$

- For every internal pion carrying momentum q assign
$$D(q) = \frac{i}{q^2 - m_\pi^2 + i\epsilon} \ .$$

- For every internal rho carrying momentum k assign
$$D^{\mu\nu} = -i\frac{g^{\mu\nu} - \frac{k^\mu k^\nu}{k^2}}{k^2 - m_\rho^2 - \Pi(k)} + i\frac{k^\mu k^\nu}{k^2}\frac{1}{m_\rho^2} \ .$$

- For every internal nucleon line carrying momentum p assign

$$D(p) = i\frac{\not{p} + M_N}{p^2 - M_N^2 + i\epsilon} \; .$$

- For every internal spin $\frac{1}{2}$ resonance line carrying momentum p assign

$$D(p) = i\frac{\not{p} + m_R}{p^2 - m_R^2 + i m_R \Gamma_R} \; .$$

- For every vertex assign a factor according to figures (3.2) - (3.5).

- Impose four-momentum conservation on each vertex.

- Integrate over every internal momentum, i.e. $\int \frac{d^4p}{(2\pi)^4}$.

- Average over all spin and isospin states.

Using the so obtained $T^{\mu\nu}$ one can now write down the forward-scattering amplitude for the diagram one is interested in (keeping in mind that the scattering ω is at rest, i.e. $\vec{q} = 0$):

$$iT(\omega) = -\frac{1}{3} g_{\mu\nu} T^{\mu\nu}(\omega) \; . \tag{5.1}$$

The prefactor i of the last equation depends on the convention of the chosen Feynman rules. (It is not present in equation (3.27).)

5.2 Imaginary part

5.2.1 1π-channel

The contribution of the 1π channel to the imaginary part of the ωN forward-scattering amplitude T is obtained by cutting (see section 1.2) the pion and an internal nucleon line in figures (4.1) - (4.9). Kinematically the internal ρ appearing in some of the diagrams is spacelike. Since spacelike $\rho' s$ do not decay into pions (see also equation (6.2)) a free ρ propagator is used here, i.e. the width of the ρ is zero. With the help of (5.1) ImT is now easily calculated. Finally every ρN-vertex is dressed with the vector meson-nucleon form factor of equation (3.23).

5.2.2 2π-channel

In the $\omega N \to 2\pi N$ channel the cutting of the ρ propagator inserts the spectral function of the ρ. This means that in the subsequent calculations an integration over this spectral function has to be carried out:

$$\mathrm{Im}\ T(\omega) = \int_{(2m_\pi)^2}^{\omega^2} \mathrm{Im}T(\omega, m)A(m)dm^2\ . \tag{5.2}$$

Here $\mathrm{Im}T(\omega, m)$ is the ωN forward-scattering amplitude with an internal ρ of mass m. The integration starts at two times the pion mass, since the ρ spectral function vanishes for smaller values of m, and ends at ω (the energy of the incoming ω meson), since the ρ decay products are outgoing particles and must obey energy conservation. Note that the incoming particles ω and N are at rest relative to each other. Therefore the maximal energy for the ρ is indeed ω. Instead of the ρN form factor in the 1π-channel here the axial form factor of equation (3.22) is used wherever there is a πN-vertex, i.e. g_A is replaced by the form factor.

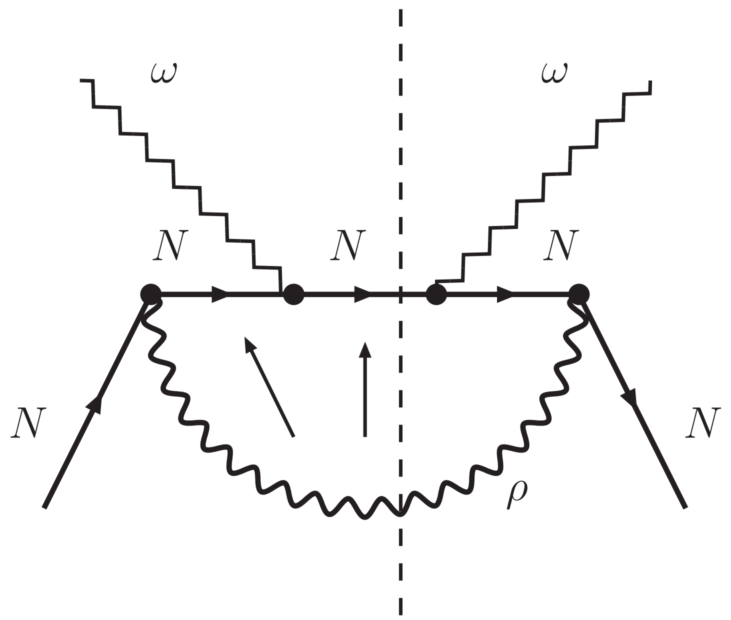

Figure 5.1: Diagram l) with cut according to Cutkosky's Cutting Rules. Here a divergence arises when the uncut nucleon propagator marked by the left arrow becomes on-shell. This can happen when the energy of the incoming ω and the off-shell mass of the ρ, which is integrated over in equation (5.2), become larger than $2M_N$.

The integration in equation (5.2) however also introduces a problem, which is the reason for the different models for the ρ spectral function introduced in Chapter 6. To understand this difficulty, one has to look in more detail at diagram l) (figure (5.1)). Since we are looking at an off-shell ω at rest (and not at a physical ω at rest), the ω can have arbitrarily high energy. When the incoming ω has an energy which is larger than two times the nucleon mass, it can decay into a nucleon-antinucleon pair (marked in figure (5.1) by the two arrows). At the same time, as one can see from equation (5.2), the integration over the ρ spectral function runs beyond $m = 2M_N$. This means that the antinucleon (left arrow) can go on-shell and annihilate with the incoming nucleon and produce the ρ with an off-shell mass $m_\rho \geq 2M_N$. However the on-shell antinucleon can basically travel an arbitrary distance before it annihilates, thus producing an infinite cross section. This is demonstrated in figure 5.2. This is of course an unphysical behavior which has its roots in the fact that in this model the actual scattering of the nucleons in the medium is not implemented. However as discussed in the beginning of this work the predictive power of our model ends at ω energies of about 1 GeV and so this divergence emerges at an energy which is not really well described.

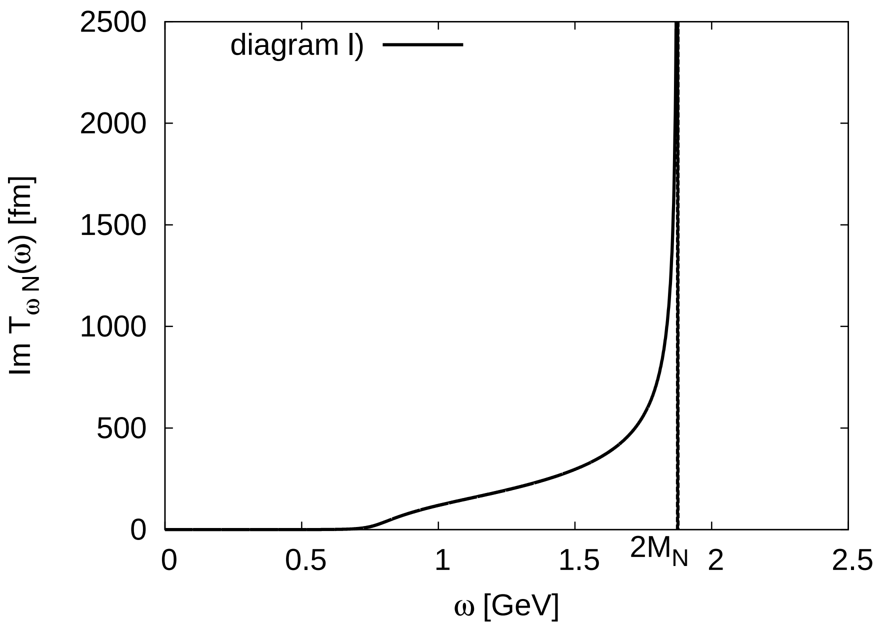

Figure 5.2: Imaginary part of the forward-scattering amplitude of Diagram l) calculated with the "standard" spectral function. The divergent behavior when approaching $\omega = 2M_N$ is obvious.

On the other hand this divergence can be suppressed if the spectral function of the ρ vanishes for $m_\rho > 2M_N$, since then the antinucleon cannot go on-shell. Exactly this is the reason to introduce the modified spectral functions presented in section 6.2 and 6.3. Two variants are developed there to explore the model dependence introduced by the recipe to cut off the ρ spectral strength. Therefore all the calculations for the 2π decay channel are done with both the modified and the simple spectral function (see Chapter 6) and the results are compared in Chapter 7.

5.2.3 Resonance channel

In this work only one diagram with a resonance (figure (4.19)) is included, namely a simple s-channel diagram. Using the Breit-Wigner parametrization as given in the Feynman rules in section (5.1) the calculation of the imaginary and the real part of the corresponding scattering amplitude is straight forward.

5.3 Real part

Having calculated the imaginary parts of the scattering amplitude for all the diagrams of sections 5.2.1 and 5.2.2 one finds that even with the suppression by the form factors given in section 3.5 these imaginary parts do not approach 0 when ω goes to infinity. This is shown in figure 5.3, where the sum of the imaginary parts of the scattering amplitudes of all diagrams a) - s) over the energy is plotted for high energies. Note here that for the contribution of the 2π-channel the function Im $T(\omega, m_\rho)$ (which is in the integrand in equation (5.2)) is plotted, since it carries all the information of the high energy behavior. Obviously $\frac{\text{Im } T_{\text{total}}(\omega)}{\omega}$ approaches a constant for $\omega \to \infty$ and thus Im $T_{\text{total}}(\omega)$ rises linearly in ω for large values of ω. Therefore it is necessary to employ a subtracted dispersion relation to obtain their corresponding real part. As argued in section 2.3.2 one finds that the once subtracted dispersion relation of equation (2.29) is sufficient to perform this task (see also [Kl97]). Thus the total real part can be found by executing a once subtracted dispersion integral over the sum of all the imaginary parts. Exactly for this step equation (2.35) was derived:

$$\text{Re } T(\omega) = \text{Re } T(0) + \frac{2\omega^2}{\pi} \int_0^\infty \frac{\text{Im } T(\omega')}{\omega'(\omega'^2 - \omega^2)} d\omega' \ . \tag{5.3}$$

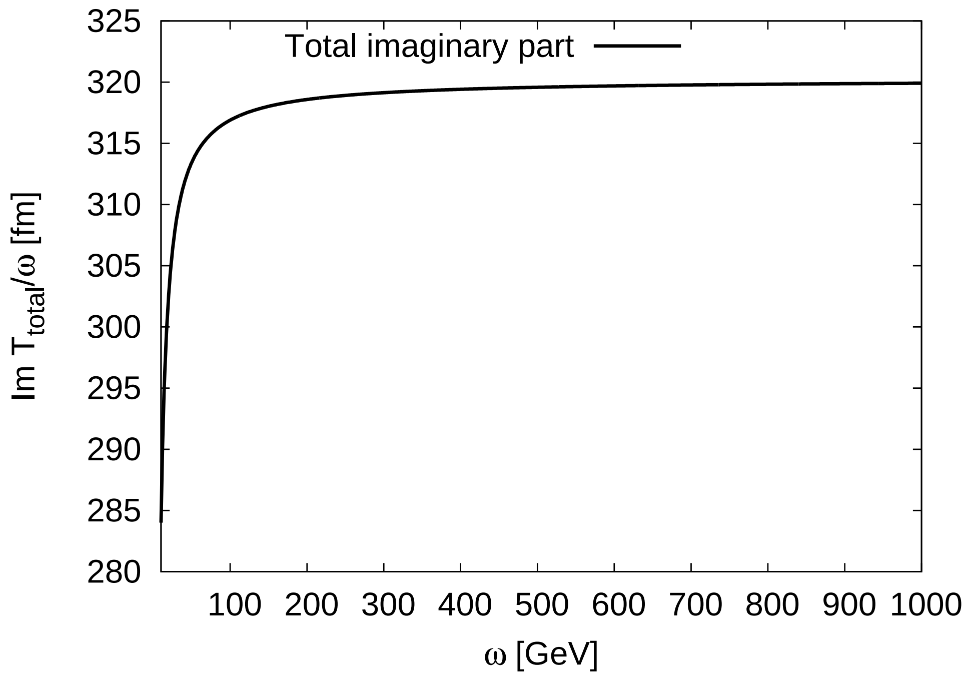

Figure 5.3: Total imaginary part of the forward-scattering amplitude of all diagrams a) - s) .

The subtraction constant Re $T(0)$ is given in analogy to the Thomson limit for Compton scattering. It is just the contribution of the two diagrams shown in figures (5.4) and (5.5) in the limit of $\omega \to 0$ [Kl97], [FB99]:

$$\text{Re } T(0) = \frac{-9g^2}{4M_N} \ . \tag{5.4}$$

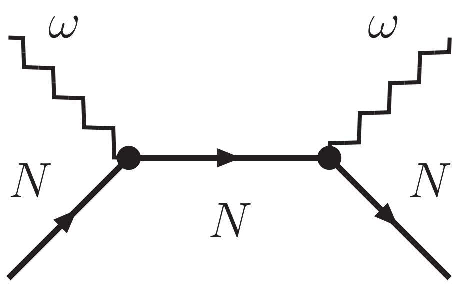

Figure 5.4: s-channel

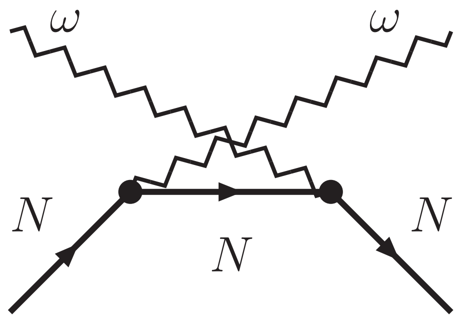

Figure 5.5: u-channel

Chapter 6

Spectral function of the ρ meson

6.1 Vacuum spectral function

The ρ meson is a vector meson (i.e. a spin 1 particle) with a vacuum mass of $m_\rho = 771.1$ MeV. It is a isospin 1 particle and in the vacuum it decays to almost 100% into two pions, thus aquiring a vacuum decay width of $\Gamma_\rho = 149.2$ MeV [PD02]. This decay and width give rise to the description of the ρ by a spectral function [Po03]:

$$A_\rho(q) = -\frac{1}{\pi}\frac{\mathrm{Im}\Pi_{vac}(q)}{(q^2-(m_\rho^0)^2-\mathrm{Re}\Pi_{vac}(q))^2+(\mathrm{Im}\Pi_{vac}(q))^2} \ . \tag{6.1}$$

Here Π_{vac} is the vacuum selfenergy of the ρ meson. By calculating Feynman diagrams for the ρ selfenergy and regulating the (divergent) real part one obtains [He93]

$$\begin{aligned}\mathrm{Im}\Pi_{vac}(q) = -\mathrm{sgn}(q_0)\frac{g^2}{48\pi}q^2\Bigg[&\theta(q^2-4m_\pi^2)\left(1-\frac{4m_\pi^2}{q^2}\right)^{\frac{3}{2}} \\ &-\theta(q^2-4\Lambda^2)\left(1-\frac{4\Lambda^2}{q^2}\right)^{\frac{3}{2}}\Bigg]\end{aligned} \tag{6.2}$$

and

$$\mathrm{Re}\Pi_{vac}(q) = -\frac{g^2}{24\pi^2}q^2\left[\mathcal{G}(q,m_\pi)-\mathcal{G}(q,\Lambda)+\frac{4(\Lambda^2-m_\pi^2)}{q^2}+\ln\frac{\Lambda}{m_\pi}\right] \ . \tag{6.3}$$

Here $\mathcal{G}$ is defined as

$$\mathcal{G}(q,m) = \begin{cases} y^{\frac{3}{2}}\arctan\left(\frac{1}{\sqrt{y}}\right) & y>0 \\ -\frac{1}{2}(-y)^{\frac{3}{2}}\ln\left|\frac{\sqrt{-y}+1}{\sqrt{-y}-1}\right| & y<0 \end{cases} \tag{6.4}$$

with

$$y = \frac{4m^2}{q^2} - 1 \ . \tag{6.5}$$

The constants have the following values:

$$g = 6.05, \tag{6.6}$$
$$m_\pi = 139.57 \text{ MeV}, \tag{6.7}$$
$$\Lambda = 1.0 \text{ GeV}, \tag{6.8}$$
$$m_\rho^0 = 875.0 \text{ MeV}. \tag{6.9}$$

The pion mass is taken from [PD02] and the regularizing Pauli-Villars parameter Λ and the bare mass m_ρ^0 from [Po03]. The coupling g is adjusted such that the on-shell width given by

$$\Gamma_\rho = -\frac{\mathrm{Im}\Pi_{vac}(q^2 = m_\rho^2)}{m_\rho} \tag{6.10}$$

obtains its proper experimental value. Using these parameters equation (6.1) is plotted in figure 6.1.

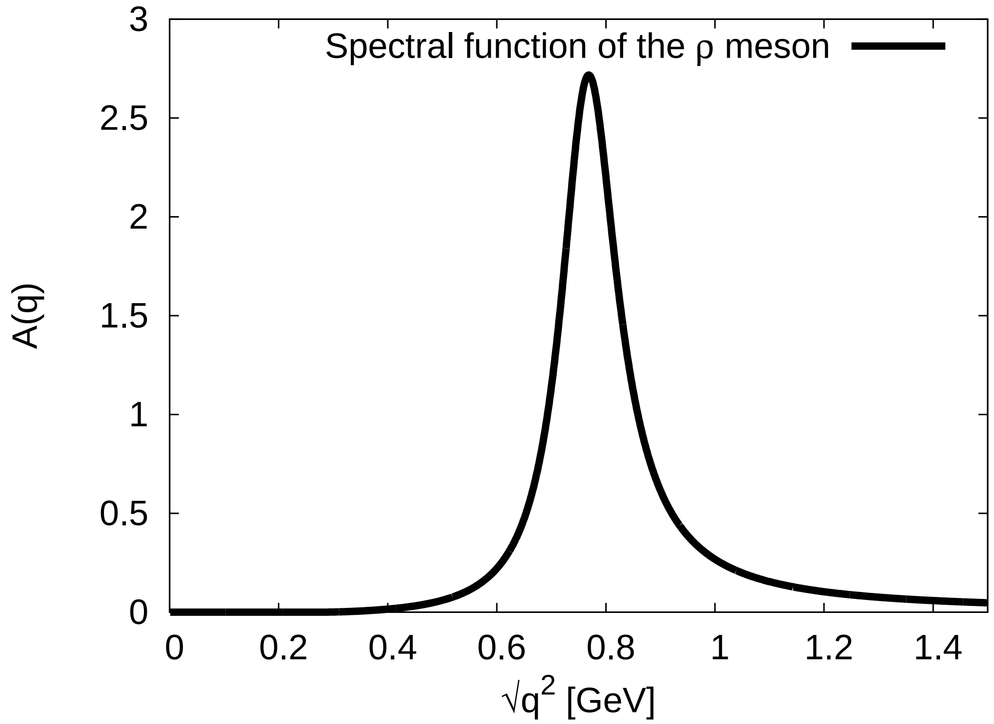

Figure 6.1: Spectral function of the ρ meson as given in equation (6.1).

As shown in [Po03] $A(q)$ is properly normalized:

$$\int_0^\infty dq^2 A(q) = 1 \ . \tag{6.11}$$

6.2 Vacuum spectral function with cutoff

The spectral function of the last section gives a very good description of the ρ meson [He93]. However for the calculation in section 5.2.2 some difficulties arise when using it for $\sqrt{q^2} \geq 2M_N$. Note that this is anyway outside of the low energy region where the model in equations (6.2) and (6.3) is made for. These problems are explained in detail in section 5.2.2. To compensate for this a modified spectral function with a cutoff [Le06] is introduced here. The modified imaginary part of the selfenergy looks as follows:

$$\mathrm{Im}\Pi_{vac}^{mod}(q) = \begin{cases} \mathrm{Im}\Pi_{vac}(q)\left(\frac{\sqrt{(2M_N)^2-q^2}}{2M_N}\right)^2 & q^2 < (2M_N)^2 \\ 0 & q^2 > (2M_N)^2 \end{cases} \tag{6.12}$$

However since (6.12) has to reproduce the width at the peak mass the coupling constant g in equations (6.2) and (6.3) has to be adapted to produce the desired result. Using equation 6.10 one obtains $\Gamma_\rho \simeq 149$ MeV for $g_{mod} = 6.58$. This modified coupling g_{mod} is only used for the imaginary part of the modified selfenergy in equation (6.12) and nowhere else.

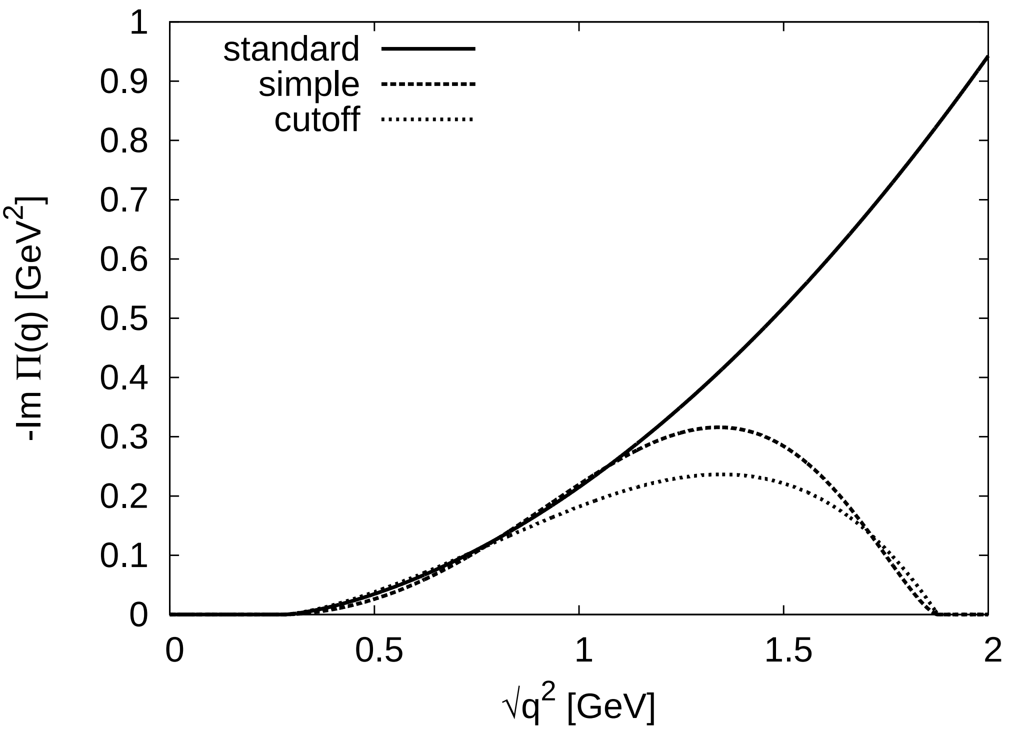

Figure 6.2: Comparison of the imaginary part of the "standard" ρ selfenergy (solid), with cutoff (short dashed) and of the simple ρ selfenergy (long dashed).

In figure 6.2 $\mathrm{Im}\Pi_{vac}$ is compared with the modified version with cutoff. At $\sqrt{q^2} = m_\rho$ the deviation is less than 2% and at $\sqrt{q^2} = 1.0$ GeV it is around 15%.

The real part of Π_{vac}^{mod} can be calculated using the dispersion relation given in equation (2.35) since, as one can see from equation (6.2),

$$\mathrm{Im}\Pi_{vac}^{mod}(-q_0) = -\mathrm{Im}\Pi_{vac}^{mod}(q_0) \tag{6.13}$$

fulfills equation (2.31). For the subtraction constant we have $\mathrm{Re}\Pi_{vac}^{mod}(0) = 0$, since at the photon point $q^2 = 0$ no mass should be generated [Kl97]. A comparison of the real parts of the unmodified and the modified selfenergies can be found in figure 6.3.

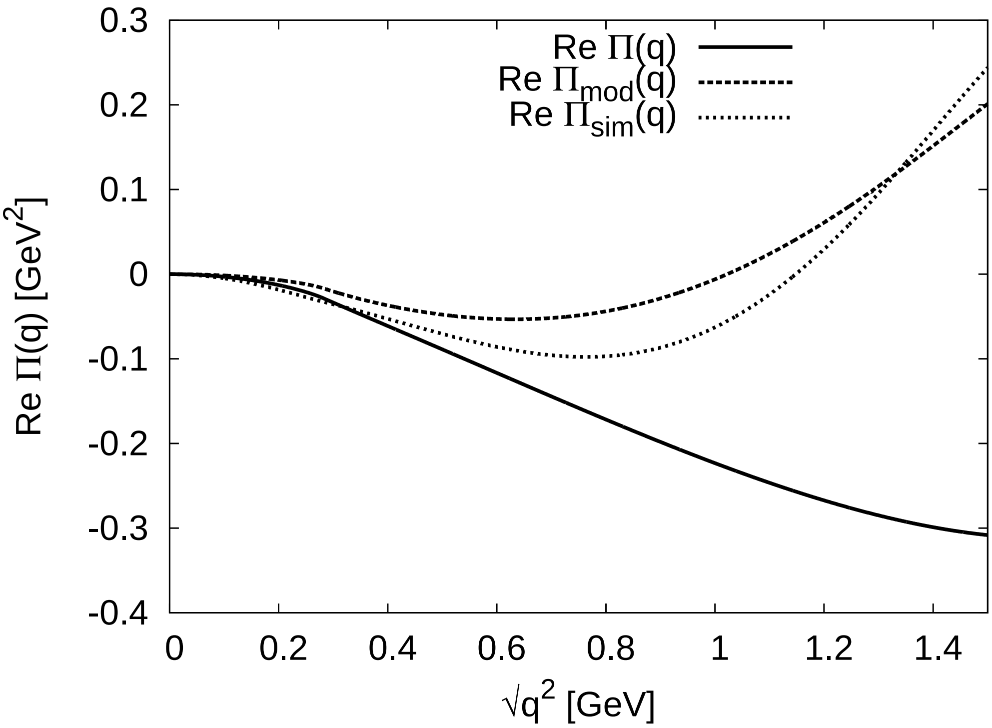

Figure 6.3: Comparison of the real part of the "standard" ρ selfenergy (solid), with cutoff (long dashed) and the simple ρ selfenergy (short dashed).

Inserting $\mathrm{Im}\Pi_{vac}^{mod}$ and $\mathrm{Re}\Pi_{vac}^{mod}$ into equation (6.1) yields:

$$A_\rho^{mod}(q) = -\frac{1}{\pi}\frac{\mathrm{Im}\Pi_{vac}^{mod}(q)}{(q^2 - (m_\rho^{mod})^2 - \mathrm{Re}\Pi_{vac}^{mod}(q))^2 + (\mathrm{Im}\Pi_{vac}^{mod}(q))^2} \tag{6.14}$$

The bare mass m_ρ^{mod} in the last equation is adjusted so that the peak of the modified spectral function is at the physical mass of the ρ. We find $m_\rho^{mod} = 811.0$ MeV.

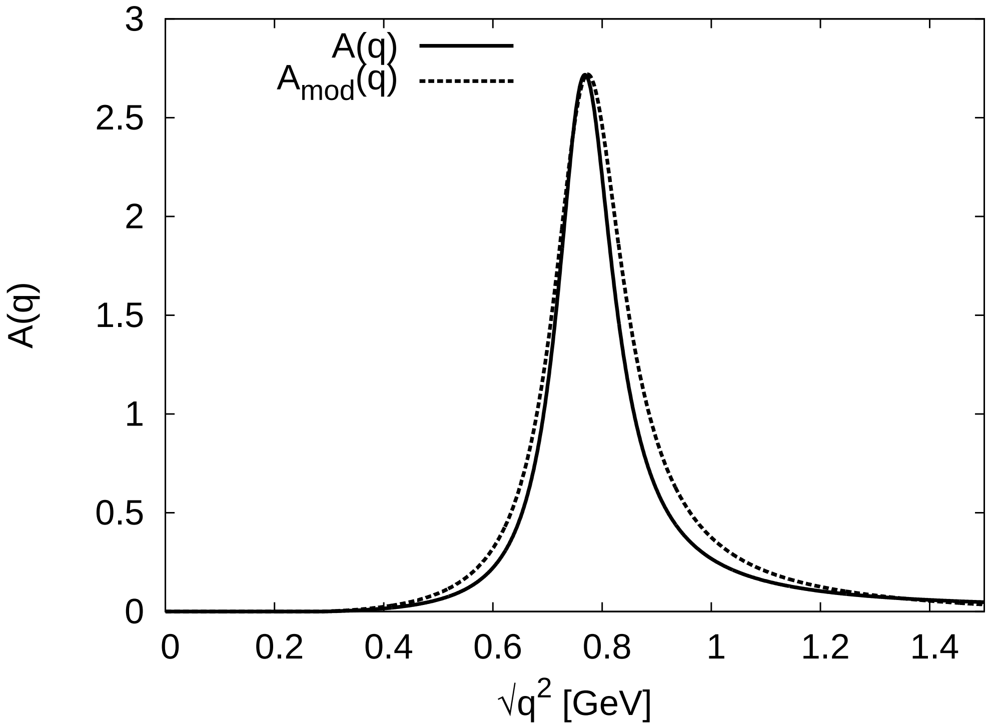

Figure 6.4: Comparison of the ρ spectral function with (dashed) and without (solid) cutoff.

In figure 6.4 the modified spectral function (equation (6.14)) is compared with the "standard" spectral function (equation (6.1)). The deviation at $\sqrt{q^2} = m_\rho$ is less than 1% and at half maximum ($\sqrt{q^2} \simeq 858$ MeV) about 25%. One can see that the modified spectral function is broader than the "standard" spectral function on both sides of the peak, although the imaginary part of the modified selfenergy (see figure 6.2) lies almost on top of the "standard" selfenergy around the peak region. This should be attributed to the large difference in the real part of the selfenergy (see figure 6.3), where the modified real part already differs significantly from the "standard" real part for $\sqrt{q^2} > 0.4$ GeV and where the modified real part is much flatter in the region of the peak mass than the "standard" real part. The modified spectral function is again properly normalized, since the real part of the ρ selfenergy was calculated using a dispersion relation:

$$\int_0^\infty dq^2 A_\rho^{mod}(q) = 1, \tag{6.15}$$

6.3 Simple spectral function

Another possibility to aquire a spectral function that fulfills the condition that it vanishes for $\sqrt{q^2} > 2M_N$ is to construct one by hand. For this one can make a reasonable ansatz for the selfenergy [Le06]:

$$\Pi_{sim}(q) = c_1 \Big[\left((q^2 - 4m_\pi^2)(q^2 - 4M_N^2) \right)^{\frac{3}{2}} - q^6 + 6(M_N^2 + m_\pi^2) q^4 \\ - 6(M_N^4 + 6M_N^2 m_\pi^2 + m_\pi^4) q^2 - 64 m_\pi^3 M_N^3 \Big] \text{ for } q_0 > 0 \ . \tag{6.16}$$

In this case one gets

$$\text{Im } \Pi_{sim}(q) = \begin{cases} -c_1 \left((q^2 - 4m_\pi^2)(4M_N^2 - q^2) \right)^{\frac{3}{2}} & 4m_\pi^2 < q^2 < 4M_N^2 \\ 0 & otherwise \end{cases} \tag{6.17}$$

Note that only the first term in the brackets in equation (6.16) leads to the imaginary part given in equation (6.17). All the other terms are only included to provide a reasonable behavior of Π_{sim} at infinity, namely $\lim\limits_{\sqrt{q^2} \to \infty} \Pi_{sim}(q) = \text{const.}$ The constant c_1 has to be adjusted to reproduce the on-shell decay width. Using equation (6.10) one obtains $c_1 = 0.0619$. For small $q^2 \geq 4m_\pi^2$ the imaginary part (6.17) shows the same q^2 behavior as (6.2). This simply reflects the proper phase space and p-wave nature of the decay $\rho \to \pi\pi$. A comparison of the imaginary and the real part of equation (6.16) with the corresponding parts of the "standard" ρ selfenergy can be found in figures 6.2 and 6.3. Inserting the real and imaginary part into equation (6.1) yields:

$$A_\rho^{sim}(q) = -\frac{1}{\pi} \frac{\text{Im}\Pi_{sim}(q)}{(q^2 - (m_\rho^{sim})^2 - \text{Re}\Pi_{sim}(q))^2 + (\text{Im}\Pi_{sim}(q))^2} \ . \tag{6.18}$$

With a bare mass $m_\rho^{sim} = 841.0$ MeV one produces a spectral function with the peak at the physical ρ mass as one can see in figure (6.5). Looking at the numbers one finds a deviation from the "standard" spectral function of 0.3% at the peak and a deviation of about 17% at half maximum.

This simple spectral function has several nice features: First of all, the selfenergy is known analytically and so there is no dispersion integration necessary to obtain the real part of the selfenergy, which allows for quick calculations. Secondly this spectral function is (by construction) again properly normalized, since Π_{sim} is an analytic function with an appropriate high-energy behavior:

$$\int_0^\infty dq^2 A_\rho^{sim}(q) = 1 \ . \tag{6.19}$$

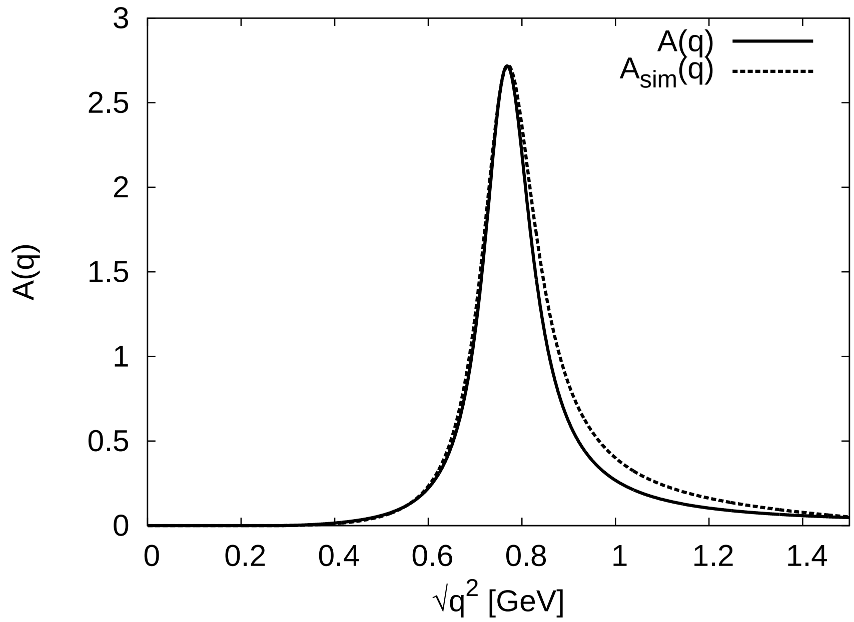

Figure 6.5: Comparison of the "standard" ρ spectral function A with the simple spectral function A_{sim}.

In this chapter three different alternatives for the ρ spectral function were introduced. The reason for this is an unphysical behavior of our hadronic model when employing the "standard" spectral function of the ρ in the later calculations. The problems arising are examined in detail in section 5.2.2. To circumvent this problems in the final calculations in the next part, mainly the modified spectral function with cutoff from the last section and the simple spectral function from this section are used.

Chapter 7

Results and comparison

7.1 Imaginary part of scattering amplitudes

7.1.1 1π-channel

Figure (7.1) shows the sum of the imaginary parts of diagrams a) - i) plotted with the vector meson-nucleon form factor (equation (3.23)).

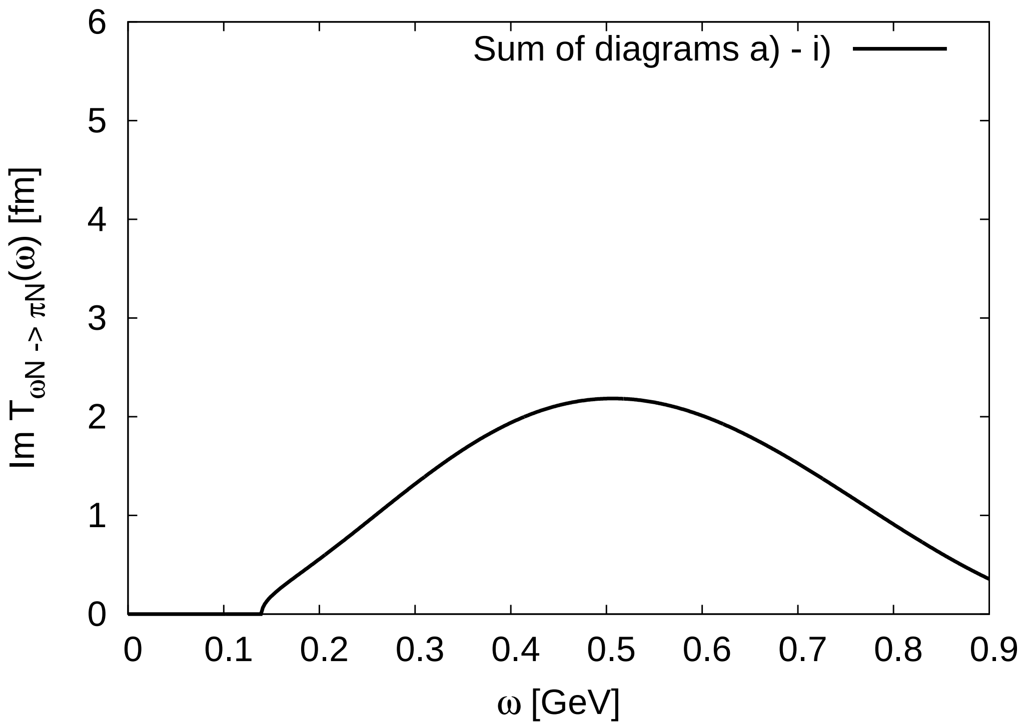

Figure 7.1: Imaginary part of the scattering amplitude for the 1π-decay channel diagrams a) - i).

This result has to be compared with the results by Klingl et al. [Kl99]. The long dashed line in figure (7.2) corresponds to the plot in figure (7.1). There are small discrepancies between the corresponding curves especially at higher energies where ImT becomes small again. However at such small values of ImT the tensor coupling between ω and nucleon might become important again. Since it was neglected in this work this could be an explanation for the deviation. We do not follow this point in more detail since at larger energies the scattering amplitude is dominated by the 2π-channel whereas the 1π-channel is practically negligible.

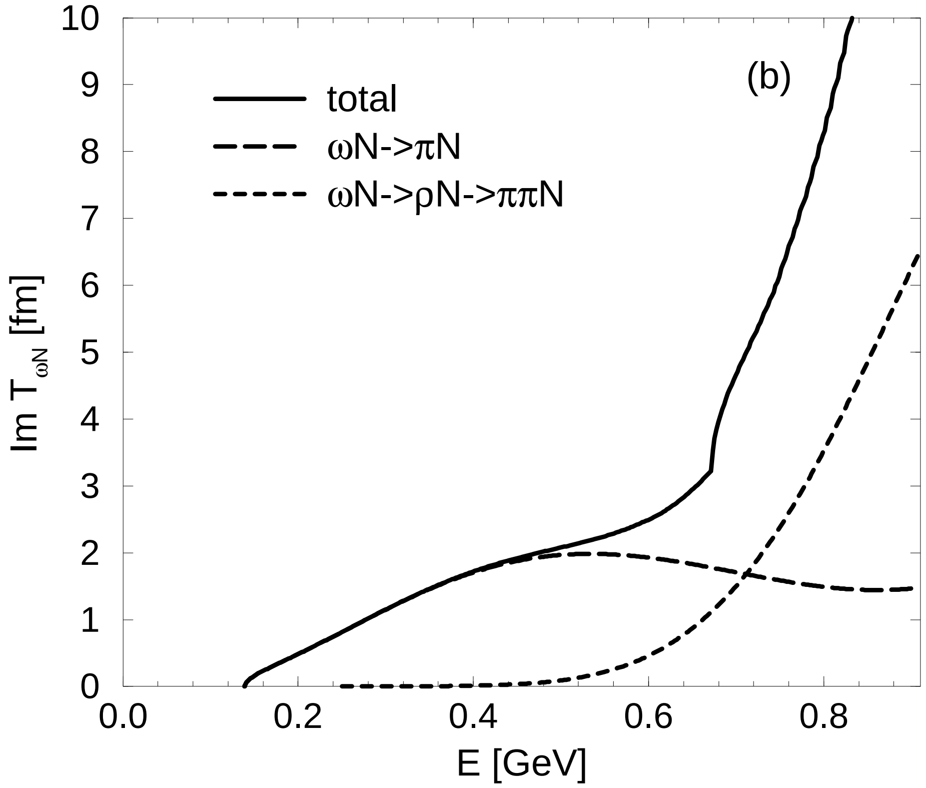

Figure 7.2: Result from Klingl et al. [Kl99]. The long dashed line has to be compared with figure (7.1) above.

7.1.2 2π-channel

In this section we will compare the calculations for the imaginary parts of diagrams j) - r) using the normal, the modified and the simple spectral function of the ρ (figure (7.3)). While the lines for the calculations with the modified and the simple spectral function lie almost on top of each other, there is a deviation of about 10% at 0.9 GeV to the calculation with the normal spectral function.

However this is still a reasonable approximation to the calculation with the "standard" ρ spectral function, which allows the calculation of the real part via the dispersion integral.

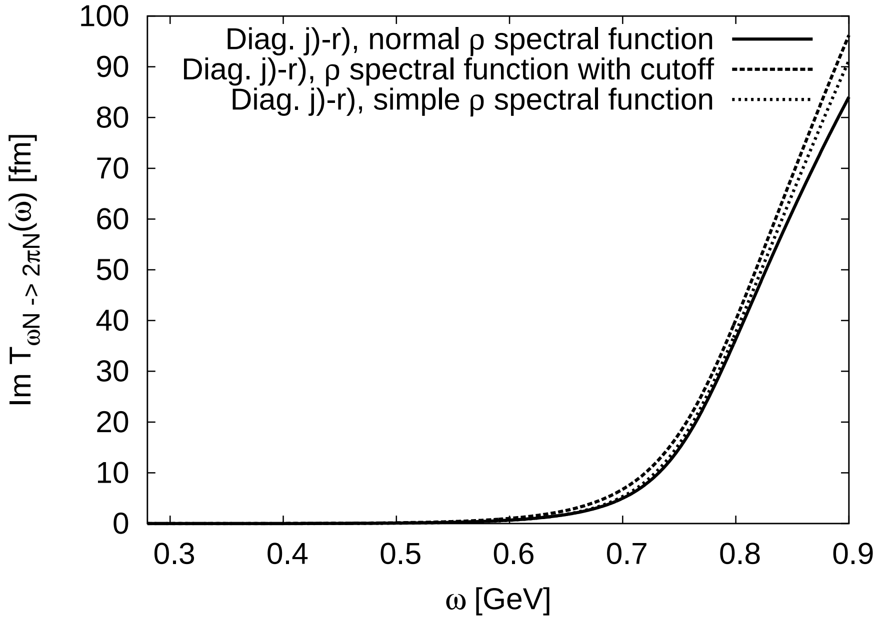

Figure 7.3: Imaginary part of the scattering amplitude for the 2π-decay channel diagrams j) - r) calculated with the "standard" ρ spectral function (solid), with cutoff (long dashed) and with the simple ρ spectral function (short dashed).

For comparison figure 7.4 demonstrates the influence of the width of the ρ meson in the intermediate state. While for the calculation with the stable ρ the imaginary part of the scattering amplitude is of course zero for $\omega < m_\rho$, it rises much faster than in the case of the calculation with the broad ρ. As will be shown in section 7.2 the corresponding real part is very sensitive to the slope of the imaginary part.

At this point it is important to note that although the divergence discussed in section 5.2.2 can be handled as explained there, diagram l) still contributes a lot to the total imaginary part in the 2π-channel. Specifically the sum of the imaginary parts of diagrams k) and l) and their interferences, namely diagrams q) and r), is much bigger than the contribution of diagram j) alone. This is shown in figure (7.5) and additionally one can see that there ImT is one order of magnitude larger than in figure (7.2). This is a striking contrast to [Kl97] where diagram j) is identified as the most important one. As described in section 4.4 diagrams k), l), q) and r) have been neglected in [Kl97] because calculations were done using a heavy baryon limit. In section 7.2 we will compare the resulting real parts and we will come back to this topic in the summary.

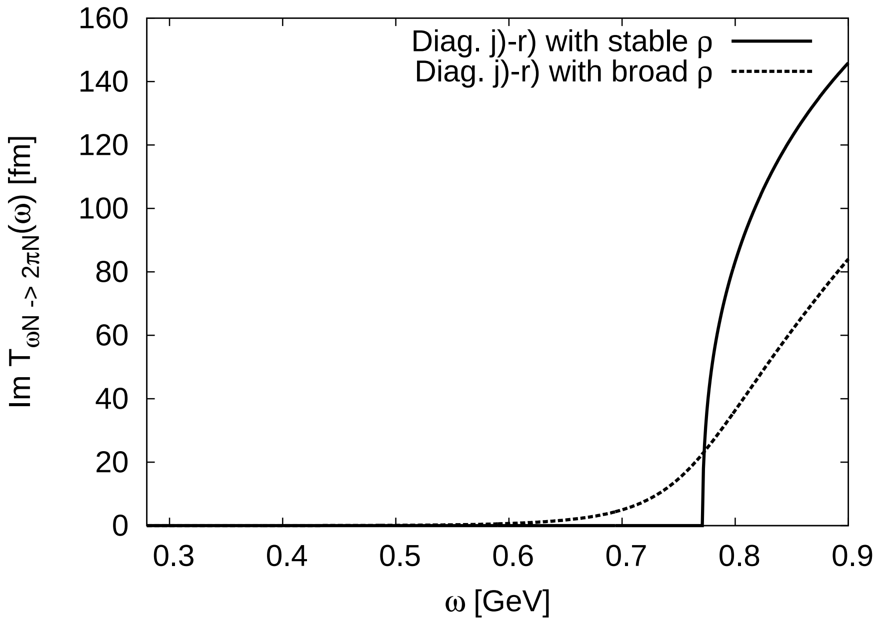

Figure 7.4: Imaginary part of the scattering amplitude for diagrams j) - r) calculated with a stable ρ and with a broad ρ ("standard" ρ spectral function).

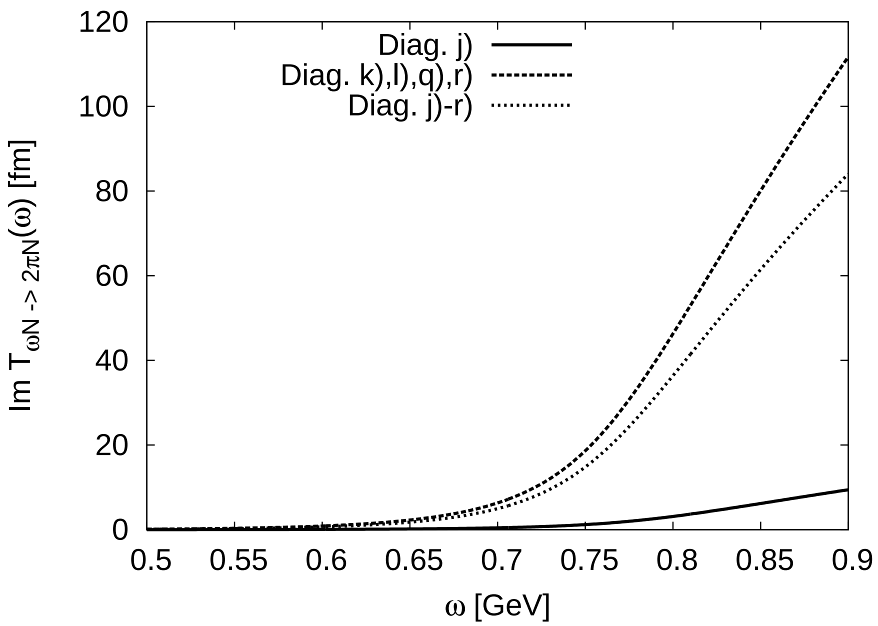

Figure 7.5: Comparison of the contributions of diagram j) alone and of the sum of diagrams k), l), q), r) with the sum over all diagrams in the 2π-channel. The imaginary parts were calculated with the "standard" ρ spectral function.

7.1.3 Resonance channel

The only resonance contribution considered in this work, namely the $\omega N \rightarrow S_{11}(1535)$ formation, is plotted in figure (7.6). It shows a typical resonance structure with the peak at about 600 MeV (which is just the difference between nucleon mass and S_{11} mass).

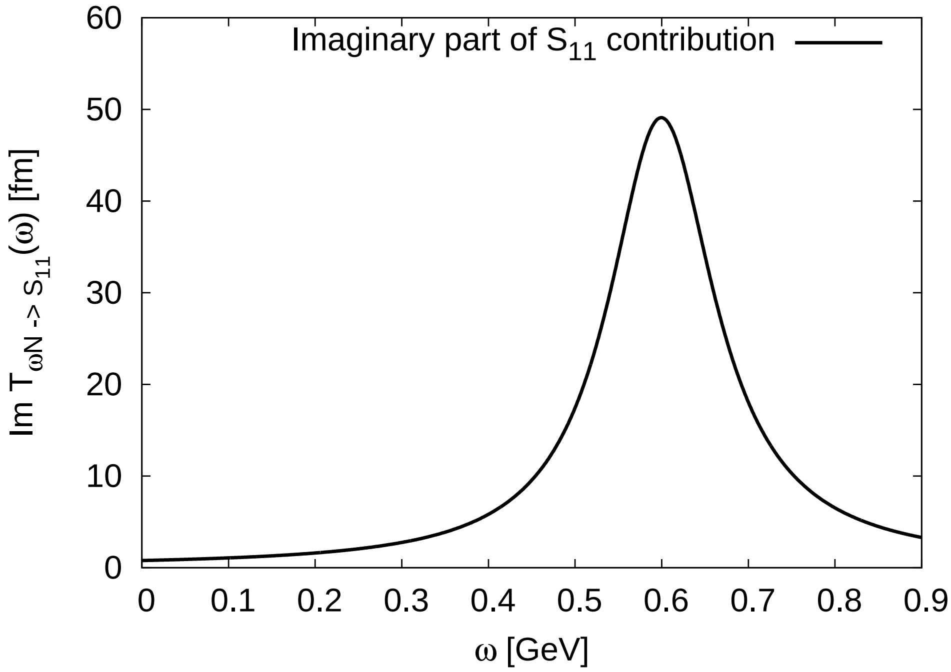

Figure 7.6: Imaginary part of the scattering amplitude for the resonance diagram s).

7.1.4 Sum of all channels

Summing up all the different channels from the previous sections the imaginary part of the forward-scattering amplitude is depicted in figure (7.7) as a comparison of the calculations with the three different ρ spectral functions. Up to about 0.85 GeV the calculated values do not differ significantly from each other. At 1 GeV the deviation to the calculation with the "standard" ρ spectral function is on the order of 15-20%. Since the dispersion integral is very sensitive to the slope of the imaginary part this might already influence the picture when one looks at the results for the real part.

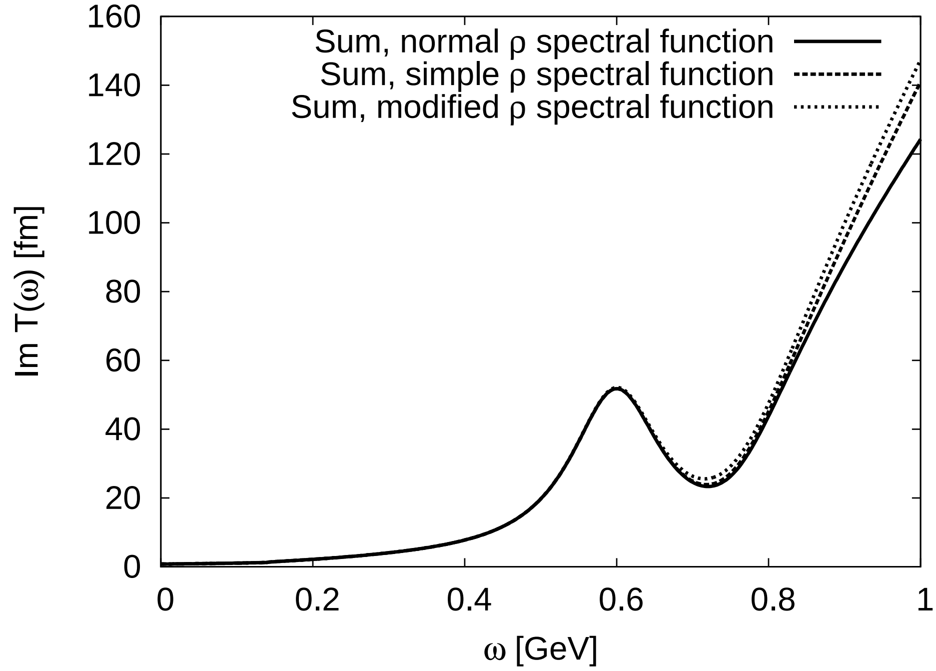

Figure 7.7: Comparison of the sum of all imaginary parts for the three different ρ spectral functions.

7.1.5 $\omega N \to 3\pi N$ contributions

So far only the $\omega N \to 1\pi N$- and the $\omega N \to 2\pi N$-channel (and one additional resonance channel) have been examined in the present work. However in [Kl98] and [Kl99] it is demonstrated, that also the $\omega N \to 3\pi N$-channel gives a sizable contribution. This is clearly visible in figure (7.2), where the difference between the total imaginary part and the sum of the two other shown contributions is comprised of the 3π-channel [WW05]. Obviously including the 3π contributions leads to an even steeper rise of the imaginary part of the forward-scattering amplitude, which allows us to speculate that this will result in an even larger real part. (The dispersion integral in equation (5.3) is very sensitive to the slope in the imaginary part; see section 7.2.) We have already found great discrepancies in the 2π-channel (by disregarding the heavy baryon limit as discussed in sections 7.1.2 and 7.2), which point to strong model dependencies. First these uncertainties should be clarified before the 3π contribution can be studied. Therefore these 3π contributions are not considered further in the present work.

7.2 Real part of scattering amplitudes

Using the imaginary parts of the scattering amplitudes shown in the last sections, the corresponding real parts obtained through the dispersion relation in equation (5.3) are now shown for the 1π and resonance contributions in figure (7.8) without the subtraction constant. One can see that the 1π contribution is attractive, especially at energies larger than the vacuum mass of the ω. The resonance contribution shows, compared to 1π, a rather strong attraction below 600 MeV, but then changes to about equally strong repulsion a little above 600 MeV. Outside this area it only plays a minor role.

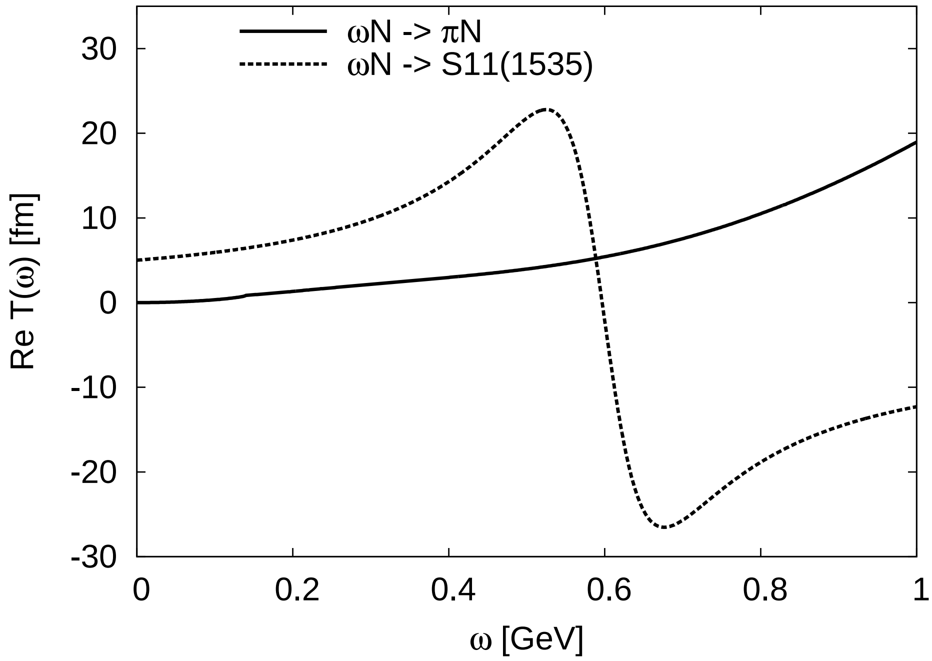

Figure 7.8: Real parts for the 1π- and the resonance-channel.

In figure (7.9) the real parts for the 2π-channel calculated with the modified ρ spectral function with cutoff and with the simple ρ spectral function are compared (again the subtraction constant is omitted here). One can see that at 1 GeV the real parts for the calculation with the ρ spectral function with cutoff and the simple ρ spectral function already differ by about 15 fm. This shows that although the corresponding imaginary parts are basically identical up to 1 GeV, the high energy behavior is quite important when using a dispersion relation. Note here that the values of the 2π-channel in figure (7.9) are at least one order of magnitude larger than those of the other contributions in figure (7.8) when looking at energies above 500 MeV. From this point on the real part is totally dominated by the 2π-channel.

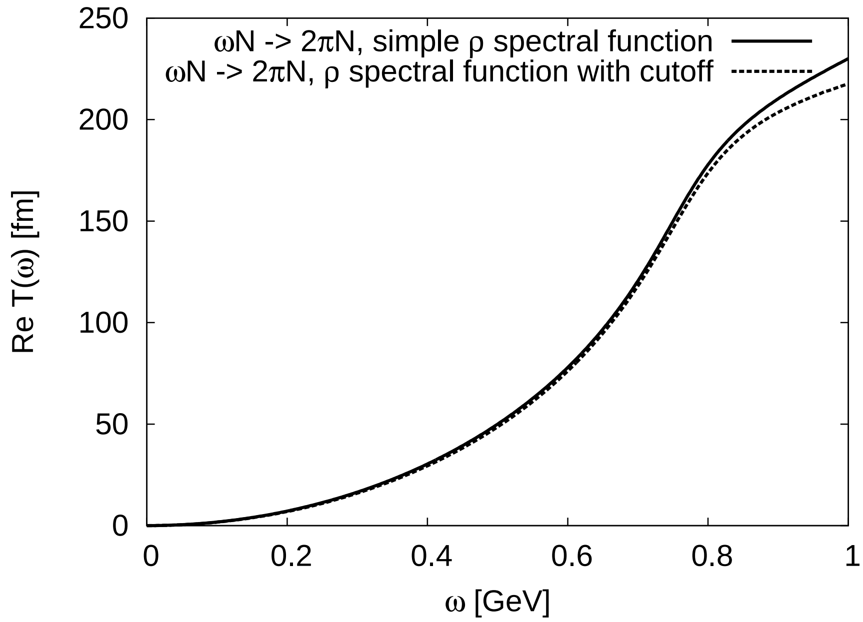

Figure 7.9: Comparison of the real part for the 2π-channel using the modified ρ spectral function with cutoff and the simple ρ spectral function.

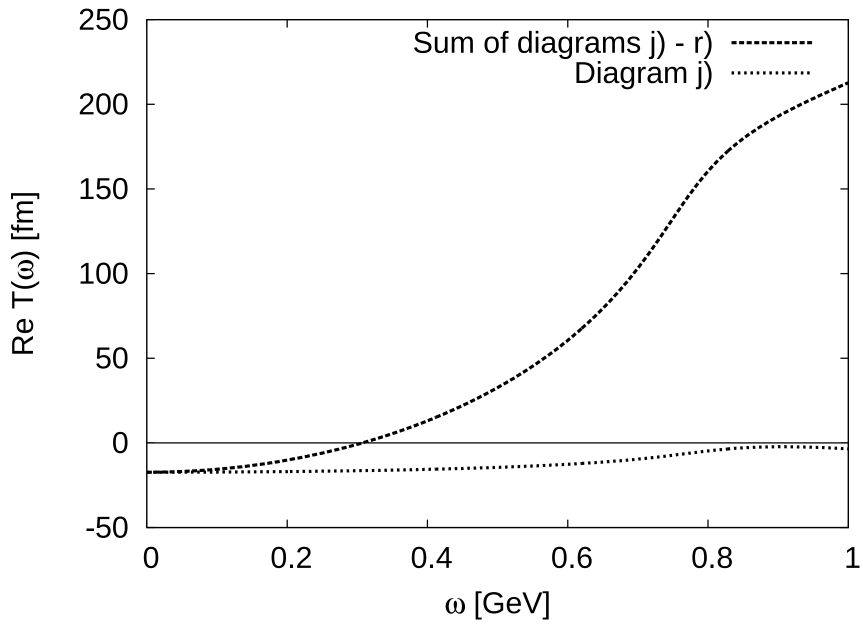

Figure 7.10: Comparison of the real part of diagram j) and the sum of diagrams j) - r) (in both cases with subtraction constant). This calculation was done using the simple ρ spectral function.

In figure 7.10 the influence of the heavy baryon limit on the real part is demonstrated. When only including diagram j) (as described in section 4.4) the real part is always negative and thus repulsive, i.e. the ω gains mass in the nuclear medium. However including all the diagrams j) - r) drastically changes the picture to strong attraction. Together with the findings concerning the comparison of the imaginary part in figure 7.5 this casts strong doubts on the use of the heavy baryon limit for vector meson-nucleon reactions.

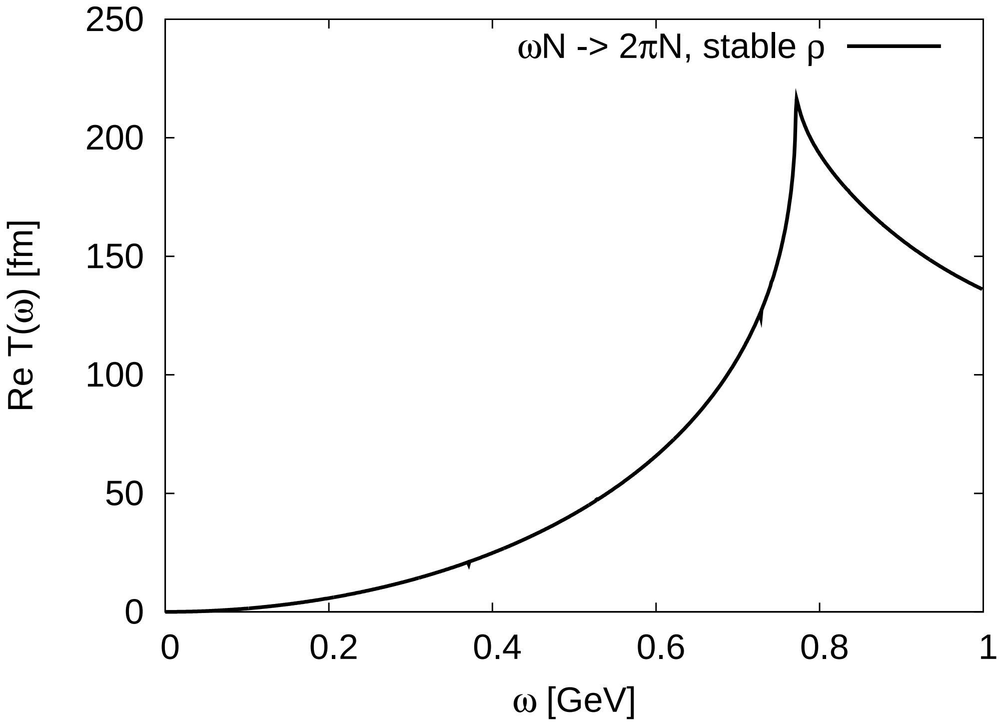

Figure 7.11: Real part for the 2π-channel with a stable ρ in the intermediate state. The strong peak at $\omega = m_\rho$ results from the sudden rise in the corresponding imaginary part (see figure 7.4).

The dispersion integral that is needed to obtain the real part of the scattering amplitudes is very sensitive to the slope of the imaginary part. This can be clearly seen in a calculation which has a stable ρ in the intermediate state as illustrated in figure 7.11: The peak is at $\omega = m_\rho$ and the real part is generally larger than in the calculations with the broad ρ (figure 7.9). This can be attributed to the sudden rise in the imaginary part of the calculation with the stable ρ, which is shown in figure 7.4.

The total real part as a sum over all the different contributions including the substraction constant is shown in figure (7.12).

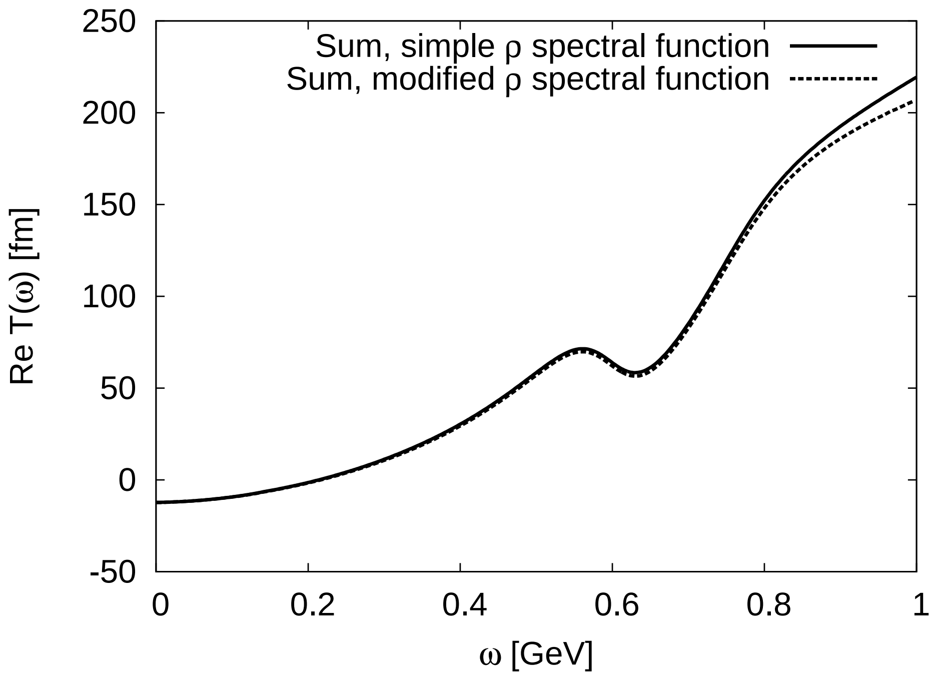

Figure 7.12: Comparison of the sum of all real parts for the calculations using the modified ρ spectral function with cutoff and the simple ρ spectral function.

7.3 Scattering lengths and cross sections

Having calculated the imaginary and the real parts of the forward-scattering amplitudes of the different channels, it is now possible to deduce from these some interesting physical quantities, namely effective scattering lengths and differential cross sections.

7.3.1 Scattering lengths

In [Kl97] the effective scattering length for "on-shell" ω mesons at rest ($\vec{q} = 0$) is defined as:

$$a_{\omega N} = \frac{M_N}{4\pi(M_N + m_\omega)} T_{\omega N}(\omega = m_\omega) \ . \tag{7.1}$$

Using our values for the scattering amplitudes we obtain for the 1π-channel only:

$$a_{\omega N \to \pi N} = (0.430 + i\ 0.044) \text{ fm} \ . \tag{7.2}$$

Note that this agrees reasonably well with constraints from the reaction $\pi^- p \to \omega n$, where an empirical value for the imaginary part of 0.03 fm is found [FR98]. For the 2π-channel (using the calculation with the simple ρ spectral function) we have:

$$a_{\omega N \to 2\pi N} = (7.100 + i\ 1.243)\ \text{fm}\ . \tag{7.3}$$

In total, including the resonance and the subtraction constant, we get:

$$a_{\omega N} = (6.132 + i\ 1.679)\ \text{fm}\ . \tag{7.4}$$

7.3.2 Cross sections

For our case of ωN scattering there is the following connection between decay width and the total cross section of the process:

$$q_0 \Gamma = \rho |\vec{q}| \sigma_{\text{tot}}\ , \tag{7.5}$$

with the energy q_0 and 3-momentum $\vec{q}$ of the ω and the nuclear matter density ρ. Now employing the low density theorem (equation (3.28)) and the relation between width and selfenergy [Po03] one obtains the optical theorem:

$$-\text{Im}\ \Pi = \rho |\vec{q}| \sigma_{tot} \tag{7.6}$$
$$\Rightarrow \text{Im}\ T = |\vec{q}| \sigma_{tot}\ . \tag{7.7}$$

Since we are looking at ω mesons at rest the total cross section in equation (7.7) is not well defined. This is not surprising for reactions where the products are lighter than the incoming particles ($M_N + m_\pi < M_N + m_\omega$) [Ko98]. Note that there is no problem for $|\vec{q}| > 0$, which is however not studied here. What one can calculate is the elastic differential cross section for forward-scattering which is simply given by [PD02] (the factor $16\pi^2$ depends on the definition of T; compare equation (7.7) with [PD02]):

$$\frac{d\sigma_{\text{elas}}}{d\Omega}(\omega; \theta = 0) = \frac{|T(\omega)|^2}{16\pi^2}\ . \tag{7.8}$$

In figure 7.13 this quantity is shown for the three different channels seperately and for the sum of the channels. We obtain an elastic differential cross section at the vacuum ω mass of the order of 1.5 barn (!) for the 2π-channel, which is a clear indication, that the imaginary parts obtained in section 7.1.2 are unrealistically large.

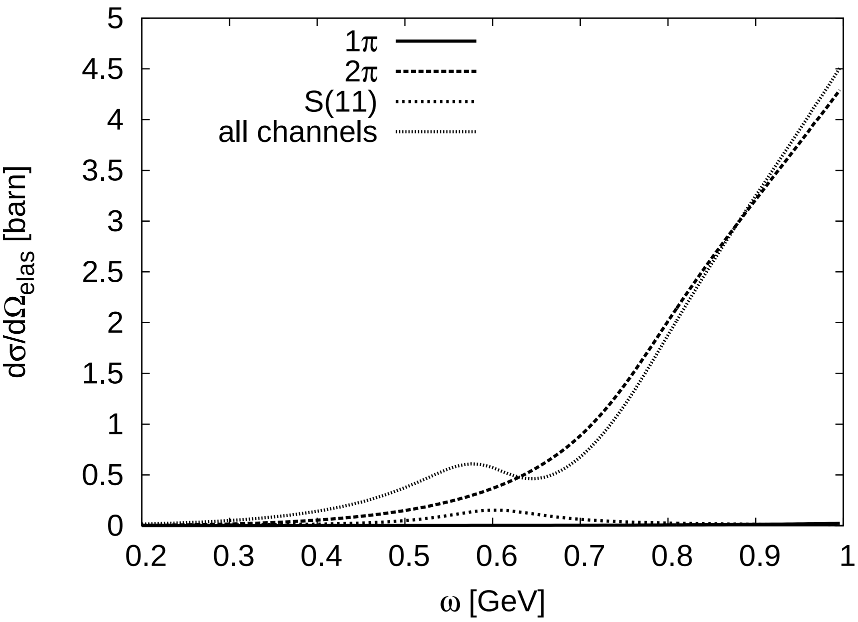

Figure 7.13: Elastic differential cross section for forward-scattering for the different channels and for the sum of all channels. Note that the 1π-channel contribution is so small, that it is not visible.

The elastic differential cross sections that result from our scattering amplitudes above are obviously far too large, which can be mainly attributed to the dominating 2π-channel. The difficulties arising in the 2π-channel that lead to this drastic behavior are described in detail in section 5.2.2. This also leads to a drastic change in the mass and the width of the ω in a nuclear medium, as one can see in the next section. The entire matter is further discussed in section 7.5.

7.4 The ω spectral function in a nuclear medium

The vacuum spectral function of the ω meson is determined by its decay into $\pi^+\pi^0\pi^-$. The imaginary part of the vacuum selfenergy $\mathrm{Im}\Pi^\omega_{vac}$ can be calculated numerically as shown in [Kl97] (equations (13) and (14)). While it is possible to obtain the real part through a dispersion relation the small vacuum width of the ω (around 8.44 MeV [PD02]) justifies to absorb it into the physical ω mass m_ω. The vacuum spectral function then can be written as:

$$A^\omega_{vac}(q) = -\frac{1}{\pi}\frac{\mathrm{Im}\Pi^\omega_{vac}(q)}{\left(q^2 - m^2_\omega\right)^2 + \left(\mathrm{Im}\Pi^\omega_{vac}(q)\right)^2} \ . \tag{7.9}$$

Now employing the low density theorem (see section 3.7) the in-medium spectral function is given by

$$A^{\omega}_{med}(q) = -\frac{1}{\pi}\frac{\mathrm{Im}\Pi^{\omega}_{med}(q)}{\left(q^2 - m_\omega^2 + \rho\ \mathrm{Re}T_{\omega N}(q)\right)^2 + \left(\mathrm{Im}\Pi^{\omega}_{med}(q)\right)^2}\ , \tag{7.10}$$

with

$$\mathrm{Im}\Pi^{\omega}_{med}(q) = \mathrm{Im}\Pi^{\omega}_{vac}(q) - \rho\ \mathrm{Im}T_{\omega N}(q)\ .$$

In figure (7.14) the vacuum and the in-medium spectral function are compared, assuming a normal nuclear matter density of $\rho_0 = 0.17\ \mathrm{fm}^{-3}$ and using the simple ρ spectral function for the calculations. Especially at half normal nuclear matter density one sees a two peak structure. Here the resonance contribution is visible, producing the right peak. The left peak originates from the genuine ω which is shifted to much lower masses due to the very large Re T obtained in the previous section. However at normal nuclear matter density the resonance-hole peak loses a lot of strength to the main peak. For normal nuclear matter density the main peak of the in-medium spectral function lies at about 486 MeV and the width at the main peak is about 228 MeV. The smaller second peak is positioned at around 632 MeV.

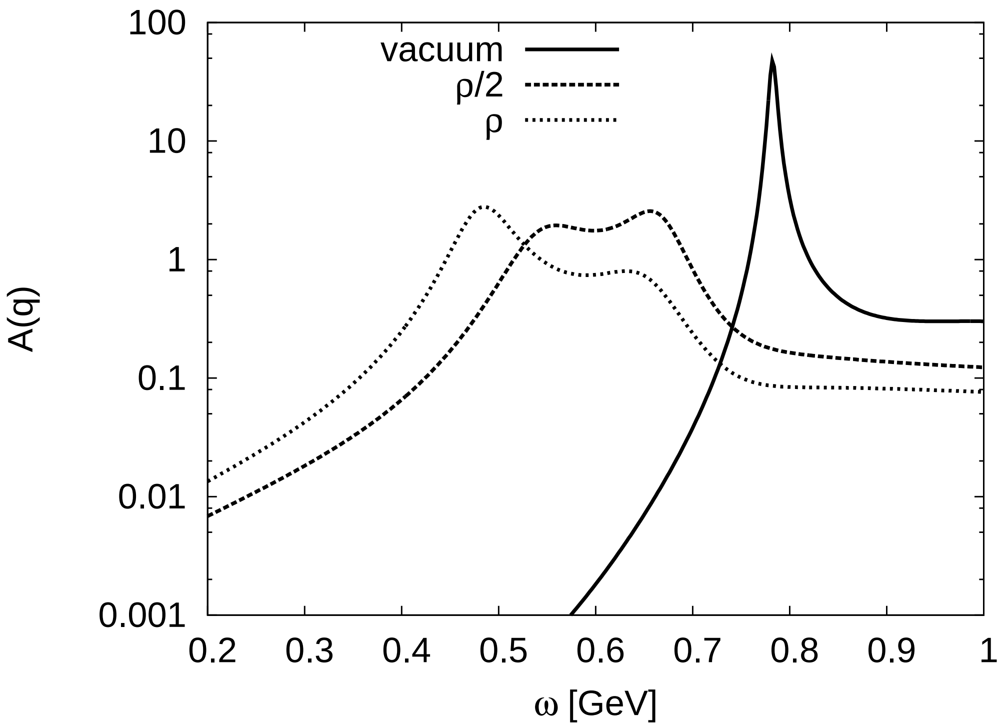

Figure 7.14: Spectral function of the ω in the vacuum and at half normal and normal nuclear matter density ρ_0. This calculation was done using the simple ρ spectral function. Note that $A(q) = A(\omega, 0)$ (vacuum data from [MuP6]).

Figure (7.15) compares the same quantities for the calculations with the modified ρ spectral function with cutoff. Here again one finds for the main peak a position of 486 MeV (normal nuclear matter density) and a width of the main peak of about 229 MeV. Here the smaller second peak is at 636 MeV. A comparison of figures (7.14) and (7.15) shows no qualitative difference and a comparison of the peak structure only negligible quantitative differences.

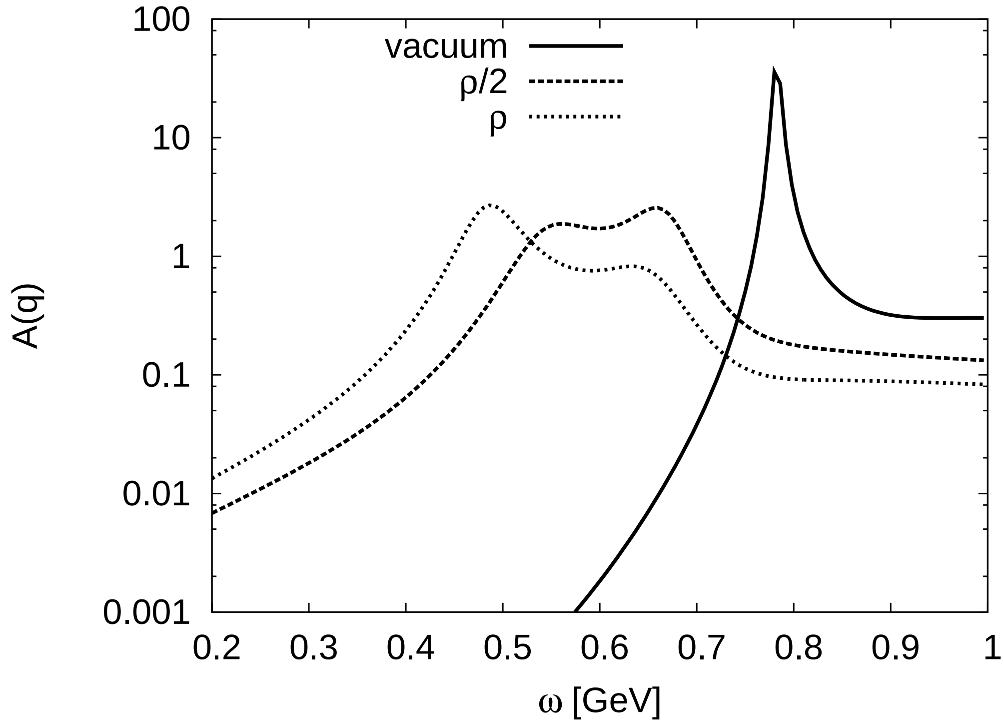

Figure 7.15: Spectral function of the ω in the vacuum and at half normal and normal nuclear matter density ρ_0. This calculation was done using the modified ρ spectral function with cutoff. Note that $A(q) = A(\omega, 0)$ (vacuum data from [MuP6]).

For further comparison a plot of the ω spectral function for the vacuum and for normal nuclear matter density obtained by Klingl et al. is shown in figure (7.16). The details concerning this figure can be found in [Kl99]. Since the authors did not take into account several diagrams as discussed before, they calculate an in-medium ω mass in the region 600-700 MeV, depending on the sets of diagrams used. This is in dramatic disagreement with what we have found in figures (7.14) and (7.15): We see a mass shift twice as large as them and we find an in-medium width about 5 times as large as the width given in [Kl99].

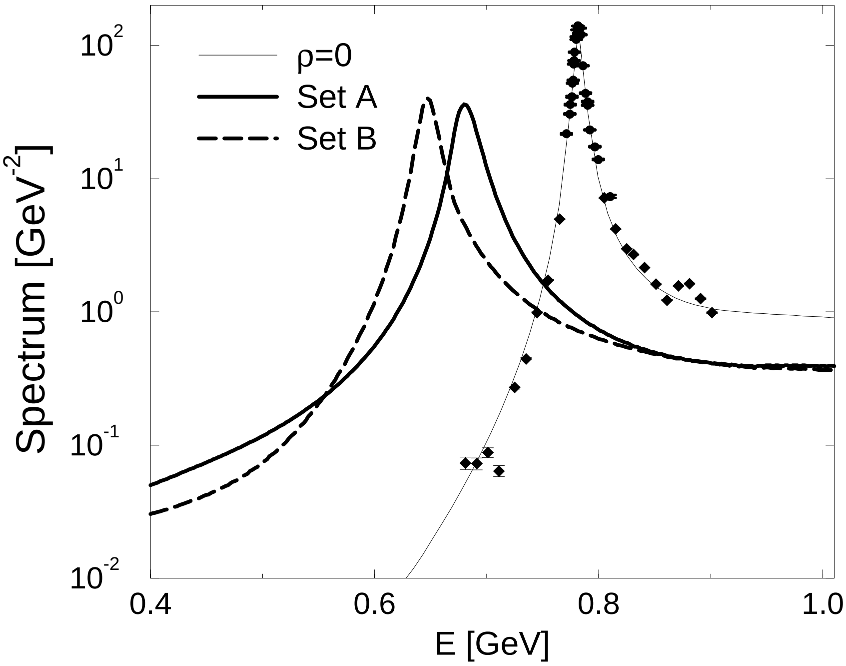

Figure 7.16: Spectral function of the ω in the vacuum and at normal nuclear matter density ρ_0 as found by Klingl et al. The details of this calculation and concerning Set A and Set B can be found in [Kl99].

7.5 Discussion

In the last section the results for the in-medium ω mass were presented, indicating a decrease of around 300 MeV from the vacuum mass. This decrease appears to be very high, especially in light of recent experiments [Tr05], which suggest an in-medium mass of 722 MeV at $0.6\rho_0$ nuclear density. In addition the width of the ω (in this work around 230 MeV) is far greater than previous predictions and experimental observations [Tr05]. There are several factors that influence this drastic behavior:

The most important factor concerns the choice which diagrams to include. This is especially the case for the 2π-channel, since the 1π-channel can basically be fit to data (as shown in [Kl99]). Figure (7.5) demonstrates, that diagrams k), l), q) and r) give the greatest contribution to the imaginary part of the scattering amplitude, compared to which e.g. diagram j) can basically be neglected. (In [Kl97] this diagram j) is found to be one of the largest contributions whereas the diagrams k), l), q), r) are not considered further, because of the heavy baryon limit approximation). In the present work these diagrams which all result from the model Lagrangian in section 3.2 were calculated fully relativistically. The comparison of our results and the results by Klingl et al. in the last section shows that by including these diagrams the results change dramatically. This makes the use of the heavy baryon limit quite doubtful. However the large contributions of these diagrams in our work are a direct result of the pole in the nucleon propagator, which was discussed in detail in section 5.2.2. The very large resulting cross sections in section 7.3 emphasize that this makes our results also doubtful since this effect is generated by our low energy hadronic model in an area which is no longer well described by it.

On top of these uncertainties we found that including the $S_{11}(1535)$ resonance produces a visible effect (especially at densities lower than normal nuclear matter density). The formation of the right peak in the in-medium spectral functions in figures (7.14) and (7.15) shows that at half normal nuclear matter density the resonance dominates over the other contributions. Hence including more resonances might also change the picture and give the mass some upward shift. Basically a better handle to decide which classes of diagrams should be regarded is necessary.

Another important point concerns the fact, that all the inelastic processes $\omega N \to \pi N$ and $\omega N \to 2\pi N$ were only treated at tree level. Here an improved calculation would be advisable, which incorporates coupled-channels and rescattering, e.g. a K-matrix approach [Fe98], [Pe02]. However the $2\pi N$-channel which proved to be so important is only very schematically included in the K-matrix calculation. This is the reason why the present work as well as the model in [Kl97], [Kl99] is limited to a tree-level calculation.

A different point of concern is the high energy behavior of the imaginary parts. Since the dispersion integrals run up to infinity, the form factors used to suppress the high energy contributions unavoidably introduce a model dependence into the real part of the scattering amplitudes. In addition the substraction constant needed for the dispersion relation is basically not fixed. In this VMD model it can be calculated in analogy to the Thomson limit for Compton scattering, but there might be additional contributions that are not covered in this theory. In total it is to be noted, that there are several uncertainties in this approach, which require a closer look to judge its predictive power.

Chapter 8

Summary and Outlook

This work was triggered by recent experimental indication [Tr05] of a significant lowering of the mass of the ω meson in nuclear matter. A prediction describing this situation rather well was made by Klingl et al. [Kl97], [Kl99] and thus their approach was well worth to be studied further. They connected the ωN forward-scattering amplitude with the in-medium ω selfenergy using the low density theorem and thus were able to make a prediction for the spectral function of the ω meson in nuclear matter.

Part I introduced some mathematical tools that were used in the calculations of this work: In Chapter 1 methods for an easy calculation of imaginary parts of scattering amplitudes, especially Cutkosky's Cutting Rules, were presented and demonstrated using a simple example. Chapter 2 provided details about dispersion relations which were used to obtain real parts of scattering amplitudes by exploiting their interdependence with the corresponding imaginary parts.

The hadronic model which was the basis of the following calculations was the matter of interest in Part II: The vector meson dominance model with its effective Lagrangians, the corresponding vertex functions and necessary form factors were shown in Chapter 3. In addition one resonance interaction was introduced which was not part of the previously used model. Chapter 4 contained a summary of all the diagrams that were calculated for this work and introduced the heavy baryon limit of [Kl97].

In Part III the details of the calculations were given and the results obtained were presented: Chapter 5 gave the Feynman rules that were employed in the calculations and covered the details for the different decay channels, as well as the matter of the dispersion relation and the subtraction constant. Since the $\omega N \to 2\pi N$ decay can have an intermediate ρN state, the spectral function of the ρ meson was needed in the calculations. The unphysical behavior of this model when going to energies outside its predictional range made it imperative to examine and modify the ρ spectral function, which was all done in Chapter 6. The results were provided in Chapter 7. First the plots of the imaginary parts of the scattering amplitudes were given and, where possible, compared with previous calculations by Klingl et al. Then the resulting effective scattering lengths and cross sections were given and it turned out that several of the diagrams in the $2\pi N$-channel, that were neglected before, give a very sizable contribution and thus influence the results for these quantities and the real part of the ω selfenergy dramatically. This is due to the heavy baryon limit employed in [Kl97], [Kl99] and this matter is discussed further in section 7.5. There also the tree-level approach to the inelastic processes considered in the present work and in [Kl97], [Kl99] is examined.

The additional resonance contribution that came along by including the S_{11} (1535) resonance in the present work proved to be not negligible especially at lower than normal nuclear matter density. This is shown in detail in section 7.2 and discussed in section 7.5.

Resulting from the imaginary and real parts the in-medium ω spectral function was finally presented in section 7.4. The very low mass and very large width obtained from it were discussed and it was found that the choice of the classes of diagrams included is crucial to the results obtained, since Klingl et al. obtained a much higher mass and much lower width in [Kl97]. It was also noted that the large contributions found in this work are connected with the unphysical behavior of this hadronic model, which is described in detail in section 5.2.2 and discussed in section 7.5.

Further working with this model poses several challenges that have to be mastered: As already mentioned one first has to clarify which physical processes and therefore which diagrams give the most important contributions. Furthermore a distinct study of the use of different form factors would have to be performed as to understand their influence to the real part of the scattering amplitudes. Additionally a deeper look into the value of the subtraction constant, which is needed as input for the dispersion relation, is of importance, since it can directly influence the resulting mass shift in the medium.

Part IV

Appendix

Appendix A

Notation and conventions

This work is presented in natural units where

$$\hbar = c = 1 \; . \tag{A.1}$$

For conversion between units, a value of

$$\hbar c = 0.197327 \text{ GeV fm}$$

is used [PD02].
We use the metric tensor (as in [PS95])

$$g_{\mu\nu} = g^{\mu\nu} = \begin{pmatrix} 1 & 0 & 0 & 0 \\ 0 & -1 & 0 & 0 \\ 0 & 0 & -1 & 0 \\ 0 & 0 & 0 & -1 \end{pmatrix} \; . \tag{A.2}$$

For the Dirac γ-matrices the following trace relation is employed:

$$\mathrm{TR}\left(\gamma_\alpha \gamma_\beta \gamma_\mu \gamma_\nu \gamma_5\right) = -4i\epsilon^{\alpha\beta\mu\nu} \; . \tag{A.3}$$

The completeness relation of the nucleon spinors read

$$\sum_s u_s(p)\bar{u}_s(p) = \frac{\not{p} + M_N}{2M_N} \tag{A.4}$$

and of the nucleon isospin vectors

$$\sum_I \chi_I \chi_I^\dagger = 2 \; . \tag{A.5}$$

Appendix B

Numerical routines

For the numerical calculations of this work a C++ program was developed, which employed the GNU Scientific Library (GSL) [http://www.gnu.org/software/gsl/]. Specifically version 1.8, released 10 April 2006, was used.

For the numerical integrations involving the ρ spectral function the adaptive integration routine *gsl_integration_qag* employing a 61 point Gauss-Kronrod rule was used to reach a relative error of max. 10^{-4}. The normalization was calculated using the adaptive routine *gsl_integration_qagiu* for infinite intervals (max. relative error 10^{-8}).

For the dispersion integrals the cauchy principle value integration routine *gsl_integration_qawc*, which uses a 25-point modified Clenshaw-Curtis rule near the singularity and a usual Gauss-Kronrod 15 point rule further away, allowed for a relative precision of 10^{-4}. Further away from the pole again a simple adaptive integration with a 61-point Gauss-Kronrod rule was used, also with a max. relative error of 10^{-4}.

Since for the modified ρ spectral function with cutoff (section 6.2) the real part of the selfenergy had to be calculated with a dispersion integral (for the "standard" and simple ρ spectral function the real part is given analytically), this spectral function was tabulated to save CPU time. For the following integration it was interpolated using the GSL interpolation routine *gsl_interp_eval*, which employed cubic splines to approximate the spectral function, which was tabulated at steps of 1 MeV.

Appendix C

Analytic expressions for the scattering amplitudes

C.1 1π-channel

In the following formulae of this section k_0 is given by

$$k_0 = \sqrt{|\vec{k}|^2 + m_\pi^2} \tag{C.1}$$

and $|\vec{k}|$ by

$$|\vec{k}| = \frac{\sqrt{\left((M_N+\omega)^2 - (m_\pi + M_N)^2\right)\left((M_N+\omega)^2 - (m_\pi - M_N)^2\right)}}{2(M_N+\omega)} \,. \tag{C.2}$$

Diagram a):

$$\mathrm{Im}\; T(\omega) = \frac{g^2 g_{\rho\omega\pi}^2}{128\pi f_\pi^2} \frac{|\vec{k}|(1+\kappa_\rho)^2\,\omega^2\,\left(4M_N^2 - m_\pi^2 + 4M_N\omega + \omega^2\right)\left({m_\pi}^2 - \omega^2\right)^2}{\left(\omega^2 - 2\omega k_0 + m_\pi^2 - m_\rho^2\right)^2 (M_N+\omega)^4} \tag{C.3}$$

Diagram b):

$$\begin{aligned}\mathrm{Im}\; T(\omega) = \frac{9g^2 g_A^2 |\vec{k}|}{128\pi f_\pi^2} & \left(\frac{(m_\pi^2 - \omega^2)(8M_N^3(2\omega + M_N) - \omega^4)}{(2M_N\omega + \omega^2)^2 (M_N+\omega)^2}\right. \\ & \left. + \frac{6M_N^2\omega^2(2m_\pi^2 - \omega^2) + 2M_N\omega^3(\omega^2 + 2m_\pi^2)}{(2M_N\omega + \omega^2)^2 (M_N+\omega)^2}\right)\end{aligned} \tag{C.4}$$

Diagram c):

$$\begin{aligned}\mathrm{Im}\; T(\omega) = \frac{9g^2 g_A^2 |\vec{k}|}{128\pi f_\pi^2} & \left(\frac{8M_N k_0^2(-k_0 M_N + (m_\pi^2 + M_N(\omega - M_N)))}{(m_\pi^2 - 2M_N k_0)^2 (M_N+\omega)}\right. \\ & \left. + \frac{(8M_N^2 m_\pi^2 - 2m_\pi^4)k_0 - 2m_\pi^2(m_\pi^2 - 4M_N^2)(M_N - \omega)}{(m_\pi^2 - 2M_N k_0)^2 (M_N+\omega)}\right)\end{aligned} \tag{C.5}$$

Diagrams d) + e):

$$\mathrm{Im}\ T(\omega) = 2\frac{-3g^2 g_A g_{\rho\omega\pi}|\vec{k}|}{64\pi f_\pi^2} \left(\frac{(m_\pi^2 - k_0^2)\ \omega^2\ (2\,M_N\,\omega + 2\,k_0\,\kappa_\rho\ (M_N + \omega))}{(2M_N\omega + \omega^2)(\omega^2 - 2\omega k_0 + m_\pi^2 - m_\rho^2) M_N (M_N + \omega)} + \frac{(m_\pi^2 - k_0^2)\ \omega^2\ (-\kappa_\rho\ ({m_\pi}^2 + \omega^2))}{(2M_N\omega + \omega^2)(\omega^2 - 2\omega k_0 + m_\pi^2 - m_\rho^2) M_N (M_N + \omega)}\right) \tag{C.6}$$

Diagrams f) + g):

$$\mathrm{Im}\ T(\omega) = 2\frac{-3g^2 g_A g_{\rho\omega\pi}|\vec{k}|}{32\pi f_\pi^2} \left(\frac{(k_0^2 - m_\pi^2)\ \omega\ (-2\,k_0\,M_N + {m_\pi}^2)}{(m_\pi^2 - 2M_N k_0)(\omega^2 - 2\omega k_0 + m_\pi^2 - m_\rho^2)(M_N + \omega)} + \frac{(k_0^2 - m_\pi^2)\ \omega\ (2\ (M_N + k_0\,\kappa_\rho)\ \omega - \kappa_\rho\,\omega^2)}{(m_\pi^2 - 2M_N k_0)(\omega^2 - 2\omega k_0 + m_\pi^2 - m_\rho^2)(M_N + \omega)}\right) \tag{C.7}$$

$$\tag{C.8}$$

Diagrams h) + i):

$$\mathrm{Im}\ T(\omega) = 2\frac{18g^2 g_A^2|\vec{k}|}{128\pi f_\pi^2} \left(\frac{k_0\,{m_\pi}^2\,\omega\ (2\,M_N + \omega) + 2k_0^2 M_N\,(2M_N^2 + 2M_N\omega + \omega^2)}{(2M_N\omega + \omega^2)(m_\pi^2 - 2M_N k_0)(M_N + \omega)} + \frac{m_\pi^2\,(-4M_N^3 - 4M_N^2\omega - m_\pi^2\omega + M_N\,(m_\pi^2 - 2\omega^2))}{(2M_N\omega + \omega^2)(m_\pi^2 - 2M_N k_0)(M_N + \omega)}\right) \tag{C.9}$$

C.2 2π-channel

In the following formulae of this section k_0 is given by

$$k_0 = \sqrt{|\vec{k}|^2 + m_\rho^2} \tag{C.10}$$

and $|\vec{k}|$ by

$$|\vec{k}| = \frac{\sqrt{((M_N+\omega)^2-(m_\rho+M_N)^2)((M_N+\omega)^2-(m_\rho-M_N)^2)}}{2(M_N+\omega)} \,. \tag{C.11}$$

Diagram j):

$$\mathrm{Im}\; T(\omega, m_\rho) = \frac{g_{\rho\omega\pi}^2 g_A^2}{16 f_\pi^4 \pi} \frac{|\vec{k}|^3\omega^2 \left(2|\vec{k}|^2 M_N - (k_0-\omega)\left((k_0-\omega)^2 - |\vec{k}|^2\right)\right)}{(\omega^2 - 2\omega k_0 + m_\rho^2 - m_\pi^2)^2 (M_N+\omega)} \tag{C.12}$$

Diagram k):

$$\begin{aligned}
\mathrm{Im}\; T(\omega, m_\rho) = & -\frac{9g^4}{128\pi}\frac{|\vec{k}|}{(2M_N\omega+\omega^2)^2(M_N+\omega)} \\
& \times \Bigg(-12\,k_0\,{M_N}^2 - 8\,{M_N}^3 + \frac{8\,{k_0}^2\,{M_N}^3}{{m_\rho}^2} - 12\,M_N\,{m_\rho}^2\,\kappa_\rho \\
& + 4\,{k_0}^2\,M_N\,{\kappa_\rho}^2 - 3\,k_0\,{m_\rho}^2\,{\kappa_\rho}^2 - 4\,M_N\,{m_\rho}^2\,{\kappa_\rho}^2 - 12\,k_0\,M_N\,\omega \\
& - 4\,{M_N}^2\,\omega + \frac{16\,{k_0}^2\,{M_N}^2\,\omega}{{m_\rho}^2} + 12\,k_0\,M_N\,\kappa_\rho\,\omega - 12\,{m_\rho}^2\,\kappa_\rho\,\omega \\
& + 8\,{k_0}^2\,{\kappa_\rho}^2\,\omega - 5\,{m_\rho}^2\,{\kappa_\rho}^2\,\omega - \frac{3\,k_0\,{m_\rho}^2\,{\kappa_\rho}^2\,\omega}{M_N} + 6\,k_0\,\omega^2 \\
& - 10\,M_N\,\omega^2 + \frac{4\,{k_0}^2\,M_N\,\omega^2}{{m_\rho}^2} + 30\,k_0\,\kappa_\rho\,\omega^2 - \frac{12\,{m_\rho}^2\,\kappa_\rho\,\omega^2}{M_N} \\
& + \frac{2\,{k_0}^2\,{\kappa_\rho}^2\,\omega^2}{M_N} + \frac{3\,k_0\,{m_\rho}^2\,{\kappa_\rho}^2\,\omega^2}{2\,{M_N}^2} - \frac{7\,{m_\rho}^2\,{\kappa_\rho}^2\,\omega^2}{2\,M_N} - 2\,\omega^3 \\
& - \frac{4\,{k_0}^2\,\omega^3}{{m_\rho}^2} + \frac{12\,k_0\,\kappa_\rho\,\omega^3}{M_N} - \frac{2\,{k_0}^2\,{\kappa_\rho}^2\,\omega^3}{{M_N}^2} + \frac{{m_\rho}^2\,{\kappa_\rho}^2\,\omega^3}{2\,{M_N}^2}\Bigg)
\end{aligned} \tag{C.13}$$

Diagram l):

$$
\begin{aligned}
\mathrm{Im}\, T(\omega, m_\rho) = &-\frac{9g^4}{128\pi}\frac{|\vec{k}|}{(m_\rho^2-2M_N k_0)^2(M_N+\omega)} \\
&\times\left(4\,{k_0}^3-4\,k_0\,|\vec{k}|^2-12\,{k_0}^2\,M_N+4\,|\vec{k}|^2\,M_N-8\,{M_N}^3+\frac{2\,{k_0}^5}{{m_\rho}^2}\right. \\
&-\frac{4\,{k_0}^3\,|\vec{k}|^2}{{m_\rho}^2}+\frac{2\,k_0\,|\vec{k}|^4}{{m_\rho}^2}-\frac{6\,{k_0}^4\,M_N}{{m_\rho}^2}+\frac{4\,{k_0}^2\,|\vec{k}|^2\,M_N}{{m_\rho}^2}+\frac{2\,|\vec{k}|^4\,M_N}{{m_\rho}^2} \\
&+\frac{8\,k_0\,|\vec{k}|^2\,{M_N}^2}{{m_\rho}^2}+\frac{8\,{k_0}^2\,{M_N}^3}{{m_\rho}^2}-18\,{k_0}^3\,\kappa_\rho+18\,k_0\,|\vec{k}|^2\,\kappa_\rho+\frac{6\,{k_0}^4\,\kappa_\rho}{M_N} \\
&-\frac{12\,{k_0}^2\,|\vec{k}|^2\,\kappa_\rho}{M_N}+\frac{6\,|\vec{k}|^4\,\kappa_\rho}{M_N}+12\,|\vec{k}|^2\,M_N\,\kappa_\rho+4\,k_0\,|\vec{k}|^2\,{\kappa_\rho}^2 \\
&+\frac{3\,{k_0}^5\,{\kappa_\rho}^2}{2\,{M_N}^2}-\frac{3\,{k_0}^3\,|\vec{k}|^2\,{\kappa_\rho}^2}{{M_N}^2}+\frac{3\,k_0\,|\vec{k}|^4\,{\kappa_\rho}^2}{2\,{M_N}^2}-\frac{9\,{k_0}^4\,{\kappa_\rho}^2}{2\,M_N} \\
&+\frac{4\,{k_0}^2\,|\vec{k}|^2\,{\kappa_\rho}^2}{M_N}+\frac{|\vec{k}|^4\,{\kappa_\rho}^2}{2\,M_N}+4\,|\vec{k}|^2\,M_N\,{\kappa_\rho}^2-4\,{k_0}^2\,\omega-4\,|\vec{k}|^2\,\omega \\
&-8\,k_0\,M_N\,\omega+8\,{M_N}^2\,\omega-\frac{2\,{k_0}^4\,\omega}{{m_\rho}^2}+\frac{4\,{k_0}^2\,|\vec{k}|^2\,\omega}{{m_\rho}^2}-\frac{2\,|\vec{k}|^4\,\omega}{{m_\rho}^2} \\
&+\frac{8\,{k_0}^3\,M_N\,\omega}{{m_\rho}^2}-\frac{8\,k_0\,|\vec{k}|^2\,M_N\,\omega}{{m_\rho}^2}-\frac{8\,{k_0}^2\,{M_N}^2\,\omega}{{m_\rho}^2}-12\,|\vec{k}|^2\,\kappa_\rho\,\omega \\
&-\frac{6\,{k_0}^3\,\kappa_\rho\,\omega}{M_N}+\frac{6\,k_0\,|\vec{k}|^2\,\kappa_\rho\,\omega}{M_N}-4\,|\vec{k}|^2\,{\kappa_\rho}^2\,\omega-\frac{3\,{k_0}^4\,{\kappa_\rho}^2\,\omega}{2\,{M_N}^2} \\
&\left.+\frac{2\,{k_0}^2\,|\vec{k}|^2\,{\kappa_\rho}^2\,\omega}{{M_N}^2}-\frac{|\vec{k}|^4\,{\kappa_\rho}^2\,\omega}{2\,{M_N}^2}\right)
\end{aligned}
\tag{C.14}
$$

Diagrams m) + n):

$$
\begin{aligned}
\mathrm{Im}\, T(\omega, m_\rho) = &\,2\frac{-3g^2 g_A g_{\rho\omega\pi}}{64\pi f_\pi^2}\frac{|\vec{k}|^3\omega^2}{(2M_N\omega+\omega^2)(\omega^2-2\omega k_0+m_\rho^2-m_\pi^2)(M_N+\omega)M_N} \\
&\times\left(4\,{M_N}^2-2\,k_0\,M_N\,\kappa_\rho+\kappa_\rho\,\left(k_0^2-|\vec{k}|^2-2k_0\omega+\omega^2\right)\right)
\end{aligned}
\tag{C.15}
$$

Diagrams o) + p):

$$
\mathrm{Im}\, T(\omega, m_\rho) = 2\frac{-3g^2 g_A g_{\rho\omega\pi}}{64\pi f_\pi^2}\frac{2|\vec{k}|^3\omega\left(-m_\rho^2+2M_N k_0+(\kappa_\rho+1)(2\omega k_0-\omega^2)\right)}{(m_\rho^2-2M_N k_0)(\omega^2-2\omega k_0+m_\rho^2-m_\pi^2)(M_N+\omega)}
\tag{C.16}
$$

Diagrams q) + r):

$$
\begin{aligned}
\mathrm{Im}\ T(\omega, m_\rho) = 2\frac{-9g^4}{128\pi}&\frac{|\vec{k}|}{(m_\rho^2 - 2M_N k_0)(\omega^2 + 2M_N\omega)(M_N+\omega)} \\
\times \Bigg(& 4\,{k_0}^2\,M_N + 4\,|\vec{k}|^2\,M_N + 8\,k_0\,{M_N}^2 - 8\,{M_N}^3 + \frac{2\,{k_0}^4\,M_N}{{m_\rho}^2} \\
& - \frac{4\,{k_0}^2\,|\vec{k}|^2\,M_N}{{m_\rho}^2} + \frac{2\,|\vec{k}|^4\,M_N}{{m_\rho}^2} - \frac{8\,{k_0}^3\,{M_N}^2}{{m_\rho}^2} + \frac{8\,k_0\,|\vec{k}|^2\,{M_N}^2}{{m_\rho}^2} \\
& + \frac{8\,{k_0}^2\,{M_N}^3}{{m_\rho}^2} + 6\,{k_0}^3\,\kappa - 6\,k_0\,|\vec{k}|^2\,\kappa + 12\,|\vec{k}|^2\,M_N\,\kappa + \frac{3\,{k_0}^4\,\kappa^2}{2\,M_N} \\
& - \frac{2\,{k_0}^2\,|\vec{k}|^2\,\kappa^2}{M_N} + \frac{|\vec{k}|^4\,\kappa^2}{2\,M_N} + 4\,|\vec{k}|^2\,M_N\,\kappa^2 + 8\,{k_0}^2\,\omega - 12\,k_0\,M_N\,\omega \\
& - 8\,{M_N}^2\,\omega - \frac{2\,{k_0}^4\,\omega}{{m_\rho}^2} + \frac{4\,{k_0}^2\,|\vec{k}|^2\,\omega}{{m_\rho}^2} - \frac{2\,|\vec{k}|^4\,\omega}{{m_\rho}^2} + \frac{8\,{k_0}^2\,{M_N}^2\,\omega}{{m_\rho}^2} \\
& - 6\,{k_0}^2\,\kappa\,\omega + 18\,|\vec{k}|^2\,\kappa\,\omega + \frac{3\,{k_0}^3\,\kappa\,\omega}{M_N} - \frac{3\,k_0\,|\vec{k}|^2\,\kappa\,\omega}{M_N} + 4\,|\vec{k}|^2\,\kappa^2\,\omega \\
& + \frac{{k_0}^2\,|\vec{k}|^2\,\kappa^2\,\omega}{{M_N}^2} - \frac{|\vec{k}|^4\,\kappa^2\,\omega}{{M_N}^2} - 8\,k_0\,\omega^2 + 4\,M_N\,\omega^2 + \frac{2\,{k_0}^3\,\omega^2}{{m_\rho}^2} \\
& - \frac{2\,k_0\,|\vec{k}|^2\,\omega^2}{{m_\rho}^2} - \frac{4\,{k_0}^2\,M_N\,\omega^2}{{m_\rho}^2} - \frac{3\,{k_0}^2\,\kappa\,\omega^2}{M_N} + \frac{|\vec{k}|^2\,\kappa\,\omega^2}{M_N}\Bigg)
\end{aligned}
\tag{C.17}
$$

C.3 $S_{11}(1535)$ resonance

Diagram s):

$$\begin{aligned}
\mathrm{Im}\, T(\omega) = {} & \frac{3\, {g_2}^2\, \omega^2\, \left(M_N + m_{S_{11}} + \omega\right) + 8\, {g_1}^2\, {M_N}^2\, \left(M_N + 2\, m_{S_{11}} + \omega\right)}{12\, {M_N}^2} \\
& \times \frac{m_{S_{11}} \Gamma_{S_{11}}}{(M_N^2 + 2M_N\omega + \omega^2 - m_{S_{11}}^2)^2 + m_{S_{11}}^2 \Gamma_{S_{11}}^2}
\end{aligned} \tag{C.18}$$

$$\begin{aligned}
\mathrm{Re}\, T(\omega) = {} & -\frac{3\, {g_2}^2\, \omega^2\, \left(M_N + m_{S_{11}} + \omega\right) + 8\, {g_1}^2\, {M_N}^2\, \left(M_N + 2\, m_{S_{11}} + \omega\right)}{12\, {M_N}^2} \\
& \times \frac{M_N^2 + 2M_N\omega + \omega^2 - m_{S_{11}}^2}{(M_N^2 + 2M_N\omega + \omega^2 - m_{S_{11}}^2)^2 + m_{S_{11}}^2 \Gamma_{S_{11}}^2}
\end{aligned} \tag{C.19}$$

Appendix D

Deutsche Zusammenfassung

Seit einiger Zeit besteht großes Interesse daran, die Eigenschaften von Hadronen in einem stark wechselwirkenden Medium zu verstehen und zu beschreiben. Dieses Interesse rührt daher, daß experimentelle Hinweise auf Änderungen von Eigenschaften von Hadronen wie Masse oder Zerfallsbreite in einem nuklearen Medium auftauchten. Insbesondere eine geringere Masse im Medium wäre hierbei interessant, da dies ein Hinweis auf eine Wiederherstellung der im Vakuum spontan gebrochenen chiralen Symmetrie bei hohen Dichten wäre. Näheres hierzu in [RW00].

Im Speziellen gab es in der Vergangenheit eine lebhafte wissenschaftliche Diskussion über die Modifikationen der Masse des ω-Mesons in einem nuklearen Medium. Es gibt eine gewisse Einigkeit darüber, daß die In-Medium-Breite in der Größenordnung von etwa 40 MeV liegt, jedoch gibt es unterschiedliche Vorhersagen für die Massenverschiebung. Während einige Gruppen abgesenkte Massen prognostizieren [Re02], [Kl97], [Kl99], gibt es auch Vorhersagen für eine steigende Masse [DM01], [PM01], [SL06], [Zs02] oder eine Spektralfunktion mit mehreren Peaks [Lu02], [Mu06]. Die kürzlich veröffentlichte Auswertung eines Experiments [Tr05] gab nun den ersten Hinweis auf eine wesentliche Absenkung der Masse im Medium, welche als erstes von Klingl et al. [Kl97] beschrieben wurde. Daher war es das Ziel dieser Diplomarbeit einen tieferen Blick in deren Zugang zu werfen und diesen genauer zu untersuchen.

Der in [Kl97] benutzte Ansatz war das Vektormesonendominanz-Modell kombiniert mit chiraler SU(3) Symmetrie, um ein hadronisches Modell für die Kopplung der Baryonen und der Pseudovektor- und Vektor-Mesonen zu konstruieren. Jedoch war in diesem Modell keine direkte ω-Nukleon-Resonanz Wechselwirkung enthalten. Aus diesem Grund wurde in dieser Arbeit eine solche Wechselwirkung mit der $S_{11}(1535)$ Resonanz eingeführt und näher untersucht. Im Rahmen dieses Modells kann man die ωN Vorwärtsstreuamplitude über ein Niedrig-Dichte Theorem mit der ω Selbstenergie im Medium in Verbindung bringen. Dieser Zugang wurde auch in dieser Arbeit benutzt.

Zuvor wurde jedoch in Teil I dieser Arbeit das mathematische Rüstzeug für die folgenden Berechnungen eingeführt. Im Speziellen waren dies in Kapitel 1 Methoden zur einfachen Berechnung der Imaginärteile der Streuamplituden. Hier wurden unter anderem Cutkosky's Schnittregeln eingeführt und anhand eines einfachen Beispiels illustriert. Kapitel 2 beschäftigte sich dann mit Dispersionsrelationen, die einem erlauben über ein Hauptwert-Integral aus den zuvor gewonnen Imaginärteilen den zugehörigen Realteil zu bestimmen. Dies war notwendig, da die Schnittregeln zwar endliche Imaginärteile liefern, die zugehörigen Realteile jedoch regularisiert werden müssen [PS95] und man die Analytizität der Streuamplitude erhalten will [BD93].

Teil II gab nun eine Übersicht über das verwendete hadronische Modell: In Kapitel 3 wurden die effektiven Lagrangedichten für die einzelnen Wechselwirkungen und die davon abgeleiteten Vertexfunktionen gezeigt, sowie die für die späteren Rechnungen notwendigen Form-Faktoren. Sämtliche Diagramme, die in dieser Arbeit Berücksichtigung fanden, wurden in Kapitel 4 aufgeführt und die Schwere-Baryonen-Näherung aus [Kl97] wurde hier näher beschrieben.

Alle Details zu den Rechnungen und den Ergebnissen waren Inhalt von Teil III: Speziell wurden in Kapitel 5 die Feynman Regeln, die zur Berechnung der Streuamplituden verwandt wurden, eingeführt und die Dispersionrelation mit, insbesondere, der notwendigen Subtraktionskonstanten beschrieben. Weil der $\omega N \to 2\pi N$-Kanal auch ein ρ-Meson im Zwischenzustand haben kann, war es notwendig, die ρ Spektralfunktion näher zu beleuchten. Insbesondere trat hier ein Problem auf, dadurch daß sich ein unphysikalisches Verhalten des Modells einstellte, allerdings in einem Bereich, der nicht mehr von der Vektormesonendominanz beschrieben wird. Dies bedingte die Einführung von modifizierten ρ Spektralfunktionen. Diese wurden in Kapitel 6 beschrieben. Die Ergebnisse der Rechnungen für die Imaginärteile der verschiedenen Kanäle, sowie Vergleiche mit früheren Ergebnissen waren Teil des Inhalts von Kapitel 7. Weiterhin wurden hier die errechneten Realteile, daraus resultierende Streulängen und Wirkungsquerschnitte und schließlich die resultierende In-Medium Spektralfunktion des ω-Mesons gezeigt.

Die für die Vorwärtsstreuamplitude wichtigen Prozesse $\omega N \to \pi N$ und $\omega N \to 2\pi N$ wurden in [Kl97] nur auf tree-level berechnet. Hier wäre es jedoch wünschenswert eine verbesserte Rechnung durchzuführen, die gekoppelte Kanäle und Rückstreuung beinhaltet, z.B. eine K-Matrix Rechnung [Fe98], [Pe02]. Allerdings ist der 2π-Kanal, der sich in der vorliegenden Arbeit als besonders wichtig herausgestellt hat, nur sehr schematisch im K-Matrix Zugang enthalten. Daher beschränkt sich auch diese Arbeit nur auf eine tree-level Berechnung.

Weiterhin wurde in [Kl97] eine Schwere-Baryonen-Näherung verwendet (siehe Sektion 4.4), aufgrund derer einige Diagramme im 2π-Kanal keine Berücksichtigung fanden. Diese Diagramme wurden in der vorliegenden Arbeit voll relativistisch berechnet. Es zeigte sich, daß diese vorher nicht enthaltenden Diagramme wesentlich größere Beiträge als die bisher in [Kl97] enthaltenden Diagramme aufwiesen, so daß diese neu hinzugekommenen Diagramme den 2π-Kanal praktisch dominierten, was die Schwere-Baryonen-Näherung doch zweifelhaft erscheinen läßt. Es ist anzumerken, daß die großen Beiträge dieser Diagramme im direkten Zusammenhang mit dem Pol im Nukleon-Propagator stehen, wie in Sektion 5.2.2 beschrieben. Daher sind die großen Beiträge, die wir finden, auch mit Zweifeln behaftet, insbesondere auch weil sie zu viel zu großen Querschnitten führten (siehe Sektion 7.3). Nichtsdestoweniger führte dies dazu, daß wir in dieser Arbeit ein ω im Medium mit stark abgesenkter Masse und stark vergrößerter Breite fanden, abweichend von den vorherigen Ergebnissen von Klingl et al. [Kl97]. Außerdem fanden wir, daß der Beitrag, den die S_{11} Resonanz lieferte, insbesondere bei Dichten eine Rolle spielt, die geringer als die Dichte normaler Kernmaterie sind. Dieser Beitrag führte zu einer Spektralfunktion mit mehreren Peaks, wobei bei halber Kernmateriedichte die Resonanz die Spektralfunktion des ω sogar dominierte. Dies ist ein Hinweis darauf, daß die Berücksichtigung weiterer Resonanzen das entstandende Bild weiter verändern kann.

Abzulesen hieran ist, daß die Wahl der zu verwendenden Diagramm-Klassen sehr entscheidend für das quantitative Ergebnis ist. Weiterhin ist zu bemerken, daß durch die verwendeten Formfaktoren eine unweigerliche Modellabhängigkeit im Realteil, der ja durch eine Dispersionrelation gewonnen wird, auftritt. Schließlich ist noch zu berücksichtigen, daß die Subtraktionskonstante der Dispersionsrelation einen direkten Einfluß auf die Massenverschiebung hat und ihr genauer Wert in diesem Modell zwar analog zum Thomsonlimit in der Comptonstreuung festgelegt ist, sie jedoch prinzipiell auch noch Einflüssen unterliegen kann, die nicht von diesem Modell beschrieben werden, und daher streng genommen nicht festgelegt werden kann.

Bibliography

[BD93] J.D. Bjorken, S.D. Drell: *Relativistische Quantenfeldtheorie*, B.I. Wissenschaftsverlag, Mannheim, 1993.

[Cu60] R.E. Cutkosky: *Singularities and Discontinuities of Feynman Amplitudes*, J. Math. Phys., 1:429, 1960.

[DM01] A.K. Dutt-Mazumder et al.: *$\rho - \omega$ mixing in asymmetric nuclear matter via QCD sum rule approach*, Phys.Rev., C63:015204, 2001.

[FB99] W. Florkowski, W. Broniowski: *Subtracted Dispersion Relations for In-Medium Meson Correlators in QCD Sum Rules*, Nucl.Phys., A651:397-410, 1999.

[Fe72] R.P. Feynman: *Photon Hadron Interactions*, Benjamin, Reading, 1971.

[Fe98] T. Feuster: *Photon- und meson-induzierte Reaktionen am Nukleon*, PhD Thesis, Institut für Theoretische Physik, JLU Giessen, 1998.

[FR98] B. Friman: *Vector meson propagation in dense matter*, Talk given at APCTP Workshop on Astro-Hadron Physics: Properties of Hadrons in Matter, Seoul, 1997, arXiv:nucl-th, 9801053v2, 1998.

[He93] M. Herrmann et al.: *Properties of ρ mesons in nuclear matter*, Nucl.Phys., A560:411-436, 1993.

[Ja99] K. Jänich: *Funktionentheorie*, Springer-Verlag, Berlin, 1999.

[Ki83] T. Kitagaki et al.: *High-energy quasielastic $\nu_\mu n \to \mu^- p$ scattering in deuterium*, Phys.Rev., D28:436-442, 1983.

[Kl96] F. Klingl et al.: *Effective Lagrangian approach to vector mesons, their structure and decays*, Z.Phys., A356:193-206, 1996.

[Kl97] F. Klingl et al.: *Current correlation functions, QCD sum rules and vector mesons in baryonic matter*, Nucl.Phys., A624:527-563, 1997.

[Kl98] F. Klingl: *Vektormesonen in dichter hadronischer Materie*, PhD Thesis, Fakultät für Physik, TU München, 1998.

[Kl99] F. Klingl et al.: *Nuclear bound states of omega mesons*, Nucl.Phys., A650:299-312, 1999.

[Ko98] L.A. Kondratyuk et al.: *ρ-meson properties at finite nuclear density*, Phys.Rev., C58:1078-1085, 1998.

[Le06] S. Leupold: *Private communications.*

[Lu02] M. Lutz et al.: *Scattering of vector mesons off nucleons*, Nucl.Phys., A706:431-496, 2002.

[Mo99] U. Mosel: *Fields, Symmetries, and Quarks*, Springer-Verlag, Berlin Heidelberg, 1999.

[Mu06] P. Mühlich et al.: *The spectral function of the ω meson in nuclear matter from a coupled-channel resonance model*, arXiv:nucl-th, 0607061v1, 2006.

[MuP6] P. Mühlich: *Private communications.*

[PD02] K. Hagiwara et al.: *Particle data group*, Phys.Rev., D66, 010001, 2002.

[Pe02] G. Penner: *Vector Meson Production and Nucleon Resonance Analysis in a Coupled-Channel Approach*, PhD Thesis, Institut für Theoretische Physik, JLU Giessen, 2002.

[PM01] M. Post, U. Mosel: *Vector Mesons and Baryon Resonances in Nuclear Matter*, Nucl.Phys., A699:169-172, 2001.

[PM02] G. Penner, U. Mosel: *Vector meson production and nucleon resonance analysis in a coupled-channel approach for energies $m_N < \sqrt{s} < 2$ GeV I: pion-induced results and hadronic parameters*, Phys.Rev., C66:055211, 2002.

[Po03] M. Post: *Hadronic Spectral Functions in Nuclear Matter*, PhD Thesis, Institut für Theoretische Physik, JLU Giessen, 2003.

[PS95] M.E. Peskin, D.V. Schroeder: *An Introduction to Quantum Field Theory*, Westview Press, USA, 1995.

[Re02] T. Renk et al.: *Phases of QCD, thermal quasiparticles and dilepton radiation from a fireball*, Phys.Rev., C66:014902, 2002.

[RW00] R. Rapp, J. Wambach: *Chiral symmetry restoration and dileptons in relativistic heavy ion collisions*, Adv.Nucl.Phys., 25:1, 2000.

[Sa69] J.J. Sakurai: *Currents and Mesons*, University of Chicago Press, Chicago, 1969.

[Sh05] V. Shklyar: *Coupled-channel analysis of the ω-meson production in πN and γN reactions for c.m. energies up to 2 GeV.*, Phys.Rev., C71:055206, 2005, Erratum-ibid. C72:019903, 2005.

[SL06] B. Steinmüller, S. Leupold: *Weighted finite energy sum rules for the omega meson in nuclear matter*, arXiv:hep-ph, 0604054v1, 2006.

[Tr05] D. Trnka et al.: *First observation of in-medium modifications of the omega meson*, Phys.Rev.Lett., 94:192303, 2005.

[WW05] W. Weise: *Private communications.*

[Zs02] S. Zschocke et al.: *In-medium spectral change of omega mesons as a probe of QCD four quark condensate*, Phys.Lett., B562:57-62, 2003.

Danksagungen

Zuallererst möchte ich Herrn Professor Ulrich Mosel für die Aufnahme in sein Institut danken, sowie dafür, daß er mir die Möglichkeit gegeben hat, diese Diplomarbeit anzufertigen. Seine vielen Anregungen, Tips und konstruktive Kritik haben mir stets weitergeholfen.

Ganz besonders will ich mich bei Dr. Stefan Leupold für seine mir geopferte Zeit und Mühe bedanken. Ohne die vielen Gespräche mit ihm über all die technischen Details und ohne die vielen Hinweise zu den Aspekten der Quantenfeldtheorie wäre die Arbeit in dieser Form nicht möglich gewesen.

Weiterhin möchte ich mich bei Dr. Vitaliy Shklyar für seine Tips und Hilfe, insbesondere bei der Einarbeitung der Resonanz, bedanken.

Der Computercrew, Oliver Buss und Frank Frömel, danke ich für die prompten und hilfreichen, Gott sei Dank nur selten notwendigen Tips und für die praktisch ausfallsfreie Zeit, was die Server und Computersysteme betrifft, die mir offen standen.

Meinen Eltern danke ich ganz besonders für jegliche, nicht nur finanzielle Unterstützung während meines Studiums, für die vielen Freiheiten, die sie mir gelassen haben und für die viele Geduld, die sie aufgebracht haben, wenn die Erledigung einiger Dinge wieder mal etwas länger dauerte.

Meinen beiden Freunden Andreas und Abdul danke ich für die viele schöne Zeit, die wir zusammen an und außerhalb der Universität verbracht haben und für den regen Austausch an Gedanken, Kritik und Hilfen, der eine Freundschaft so wichtig sein läßt. Ohne sie hätte das Studium sicher nicht soviel Spaß gemacht.

Meinem Zimmerkollegen David danke ich für die gute Atmosphäre während der Arbeitszeit und für die vielen physikalischen und auch unphysikalischen Gespräche, sowie für die Durchsicht dieses Manuskripts.

Bei allen anderen Institutsmitgliedern bedanke ich mich für das gute Arbeitsklima, die schönen gesellschaftlichen Veranstaltungen und die vielen Besuche und Unterhaltungen im Partyzimmer, durch die ich alle noch ein bißchen besser kennenlernen konnte.

Dem wichtigsten Menschen in meinem Leben, meiner Partnerin Kathrin, möchte ich für die viele Unterstützung, gerade auch neben dem Studium, danken und für ihre Geduld und für ihr Verständnis, wenn ich sie wieder mal mit Physik genervt habe oder später nach Hause kam, wenn ich wieder ”noch schnell was rechnen" wollte.

Last but not least bedanke ich mich bei Elke Jung für alle Hilfe was Organisatorisches und Bürokratie betrifft. Sie war stets tätig und erfolgreich bemüht den "Papierkram" und alles was damit zusammen hängt schnellstmöglich zu erledigen und hat mir damit viel Arbeit und Aufwand erspart.

Ich versichere hiermit, daß ich diese Diplomarbeit selbstständig verfasst und keine anderen als die angegebenen Quellen und Hilfsmittel benutzt habe.

________________________ Gießen, den ____________________